INFORMATION TO USERS

This manuscript has been reproduced from the microfilm master. UMI films the text directly from the original or copy submitted. Thus, some thesis and dissertation copies are in typewriter face, while others may be from any type of computer printer.

The quality of this reproduction is dependent upon the quality of the copy submitted. Broken or indistinct print, colored or poor quality illustrations and photographs, print bleedthrough, substandard margins, and improper alignment can adversely affect reproduction.

In the unlikely event that the author did not send UMI a complete manuscript and there are missing pages, these will be noted. Also, if unauthorized copyright material had to be removed, a note will indicate the deletion.

Oversize materials (e.g., maps, drawings, charts) are reproduced by sectioning the original, beginning at the upper left-hand corner and continuing from left to right in equal sections with small overlaps.

Photographs included in the original manuscript have been reproduced xerographically in this copy. Higher quality 6" x 9" black and white photographic prints are available for any photographs or illustrations appearing in this copy for an additional charge. Contact UMI directly to order.

ProQuest Information and Learning
300 North Zeeb Road, Ann Arbor, MI 48106-1346 USA
800-521-0600

UNIVERSITY OF OKLAHOMA

GRADUATE COLLEGE

ELUCIDATING THE CATALYTIC MECHANISM OF MALIC ENZYME via SITE-DIRECTED MUTAGENESIS STUDIES.

A Dissertation

SUBMITTED TO THE GRADUATE FACULTY

in partial fulfillment of requirements for the degree of

Doctor of Philosophy

By

Dali Liu
Norman Oklahoma
2001

UMI Number: 3028803

UMI®

UMI Microform 3028803
Copyright 2002 by Bell & Howell Information and Learning Company.
All rights reserved. This microform edition is protected against unauthorized copying under Title 17, United States Code.

Bell & Howell Information and Learning Company
300 North Zeeb Road
P.O. Box 1346
Ann Arbor, MI 48106-1346

© Copyright by DALI LIU 2001

All Rights Reserved.

ELUCIDATING THE CATALYTIC MECHANISM OF MALIC ENZYME via SITE-DIRECTED MUTAGENESIS STUDIES.

A Dissertation **APPROVED FOR THE DEPARTMENT OF CHEMISTRY AND BIOCHEMISTRY**

BY

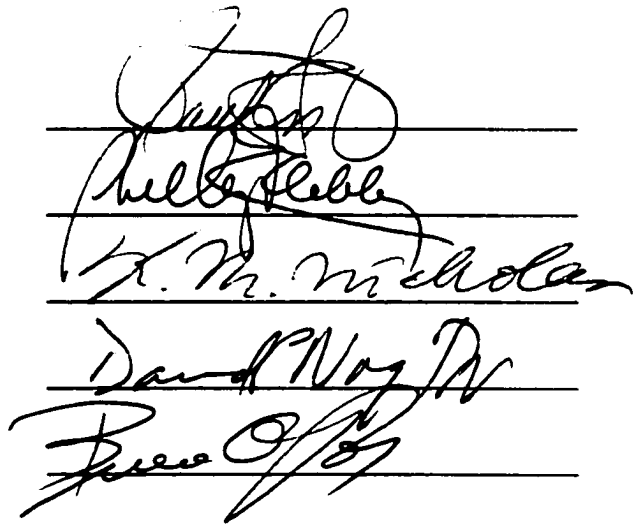

ACKNOWLEDGEMENTS

First of all, I would like to express my gratitude to my research advisor, Dr. Paul F. Cook, who is a dream boss for a graduate student. I feel blessed to have had the chance of studying and working under his guidance for the past five years. I also want to thank the other members of my graduate advisory committee, Dr. Bruce A. Roe, Dr. Phillip E. Klebba, Dr. Kenneth M. Nicholas, and Dr. David P. Nagle, Jr., for constantly motivating me and helping me improving.

I am extremely grateful for Drs. Bill Karsten and Lillian Chooback. They have taught me every technique I use in the lab as well as given invaluable advice on my project, and more importantly, their enormous patience with me helped me to overcome every mistake I made and become a confident researcher. The same thankfulness goes to Ms. Jean Keil for helping me on a daily base in the past five years. I appreciate every other member in Dr. Cook's lab, for being my friend and helping me. I give special thanks to Dr. Ann West and every member in her lab, for treating me as their own and helping me in whatever way they could.

At last, I want to dedicate this dissertation to my dear wife, Dr. Lei Zhang, and my family in China, whose love makes my life meaningful.

TABLE OF CONTENT

LIST OF TABLES

LIST OF FIGURES

LIST OF ABBREVIATIONS

APAD, 3-acetylpridine adenine dinucleotide

ADP, adenosine diphosphate

ATP, adenosine triphosphate

AsME, *Ascaris suum* malic enzyme

BSA, bovine serum albumin

Caps, 3-(cyclohexylamino)-1-propane-sulfonic acid

CD, circular dichroism

cDNA, complementary deoxyribonucleic acid

Ches, 2-(*N*-cyclohexylamino)ethanesulfonic acid

DEAE, diethylaminoethylcellulose

dsDNA, double stranded deoxyribonucleic acid

DTNB, 5,5-dithiobis(2-nitrobenzoic acid)

ESEEM, electron spin echo envelope modulation spectroscopy

Hepes, *N*-(2-hydroxyethyl)piperazine-*N'*-2-ethanesulfonic acid

HPLC, high performance liquid chromatography

ICDH, isocitrate dehydrogenase

IPMDH, isopropylmalate dehydrogenase

IPTG, isopropyl-β-D-thiogalactopyranoside

LB, Luria-Bertani

ME, malic enzyme

Mes, 2-(*N*-morpholino)ethanesulfonic acid

NAD^+, nicotinamide adenine dinucleotide

NADH, reduced nicotinamide adenine dinucleotide

$NADP^+$, nicotinamide adenine dinucleotide 2'-phosphate

NADPH, reduced nicotinamide adenine dinucleotide 2'-phosphate

Ni-NTA, Ni^{2+}-nitrilo-tri-acetic acid

OAA, oxalacetate

PAAD, 3-pyridinealdehyde adenine dinucleotide

PAGE, polyacrylamide gel electrophoresis

PCR, polymerase chain reaction

PEP, phosphoenolpyruvate

6PG, 6-phosphogluconate

6PGDH, 6-phosphogluconate dehydrogenase

Pipes, piperazine-*N*, *N*'-bis-(2-ethanesulfonic acid)

SDS, sodium dodecyl sulfate

ssDNA, single stranded deoxyribonucleic acid

Taps, 3-[[tris(hydroxymethyl)methyl]amino]-propanesulfonic acid

TDH, tartrate dehydrogease

WT, wild type

ABSTRACT

Malic enzyme catalyzes the metal-ion dependent oxidative decarboxylation of L-malate with $NAD(P)^+$ as a cofactor. NAD-dependent malic enzyme from *Ascaris suum* was used in the research of this dissertation to elucidate the catalytic mechanism of the malic enzyme reaction, especially the identities of catalytic groups.

Based on homology search results and the three-dimensional structures of malic enzymes, 12 highly conserved ionizable residues were selected as potential general acid/base in the malic enzyme reaction. Site-directed mutagenesis studies were carried out to eliminate the potential catalytic groups on the targeted residues. One lysine (199), and four glutamates (58, 107, 271, 440) were mutated to alanine (alanine scanning), while one tyrosine (126) was mutated to phenylalaine. The alanine and phenylalanine mutant proteins were expressed and purified. The initial velocity studies were carried out on the purified mutant proteins. The K199A mutant enzyme and the Y126F mutant enzyme exhibited decreases in turnover number by 10^5- and 10^3-fold, respectively, compared to that of the wild type AsME, the two most significant decreases in enzyme activity observed for the mutant enzymes studied. Therefore, K199 and Y126 were considered viable candidates for a catalytic residue.

Other mutations were thus prepared, changing K199 and Y126 to other residues. In the case of K199, the R mutant enzyme gave only a 10-fold decrease in turnover number compared to that of the WT AsME, while the K199E and K199Q mutant enzymes gave decreases in turnover number of about 10^4- and 10^5-fold, respectively. The much higher activity of the K199R mutant enzyme compared to K199A supports the assignment of K199 as a proton donor in the malic enzyme reaction. The V/K_{malate} pH-rate profile of the K199R mutant enzyme is pH independent over the pH range 8-10, while a pK of 9 is observed for the WT enzyme. These data are also consistent with K199 as general acid, given the higher pK of the R side chain compared to that of K in the malic enzyme reaction. Exchange of tritium from solvent into the methyl group of pyruvate, catalyzed by the WT enzyme, is eliminated in the K199A mutant enzyme, also consistent with the general acid function of K199. Thus, K199 serves as the general acid in the malic enzyme reaction. Partitioning of the oxalacetate intermediate with the K199A mutant enzyme is also consistent with the general acid function of K199, and further suggests that K199 also plays a structural role in the conformational change that must occur in the malic enzyme reaction. In this regard, K199 is in the hinge area in the active site, nestled between two subdomains involved in the conformational change.

The facts that no other ionizable residue can replace the function of Y126, and that the Y126F mutant enzyme is the most active among all mutants made at the 126 position, suggest that Y126F is not a catalytic group but structurally important in the active site area. The pH study and the oxalacetate partitioning results on Y126F are consistent with the idea that Y126 plays only a structural role in the malic enzyme reaction.

CHAPTER 1

INTRODUCTION

1.1. The Physiological Significance of the Malic Enzyme Reaction.

It was in the late 1940's that the evidence for the biological oxidative decarboxylation of malate was obtained independently by several scientists (Moulder et al., 1940; and Ochoa et al., 1947). Eventually, a divalent metal ion dependent enzyme, which catalyzes the reversible oxidative decarboxylation of L-malate to pyruvate and CO_2 with concomitant reduction of $NADP^+$, was identified in avian liver and named malic enzyme by Ochoa et al. (1947). Malic enzyme has since been isolated from most living organisms, including microorganisms, plants, and animals including humans.

As indicated by its wide distribution in nature, malic enzyme plays a significant role in a number of biological processes. The products of the malic enzyme reaction, pyruvate, CO_2 and the NAD(P)H, may subsequently serve as precursors or intermediates in many important metabolic pathways. For example, in the photosynthetic reactions in C4 plants, CO_2 is first carried by C4 compounds like oxalacetate and malate from mesophyll cells to bundle-sheath cells. Then the CO_2 is released via the malic enzyme reaction to maintain the concentration of CO_2 required by the Calvin cycle (Stryre, 1995).

Early investigations have also suggested that the oxidative decarboxylation of malate can be driven in the reverse direction by coupling it to the generation of NADPH in another system (Gornall et al., 1949; Shifrin and Kaplan, 1960; Rutter and Lardy, 1958). Possible reversal of the malic enzyme reaction suggested that it might participate

in gluconeogenesis by converting pyruvate to malate which could then be oxidized to the precursor of phosphoenolpyruvate, oxalacetate. However, malic enzyme activity in rat liver was proven insufficient for the needed rate of pyruvate conversion to carbohydrate. So, it is unlikely that malic enzyme contributes to gluconeogenesis in this manner, but the production of pyruvate as a gluconeogenic precursor is still a legitimate possibility. The amount of malic enzyme was found to increase under conditions favoring lipogenesis (Shrago, E. et al., 1963; Lardy, H.A., et al., 1964), leading to the suggestion that the malic enzyme reaction may supply lipogenesis with NADPH. Today, it is known that cytosolic NADP-dependent malic enzyme in mammals is involved in the generation of NADPH for the biosynthesis of fatty acids and steroids in liver and adipose tissues. Furthermore, cytosolic NADP-ME in mammals may also play a role in microsomal drug detoxification (Sanz et al., 1997).

Another malic enzyme isoform, mitochondrial NAD-dependent malic enzyme, plays an important role in energy production, via the production of NADH and pyruvate, in rapidly proliferating tissues such as spleen, thymus, mucosal cells of the small intestine, and particularly in tumors (Loeber et al., 1994; Baggetto., 1992). In tumor cells, the major sources of respiratory energy have been shown to be glutamine and glutamate, instead of glucose as in normal cells. Oxidation of glutamate in tumor cell mitochondria occurs initially via transamination of L-glutamate (which can be produced from L-glutamine via the glutaminase reaction) and OAA to L-aspartate and α-ketoglutarate. The α-ketoglutarate produced is then converted to malate via the Kreb's cycle generating 8 ATPs. The mitochondrial NAD-dependent malic enzyme in tumor mitochondria then converts malate to pyruvate, CO_2 and NADH, which generates another 3 ATPs. The pyruvate product can then be converted to OAA via the pyruvate carboxylase reaction, utilizing 1 mole of ATP. The pathway overall is called glutaminolysis, in contrast to glycolysis, which converts glucose to pyruvate (Mckeehan,

1982). Mitochondrial NAD-malic enzyme also plays a role in converting amino acids to pyruvate in mitochondria.

In 1956, malic enzyme was isolated from a rather unique creature, the parasitic nematode *Ascaris lumbricoides var suum* (Saz and Hubbar., 1957). Another variety of the same roundworm, *Ascaris lumbricoides*, infects humans, and is responsible for ascariasis in about 25% of the world's population. The life cycle of *Ascaris suum* is interesting. The eggs of the worm hatch to become larvae in the stomach and small intestine after being swallowed by the host. The larvae wander through host's body via the venules of the hepatic portal system, they migrate through the liver, heart, and enter the veins of the lungs, they penetrate the lung wall, reach the trachea, and are eventually swallowed. Their adult life is spent in the intestine of the host. During their journey, the larvae transform though four stages and finally develop to adults (Olsen, 1974). The adult form of the parasite resides in the small intestine, which is an environment with very low oxygen concentration. As a result, the parasite correspondingly has a special anaerobic mitochondrial energy metabolism (Fig 1), in which the Kreb's cycle is not functional and the electron-transport chain is surprisingly antimycin and cyanide resistant (Saz, 1981; Ward and Fairbain, 1970; Kohler and Bachman, 1980). During times of host feeding, the free-swimming parasite stores most of its glucose as glycogen in specialized muscle cells. In the cytosol of *Ascaris*, one equivalent of glucose from glycogen is converted to two equivalents of phosphoenolpyruvate as in the glycolytic pathway of the pig or human host. Phosphoenolpyruvate is then converted to oxalacetate by PEP carboxykinase, and oxalacetate is next converted to malate by malate dehydrogenase. Malate is transported into the mitochondria and undergoes a dismutation reaction. The NAD-malic enzyme catalyzes the oxidative decarboxylation of malate to produce pyruvate, CO_2 and intramitochondrial NADH while fumarase converts malate to fumarate to keep the malate pool in equilibrium with fumarate.

Figure 1. An Abbreviated Metabolic Pathway of the Parasitic Nematode, *Ascaris suum*. The pathway has a glycolytic portion in the cytoplasm to convert glucose to phosphoenolpyruvate. Phosphoenolpyruvate is then converted to L-malate via. the PEP carboxylkinase and malate dehydrogenase reactions. L-Malate is transported into the mitochondrion to undergo a dismutation reaction. The malic enzyme reaction is a key reaction in the dismutation and is ultimately the sole source of mitochondrial ATP. The mitochondrial membrane is shown in the middle of the figure. The key enzymes involved are underlined. The regulation of the malic enzyme reaction by fumarate is shown with a dashed arrow.

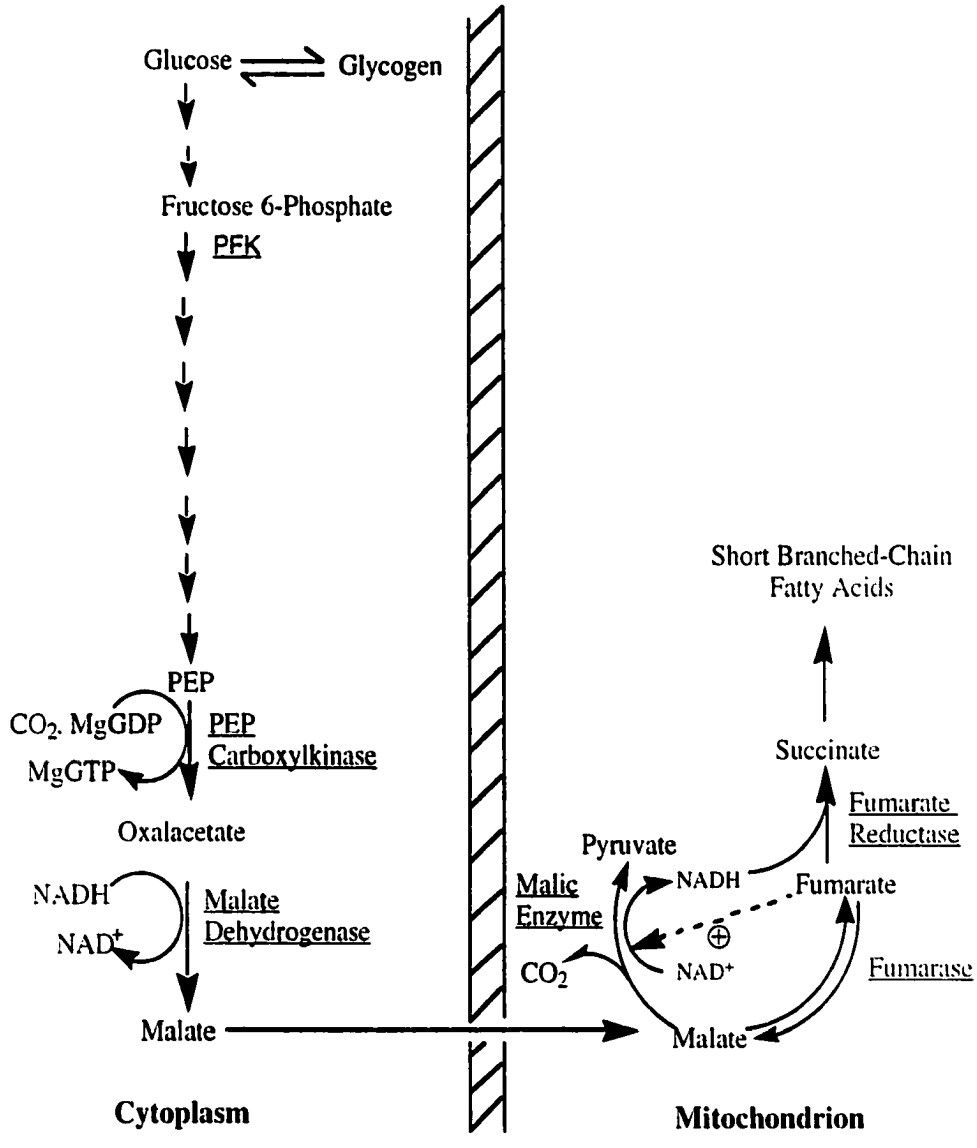
Glucose
Glycogen
Fructose 6-Phosphate
PFK
PEP
CO_2. MgGDP
MgGTP
PEP Carboxylkinase
Oxalacetate
NADH
NAD^+
Malate Dehydrogenase
Malate
Cytoplasm
Short Branched-Chain Fatty Acids
Succinate
Fumarate Reductase
Pyruvate
Malic Enzyme
NADH
Fumarate
CO_2
NAD^+
Fumarase
Malate
Mitochondrion

Fumarate is then reduced to succinate by a membrane-bound flavoprotein-linked succinate dehydrogenase, consuming the NADH produced by the malic enzyme reaction. Fumarate reduction is also coupling to a rotenone-sensitive, electron transport-associated ADP phosphorylation (site I ADP phosphorylation) (Saz, 1970; 1971; Seidman and Entner, 1961). The final electron acceptor is the unsaturated organic acid fumarate, and not oxygen. The branched-chain fatty acids, 2-methylbutyrate and 2-methylvalerate, which are produced from succinate, are major end products of metabolism of the worm. This pathway is confirmed to be the sole source of the mitochondrial ATP for the parasite.

1.2. Pyridine-Nucleotide Dependent Oxidative Decarboxylases

The physiological significance of malic enzyme is not the only thing that makes it worthy of study. The overall reaction catalyzed by malic enzyme places it in the class of pyridine nucleotide-linked β-hydroxyacid oxidative decarboxylases (Fig. 2). Enzymes in this class include isocitrate dehydrogenase (ICDH), isopropylmalate dehydrogenase (IPMDH), tartrate dehydrogenase (TDH), 6-phosphogluconate dehydrogenase (6-PGDH), malic enzyme (ME), and cholestenoate dehydrogenase (CDH) (Karsten and Cook, 2000). However, CDH has only been characterized in crude form. All of the above enzymes catalyze the oxidative decarboxylation of a β–hydroxyacid with $NAD(P)^+$ as the oxidant to generate NAD(P)H, CO_2 and a ketone product (Fig. 2).

Structurally, enzymes in this class are all multimeric proteins, either homotetramers (e.g. malic enzymes) or homodimers (e.g. IPMDH). Allosteric sites have been identified in some enzymes in this class, e.g. ICDH and ME. Based on amino acid sequence homology, enzymes in this class can be divided into three structural classes. IPMDH, ICDH and TDH are homologous of one another at the

Figure 2. The General Reaction Catalyzed by the Pyridine-Nucleotide Dependent Oxidative Decarboxylases. R_1 = H, OH, $CH_2CO_2^-$, $CH(CH_3)_2$. R_2 = CO_2^-, $CH(OH)CH(OH)CH_2OPO_3^{2-}$. M^{2+} stands for the divalent metal ion required by this category of enzymes with the exception of 6PGDH.

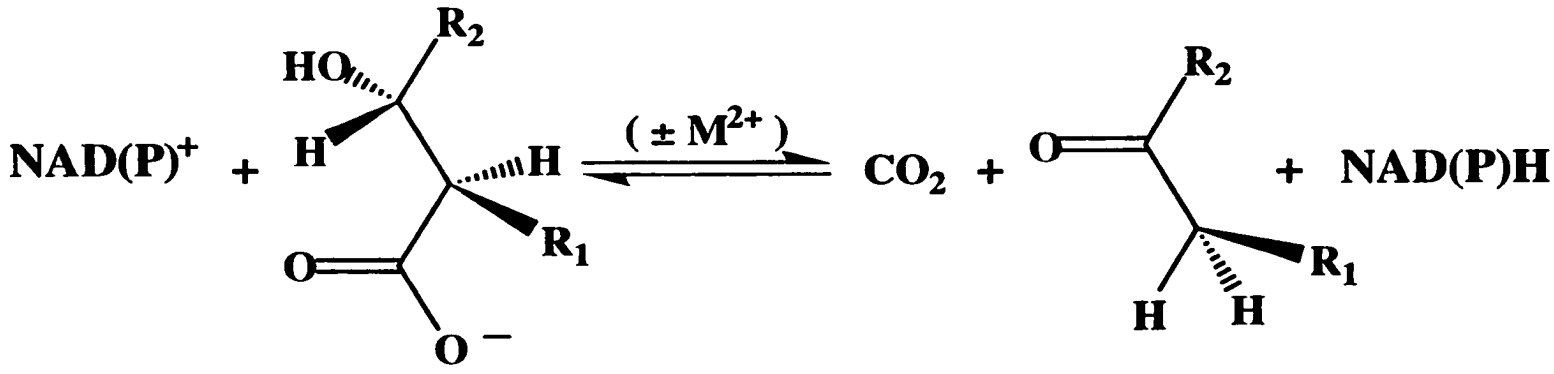

8

amino acid sequence level. However there is only a low degree of homology among the above subclass, 6-PGDH, and ME. Three-dimensional structures are available for IPMDH, ICDH, ME, and 6-PGDH. Among the above enzymes, only IPMDH and ICDH are structurally similar to one another. In this case, three structural classes are confirmed and represented by the three-dimensional structures of IMPDH and ICDH (class A), ME (class B), and 6-PGDH (class C) (Karsten and Cook, 2000).

Because of the existence of electron-withdrawing groups in the vicinity to the β-hydroxyl in the substrates, 6-PGDH is metal ion independent, while all others require a divalent metal ion (usually Mg^{2+} or Mn^{2+}) for catalysis (Zhang and Cook, 2000). Tartrate dehydrogenase requires a divalent and a monovalent metal ion to facilitate catalysis (Tipton, 1993).

All of the enzymes in the class have the same general acid-base mechanism (see 1.3.5. below). First, a general base aids in the oxidation of the β-hydroxyacid to produce the β-ketoacid. The β-ketoacid then undergoes decarboxylation assisted by a metal ion, which acts as a Lewis acid, and the protonated general base, which acts as a general acid in this step, to give an enol (or enediol) intermediate. As mentioned above, 6-PGDH is the only exception that does not require a divalent metal ion for decarboxylation. The general base in the 6-PGDH reaction is a lysine, which will facilitate decarboxylation in its protonated form (Zhang and Cook, 2000). The final step in the overall reaction is the tautomerization of the enol (or enediol) intermediate to give the final ketone product with the assistance of a second enzyme group that acts as a general acid. All enzymes in the class are reported to have a random kinetic mechanism with the exception of TDH, which has an ordered kinetic mechanism (Tipton and Peisach, 1990).

Overall, the enzymes in this class provide a superb example of multistep catalysis and give us the opportunity to carry out research on the coupling of transition

state/intermediates as the reaction pathway is traversed. Hence, the research on malic enzyme will have an impact not only on this class of enzymes, but also on the fundamental principles of enzymatic reactions in general.

1.3. Malic Enzymes and NAD-Malic Enzyme from *Ascaris suum* (AsME)

Since the identification of the first malic enzyme, dozens of malic enzymes have been isolated from different sources. All of the enzymes catalyze the metal-dependent oxidative decarboxylation of L-malate (Fig. 3, I.) with NAD^+ or $NADP^+$ as a cofactor. Some of the malic enzymes additionally catalyze the decarboxylation of oxalacetate (Fig. 3, II.) and the reduction of α-ketoacids such as pyruvate, ketomalonate, and oxalacetate (Fig. 3, III.).

Based on their dinucleotide specificity and oxalacetate decarboxylase activity, malic enzymes are divided into three classes (EC 1.1.1.38-40) (Park et al., 1986). Enzymes in the class EC 1.1.1.40, including malic enzymes from the livers of pigeons and chickens, are NADP-dependent oxidoreductases (oxalacetate-decarboxylating). Enzymes in the class EC.1.1.1.39, including malic enzymes from the group D *streptococcus*, potato tuber, and cauliflower, are NAD-dependent oxidoreductases (decarboxylating). Enzymes in the class EC 1.1.1.38, including malic enzymes from *Ascaris suum*, *Lactobacillus arabinosus*, and the dung beetle *Catharsius*, are NAD-dependent oxidoreductases (oxalacetate-decarboxylating).

Because *Ascaris suum* was an excellent source for the isolation of NAD-malic enzyme, prior to obtaining recombinant proteins, the *Ascaris suum* malic enzyme has been a major research target. Thus far, *Ascaris suum* malic enzyme is one of the best studied malic enzymes, and the best studied member of class EC 1.1.1.38. The work involved in this dissertation is based on the studies of the *Ascaris suum* malic enzyme.

Figure 3. The Three Reactions Catalyzed by Malic enzymes. I. Oxidative Decarboxylation of L-Malate. II. Decarboxylation of Oxalacetate. III. Reduction of α-Ketoacids. R stands for CO_2^-, $CH_2CO_2^-$, or CH_3. M^{2+} stands for the divalent metal ion.

I.

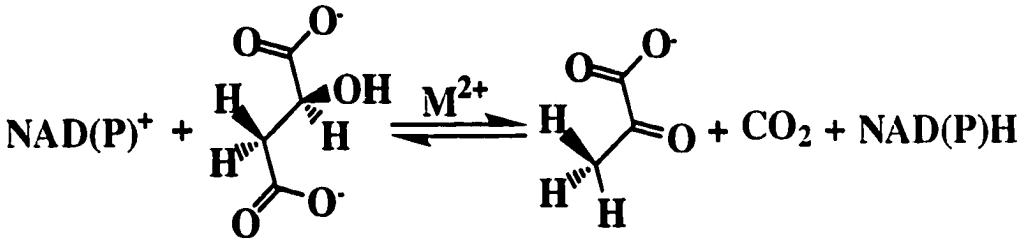

L-Malate Pyruvate

II.

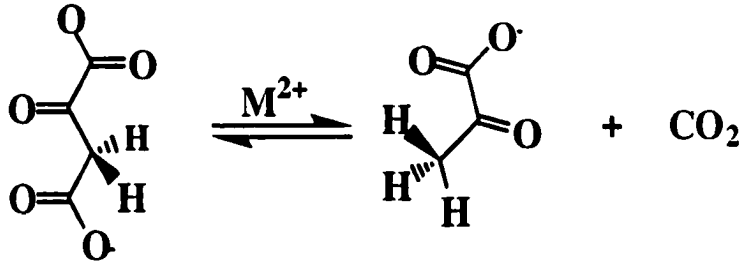

Oxalacetate Pyruvate

III.

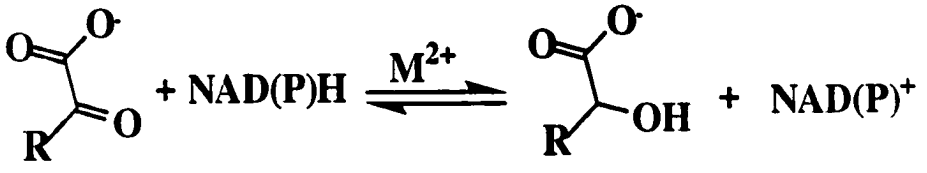

α–Ketoacid α-Hydroxyacid

1.3.1. Purification, Cloning and Expression of AsME.

Ascaris suum malic enzyme was partially purified from *Ascaris suum* (Saz and Hubbard. 1957), and eventually purified to the homogeneity (Fodge et al., 1972; Landsperger and Harris, 1976; Landsperger et al., 1978; Allen and Harris, 1981). The purification generally included an ammonium sulfate fractionation, cellulose phosphate and DEAE-cellulose column chromatographies to purify the ascarid malic enzyme to homogeneity. More recently, Karsten and Cook (1994) developed a procedure that could be carried out in two days using a tandem-column-affinity-chromatography step with Blue-B agarose and Orange-A agarose. The purified enzyme has a specific activity of 35 U/mg with a yield > 50%.

With the dramatic developments in molecular biology, the primary structure of the enzyme was obtained by Kulkarni et al (1993). A cDNA library was developed and screened with anti-malic enzyme antibodies and oligonucleotide probes. A clone encoding the complete sequence of the *Ascaris suum* malic enzyme protein was isolated and the cDNA, with an overall length of 2269 bases and an open reading frame of 1851 nucleotides was sequenced. Analysis gave a final deduced amino acid sequence of 618 amino acid residues. The N-terminal sequence of the purified *Ascaris suum* malic enzyme as well as five typical peptides was determined by solid-phase microsequencing, with a perfect match between those and the deduced sequence. The calculated subunit molecular mass is 68,478 Da. for the mature protein without the first 13 amino acids. The *Ascaris suum* malic enzyme is nuclear encoded and must be transported into the mitochondrion. The first 13 amino acids of the *Ascais suum* malic enzyme sequence represent a leader sequence needed for transport of the enzyme into the mitochondrion.

To take full advantage of the cloned AsME cDNA, Chooback et al. (1997) subcloned the cDNA into expression vector, pKK223-3. The recombinant protein, which has been purified and characterized, behaves kinetically in a manner identical to

the malic enzyme purified directly from *Ascaris suum*. Thus, purification of the enzyme was further simplified, and site-directed mutagenesis made possible.

1.3.2. Regulation of AsME and Other Malic Enzymes.

As stated in 1.1., *Ascaris suum* malic enzyme (AsME) plays a critical role in a rather unique energy metabolism. Therefore, research on AsME becomes more important, since a knowledge of its regulatory properties and control could not only lead to a clearer comprehension of carbohydrate metabolism, but also to a possible approach to eliminating the intestinal parasitic nematode. In the energy metabolism of the parasite, there is a competition between malic enzyme and fumarase for malate as it enters the mitochondrion. Considering that this pathway is the sole source of mitochondrial ATP for the worm, it is reasonable to expect that some type of regulation of malate flux must exist in order to maintain a balance between the production of NADH and fumarate.

Landsperger and Harris (1976) first reported on inhibition and activation of malic enzyme by a number of physiological metabolites. The results showed that effectors, including fumarate, branched-chain fatty acid excretion products, and oxalacetate, were all competitive with malate.

However, inhibitors such as branch-chain fatty acids and oxalacetate, were shown to generate their effect by depleting free Mg^{2+} concentration required for activity (Lai et al., 1992). Among the effectors, oxalacetate was reported as the most potent inhibitor of the ascarid malic enzyme. The end products of the metabolic pathway, including tiglate, 2-methylbutenoate, and 2-methylpentenoate, are all competitive inhibitors against malate. Thus, end product inhibition could also contribute to the overall control of the malic enzyme activity. Surprisingly, ATP and several other nucleotides did not inhibit the ascarid malic enzyme, while most of the other malic

enzymes studied so far are strongly inhibited by ATP. This result suggested that there were some structural difference between ascarid malic enzyme and other malic enzymes.

Fumarate is the only effector tested that activated the ascarid malic enzyme (Fig. 1), and the stimulation occurred at low concentrations of malate and fumarate, within the reasonable physiological range (Lai et al., 1992; Landsperger et al., 1978). Hence, a metabolic control mechanism might exist to regulate, in part, the flux of malate through the two enzymes of the dismutation reaction (Fig. 1). When fumarate production is increased by the fumarase reaction, the fumarate activates the malic enzyme by increasing the affinity of the enzyme for malate. The production of NADH by the malic enzyme reaction then increases to satisfy the need for reducing potential for fumarate reduction and the concomitant production of ATP. Fumarate was confirmed as a positive heterotropic effector of the NAD-malic enzyme at low concentrations (K_{act} = 0.05 mM) and an inhibitor competitive against malate (K_i = 25 mM) (Lai et al., 1992). There is a discrimination between active and activator sites for binding dicarboxylic acids. The active site prefers a configuration in which 4-carboxyl is twisted out of the C1-C3 plane.

Other than the regulation discussed above for AsME, the cytosolic NADP-malic enzyme in mammals plays an important role in fatty acid synthesis, and this NADP-malic enzyme isoform is under dietary control and can be induced by a carbohydrate-rich diet or thyroid hormone (Fraenkel, 1975; Dozin et al., 1985). A thyroid response element is present in the promoter region of the cytosolic NADP-ME gene.

1.3.3. Physical Properties and Crystal Structure of Malic Enzymes

Gel filtration, sedimentation velocity and sedimentation equilibrium ultracentrifugation have been used to determine the size of the protein. The enzyme was proven to be a homotetramer with a monomer molecular mass around 65,000 Da. The

molecular weight was then corrected to 68,478 Da. after sequencing the AsME cDNA. The apparent isoelectric pH is 6.63 (Fodge et al., 1972).

When the pigeon liver malic enzyme was embedded in a reverse micellar system prepared by dissolving the surfactant sodium bis(2-ethylhexxyl)-sulfosuccinate(AOT) in isooctane, the tetrameric enzyme dissociated into monomers (Chang et al. 1994). The dissociated monomers are also enzymatically active, but with diminished specific activity in reverse micelles relative to the activity in aqueous media. The decreased enzyme activity in reverse micelles was due to interactions of the surfactant with the enzyme molecules, suggesting that the cytosolic malic enzyme is located near the plasma membrane. Because a difference exists between the dissociation constants of tetramer to dimer and dimer to monomer, an asymmetric model of the quaternary enzyme was proposed.

The first malic enzyme structure, from human mitochondria, has recently been solved (Xu et al., 1999). The published structure has a 2.1 Å resolution (Fig. 4A). The tetrameric structure appears to be a dimer of dimers, which confirms the so-called asymmetric quaternary model. The structure of the monomer can be divided into four domains (Fig. 5A). Domain A is helical and contributes to the association to give the dimer and tetramer. Domain B consists of two fragments of polypeptite chain with a portion of the primary structure between the two forming domain C. Overall, domain B consists of a five-stranded β-sheet with helices on both sides, and it contributes to binding malate and metal ion. Domain C also has a β-sheet structure surrounded by helices and contributes to binding NAD^+. Domain D contains one helix and a long tail, and contributes to the association of the dimers to give the tetramer. Overall, the structure of malic enzyme has little similarity to ICDH, IPMDH or 6-PGDH. Thus, malic enzyme is in a unique structural class of oxidative decarboxylases.

The active site of the enzyme is located in a deep cleft at the interface among

Figure 4. The Tetrameric Structure of Malic Enzymes. A. NAD-Dependent Malic Enzyme from Human Mitochondrion. B. NAD-Dependent Malic Enzyme from *Ascaris suum.* In each tetramer, a dimer is shown in red, while two monomers are shown in blue and yellow.

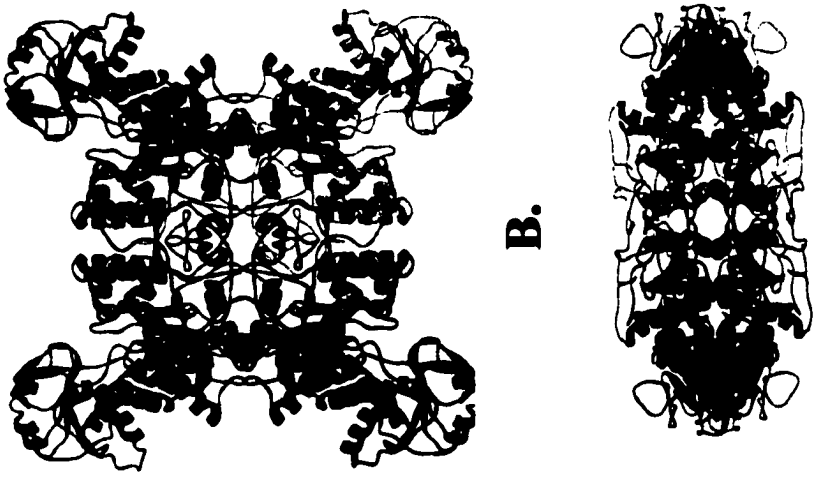
B.


A.

Figure 5. Monomeric Structure of Malic Enzymes. A. NAD-Dependent Malic Enzyme from Human Mitochondrion. B. NAD-Dependent Malic Enzyme from *Ascaris suum*. Domain A is red. Domain B is blue. Domain C is yellow. Domain D is green. The location of the active site in the Human malic enzynme is indicated with a bound NAD^+ in stick form.

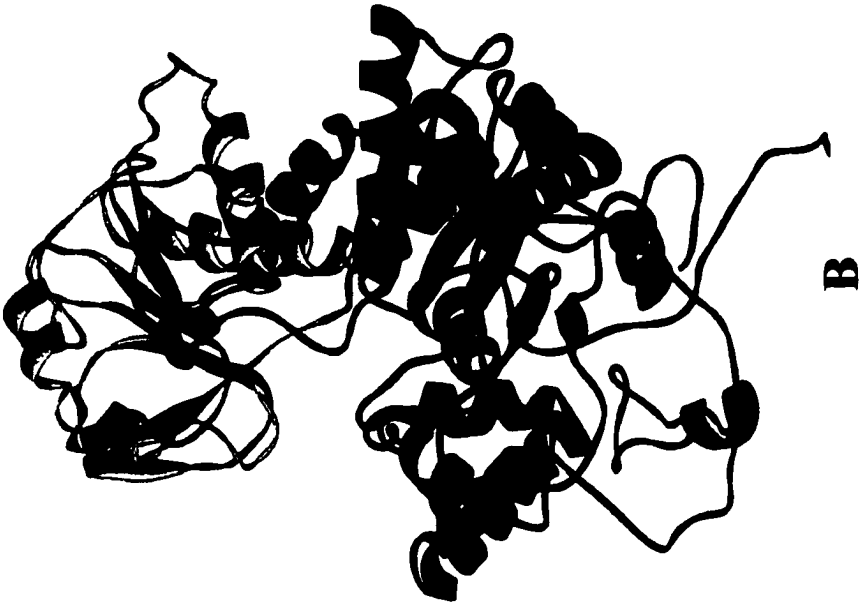
B


A

three domains (domain A, B, and C) and is far from the tetramer interface (Figs. 4, 5). Moreover, a second NAD^+ binding site exists in each monomer of the human enzyme (domain B). The natural ligand for this site may be ATP, an allosteric negative effector of the human NAD-malic enzyme.

Although tartronate had been added to the crystallization solution, this first human NAD-malic enzyme structure had no tartronate bound. A conformational change was expected upon the binding of malate. The crystal structure of the human NAD-dependent malic enzyme in a quaternary complex with NAD^+, Mn^{2+}, and oxalate has been obtained at 2.2 Å resolution (Yang et al., 2000). In the same study the structures of the quaternary complexes with NAD^+, Mg^{2+}, and tartronate (Fig. 6B) or ketomalonate were also determined to 2.6 Å resolution. These structures showed the expected conformational change with domains B and C closer to each other after binding the substrate analogs and cofactor (Fig. 6).

The ascarid malic enzyme was first crystallized by Clancy et al. (1992). Crystals diffracted to 3.0 Å, but heavy atom derivatives were not obtained. Results did indicate that the malic enzyme tetramer has 222 symmetry. Soon after solving the human malic enzyme structure, a breakthrough was made on the AsME structural studies. The structure of AsME was recently solved to a resolution of 2.3 (Coleman et al., 2001), indicating that the AsME structure is very similar to the human NAD-malic enzyme (Figs. 4, 5). This is not a surprise, since the human NAD-malic enzyme amino acid sequence has a very high identity, 51%, to the ascarid malic enzyme sequence. One difference is that the ATP inhibitory binding-site of the human enzyme is not present.

1.3.4. Kinetic Mechanism of the Malic Enzyme Reaction.

Despite differences in cofactor specificity and oxalacetate decarboxylating

Figure 6. Open Form vs. Closed Form Monomeric Structure of Human NAD-Dependent Malic Enzyme. Open form structure is in gray. Closed form structure is shown in colours. Domain A is red. Domain B is blue. Domain C is yellow. Domain D is green. Bound NAD^+ and tartronate in the closed form enzyme are shown in stick form in colours. Bound Mg^{++} is also shown in space-filled form in colour.

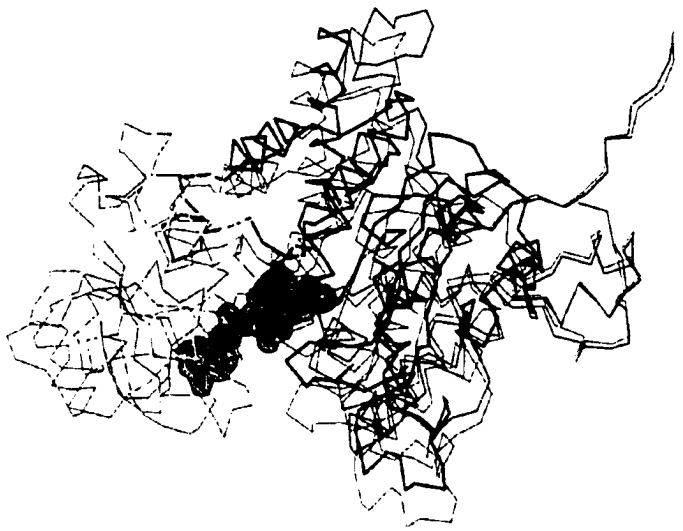

activity, all malic enzymes catalyze the metal-dependent oxidative decarboxylation of L-malate with a similar kinetic mechanism (Fig. 7 , Table 1.).

Initial velocity studies in both forward and reverse directions were first carried out by Landsperger et al. (1978) and results showed a sequential kinetic mechanism. Product and dead-end inhibition patterns by several substrate analogs showed randomness in binding of malate and NAD^+. However, correction for chelation between metal ion and substrates was not considered, and the qualitative and quantitative data had to be repeated.

Comprehensive initial velocity studies showed the free metal and uncomplexed reactants were substrates (Park et al., 1984). Utilizing chelate correction, kinetic parameters were established by fitting initial velocity data using a random terreactant reaction equation. Kinetic parameters were estimated as follows: V_{max} = 32 s^{-1}, K_{malate} = 1.18 mM, K_{NAD} = 0.011 mM. The kinetic mechanism changes with different metal and malate concentrations. When metal concentrations are low, the mechanism is ordered with NAD^+ adding prior to Mg^{2+} and then malate. But when a boarder range of metal and malate concentrations are used, the steady state random kinetic mechanism is observed with the requirement that Mg^{2+} must add in rapid equilibrium prior to malate. The low concentration range used is likely in the physiological concentration range, so the mechanism of this enzyme is considered ordered *in vivo*. Isotope partitioning studies confirmed the steady state random mechanism in the oxidative decarboxylation direction (Chen et al., 1987).

The reverse reaction was first thought to be a rapid equilibrium random mechanism, but later research proved that the reductive carboxylation has a steady state random mechanism with the requirement of metal ion binding prior to pyruvate (Park et al., 1986; Mallick et al., 1991). No binding site was found for CO_2. Extensive kinetic studies on other malic enzymes showed that all are likely steady state random.

Figure 7. Kinetic Mechanism and Kinetic Constants in the *Ascaris suum* Malic Enzyme Reaction. a. Random Kinetic Mechanism of *Ascaris suum* Malic Enzyme Reaction. b. Known Rate Constants. A, B, C, X, R, P and Q represent NAD^+, divalent metal ion, L-malate, oxalacetate, NADH, CO_2 and pyruvate respectively. Known dissociation constants are indicated according to steps, and the values are shown in Table I.

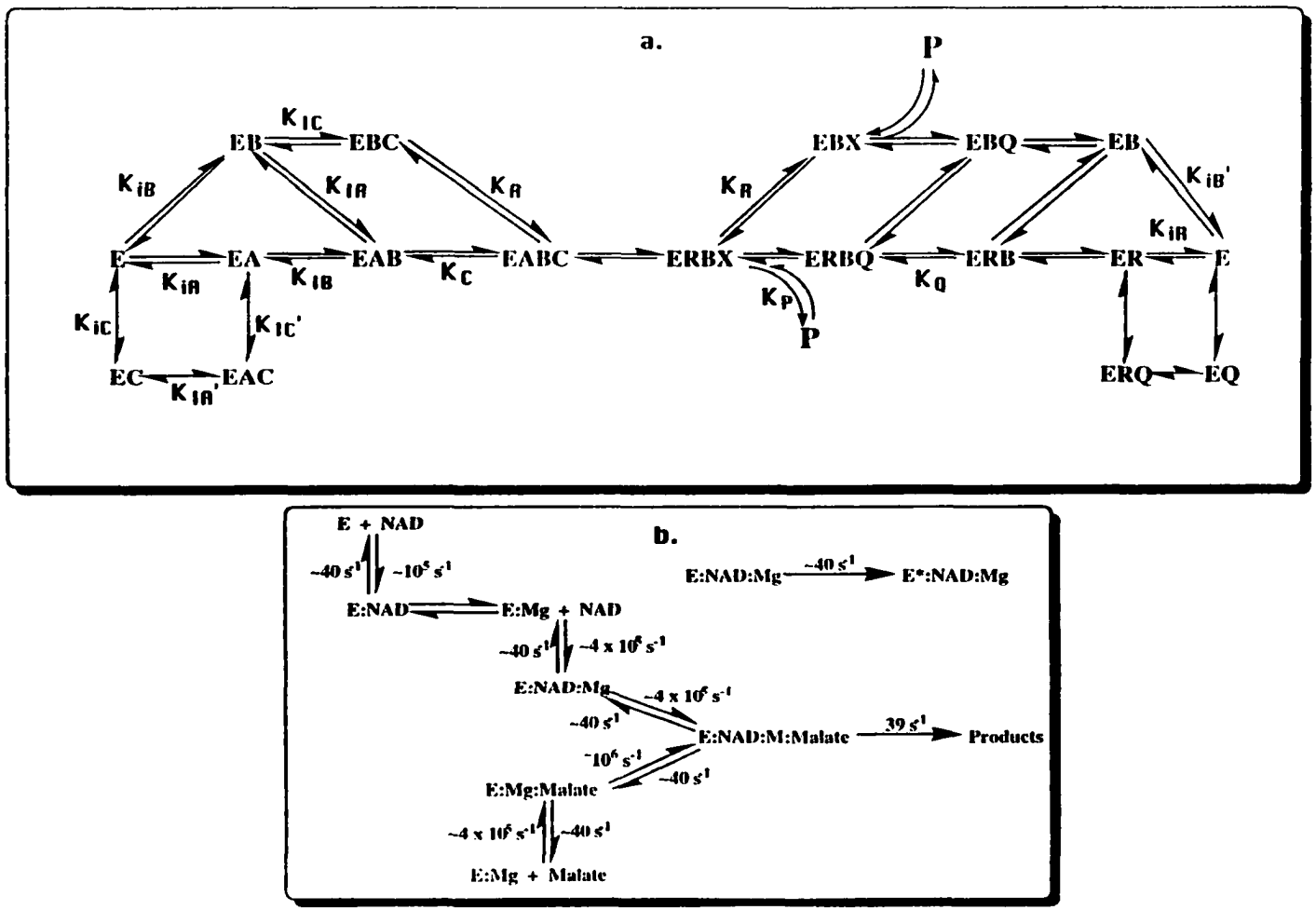
a.
P
EB
EBC
EBX
EBQ
EB
E
EA
EAB
EABC
ERBX
ERBQ
ERB
ER
E
EC
EAC
ERQ
EQ
b.
E + NAD
E:NAD
E:Mg + NAD
E:NAD:Mg
E:NAD:Mg
E*:NAD:Mg
E:NAD:M:Malate
Products
E:Mg:Malate
E:Mg + Malate

Table 1. Known Dissociation Constants in the AsME Malic Enzyme Reaction

Dissociation Constants (mM)	Mg^{2+} as Cofactor	Mn^{2+} as Cofactor
K_A	0.005 ± 0.001	0.042 ± 0.016
K_{iA}	0.080 ± 0.001	
K_{IA}	0.078 ± 0.004	
K_{IA}'	0.14 ± 0.03	
K_B		-1.1 ± 0.7
K_B'		4.3 ± 0.2
K_{iB}	14.0 ±1.0	9 ± 7
K_{IB}	29.3 ± 1.3	
K_{iB}'		0.7 ± 0.4
K_C	1.2 ± 0.1	0.4 ± 0.2
K_{iC}	20.0 ± 2.0	
K_{IC}	1.6 ± 0.3	
K_{IC}'	35.0 ± 0.8	
K_Q		45 ± 9
K_R		0.05 ± 0.02
K_{iR}		0.003 ± 0.002
K_P		4 ± 1

Location of the rate determining steps for *Ascaris suum* malic enzyme reaction was carried out using a number of approaches (Park et al., 1984; Kiick et al., 1986; Chen et al., 1987; Rajapaksa et al., 1993; Weiss et al., 1993). Deuterium isotope effects were measured with L-malate-2-H, D giving approximately equal isotope effects on V_{max} and V_{max}/K_m for both malate and NAD^+. Data indicated that hydride transfer is a rate-determining step and that both NAD^+ and malate are released from the Michaelis complex at about the same rate. Furthermore, the hydride transfer step cannot be the only rate-determining step because the observed isotope effect of 1.45 is small compared to the expected maximum of 6-8 (Cook, 1991).

Since the ascarid malic enzyme can also catalyzes the decarboxylation of oxalacetate, which is considered an intermediate in the oxidative decarboxylation of malate, the kinetic parameters of decarboxylation of oxalacetate were determined and compared to the ones in the direction of oxidative decarboxylation of malate (Park et al., 1986). The turnover numbers in those two reactions are very similar with a slightly larger value for the decarboxylation of oxalacetate. The comparison indicated that the decarboxylation step might be the major rate-determining step in the overall reaction. Primary ^{13}C isotope effects then provided evidence that decarboxylation is the major rate-determining step (Weiss et al., 1991).

The pH dependence of kinetic parameters of the ascarid malic enzyme gave a decrease in logV at low pH with a pK of 4.9 (Kiick et al., 1986). The isotope effects on V_{max} went to a value of 1 as the pH decreased to 4. Two possibilities could account for these data. Either NADH release is slow at low pH or there is a slow isomeriztion step, which is pH dependent as indicated in the pH profile. Presteady state kinetic studies (Rajapaksa et al., 1993) confirmed the latter possibility as evidenced by a lag in the time course reacting either E:Mg or $E:NAD^+:Mg$ with malate. Preincubation with Mg^{2+} and malate eliminates the lag. These data also confirm the random mechanism.

Chemical modification with bulky reagents of a nonessential thiol group near the active site can inactivate the malic enzyme activity. Binding of the different substrates protects the activity of the enzyme to different extents. In this case, the dissociation constants of all substrates in both reaction directions were measured by modulation the thiol inactivation rate (Kiick et al, 1984). Other rate constants were also found via isotope partitioning studies (Chen et al., 1987) and isotope effect studies (Kiick et al., 1986; Karsten and Cook, 1994). Results confirm the steady state random mechanism with the requirement that metal ion binds prior to malate or pyruvate.

1.3.5. Chemical Mechanism of the Malic Enzyme Reaction

How exactly the enzyme converts substrates to products is always of great interest to enzymologists. The pH dependence of the kinetic parameters in the direction of oxidative decarboxylation of malate showed that two enzyme groups are necessary for binding the substrates and catalysis (Schimerlik and Cleland, 1977; Kiick et al., 1986). In the case of AsME, a group with pK of 4.9 must be unprotonated while the other with a pK of 8.9 must be protonated for optimum binding and activity. The pH dependence of dissociation constants for competitive inhibitors against malate (such as tartronate) was consistent with the result obtained from V/K pH profiles. A general acid/general base mechanism was proposed, Fig. 8.

In addition to contributing to binding the substrate, the unprotonated group with pK of 4.9 serves as a general base required to deprotonate the β-hydroxyl group of malate in the hydride transfer step. Hydride transfer produces NADH and oxalacetate as an intermediate. The oxalacetate binds to the enzyme tightly and is not released during the reaction. In the following steps, decarboxylation and tautomerization, the same general base group shuttles the proton back and forth between the oxygen of the β-carbonyl group and itself to assist in the conversion of oxalacetate to enol-pyruvate

Figure 8. Chemical Mechanism for The *Ascaris suum* Malic Enzyme Rreaction. –B:(H) represents deprotonated (protonated), catalytic enzyme group. M^{2+} represents divalent metal ion. The catalytic process consists of three steps, the hydride transfer step assisted by metal ion and the deprotonated general base group, the decarboxylation step assisted by metal ion and the protonated general base group, and the tautomerization step assisted by the depronated general base group and the protonated general acid group.

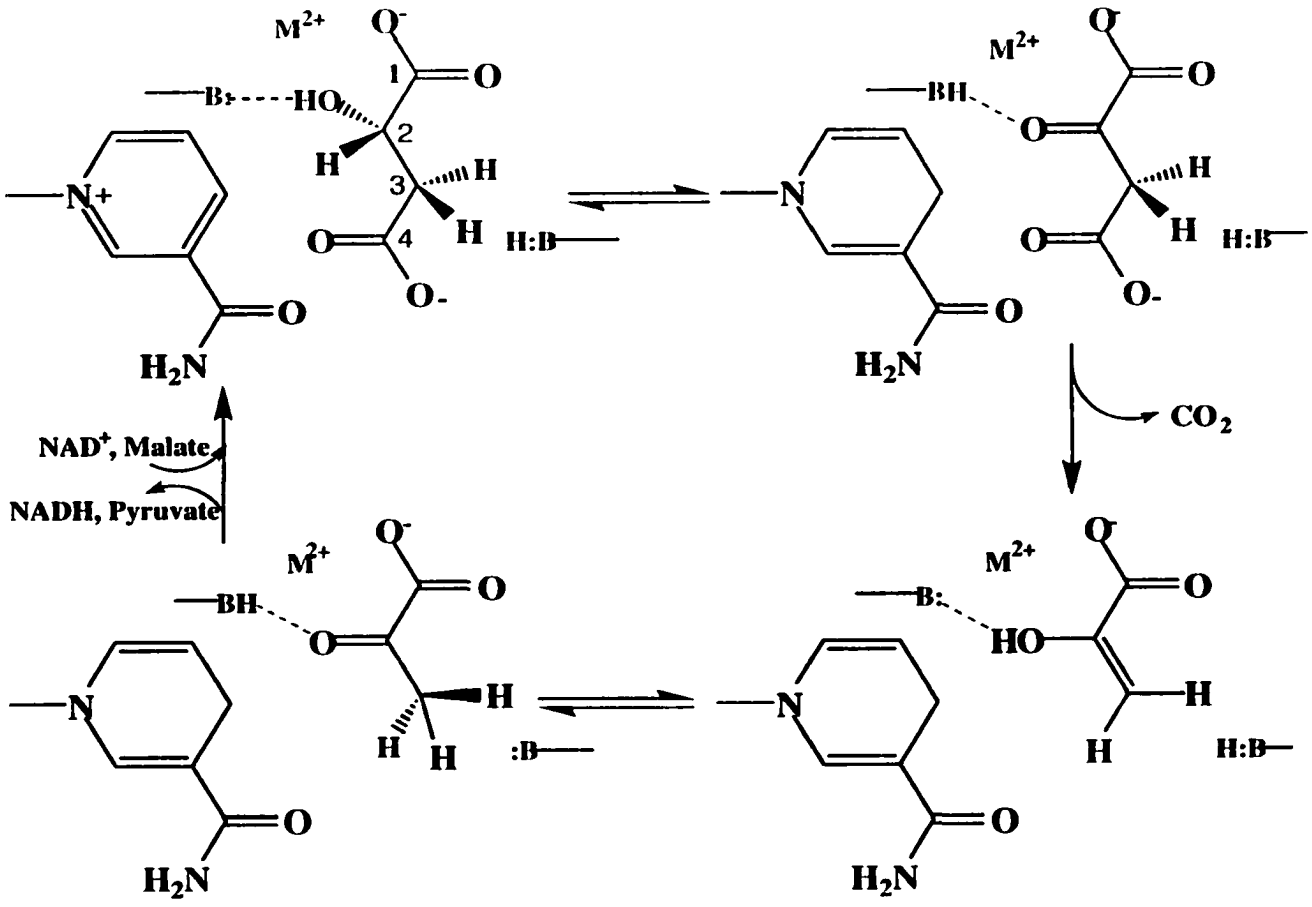
M2+
O-
1
O
B:----HO
2
H
3
H
N+
O
4
H
H:B
O-
O
H2N
NAD+, Malate
NADH, Pyruvate
BH
:B
CO2
B:
HO
N

and then the final product, pyruvate. The protonated group with a pK of 8.9 contributes to binding substrate correctly and acts as a general acid to protonate C3 of malate during the tautomerization step, in which enolpyruvate is converted to pyruvate.

As we know, the above enzyme-catalyzed reaction is metal ion dependent. Although a number of divalent metal ions can be used as activators in malic enzyme reaction, Mg^{2+} has been tagged as the physiological activator *in vivo* (Park et al., 1984; Karsten et al., 1995). Bound malate was shown by ESEEM studies (Tipton et al., 1996) to be positioned with its β-hydroxyl group in the vicinity of the divalent metal ion. Based on this and the mechanism of the nonenzymatic metal-ion catalyzed decarboxylation of oxalacetate, the role of Mn^{2+}, used as a divalent metal ion is proposed as a Lewis acid that assists in the decarboxylation of the oxalacetate intermediate to give enolpyruvate. A study of malate inhibitory analogs indicates that the metal ion provides a major determinant for substrate binding. The fact that Mg^{2+} must bind to the enzyme prior to malate or pyruvate also supports this conclusion. The identity of the metal ion used can affect the transition state of the reaction. The position of malate relative to NAD^+ could be expected to be a function of the size of the metal. A bigger metal ion would lead to a smaller distance between the malate and the pyridinium ring of NAD^+. The smaller distance leads to a compressed reaction coordinate that would favor a tendency for quantum mechanical tunneling. Isotope effect results using divalent metal ions of different ionic radius corroborated the hypothesis (Karsten et al., 1995).

A number of isotope effect studies have been carried out to clarify the sequence of the multiple step reaction (Schmerlik et al., 1977; Hermes et al., 1982; Weiss et al, 1991; Karsten and Cook, 1994). When NAD^+ is used as dinucleotide substrate, multiple primary deuterium/primary ^{13}C isotope effects suggest that the reaction has a stepwise mechanism with hydride transfer preceding decarboxylation. However, the mechanism changes to an asynchronous concerted mechanism when other dinucleotide

substrates like 3-APAD or PAAD, which have more positive redox potential, are used. The most likely explanation for this change is either a difference in the configuration of bound malate when alternative dinucleotide substrates are used (Karsten and Cook, 1994), or a shallow potential energy well for the oxalacetate intermediate that is eliminated as the dinucleotide substrate changes and hydride transfer becomes more rate limiting compared to decarboxylation. The concerted mechanism was confirmed by the work of Edens et al. (1997) who measured primary ^{13}C/primary D multiple isotope effects at C2 and C3 of L-malate.

1.3.6. Identification of Functional Groups in the Malic Enzyme Reaction.

While research on the chemical mechanism was being carried out, the identity of functional groups in the active site remained unknown. It is important to identify the functional groups to disclose the details of catalysis and the catalytic advantage of each of the residues.

Initial efforts in identifying the important functional groups in the malic enzyme reaction were by chemical modification of the pigeon liver malic enzyme. Histidine and lysine residues were proposed to be involved in dinucleotide binding upon treatment with ethoxyformic anhydride (Chang and Hsu, 1977) and 3-aminopyridine adenine dinucleotide phosphate with sodium periodate (Chang et al., 1989). The chemical modification of the sulfhydryl-masked pigeon liver malic enzyme with tetranitromethane or N-acetylimidazole suggested that a tyrosine residue may be hydrogen bonded to C-4 of L-malate (Chang and Huang, 1980). Based on the results of treatment with dicarbonyl compounds (2,3-butanedione, methylglyoxal, 2,4-phenylglyoxal), an arginine residue was also proposed to be ion-paired to C-1 of L-malate (Chang and Huang, 1981). The pigeon liver malic enzyme can be inactivated by N-ethyl-5-phenylisoxazolium-3'-sulfonate (Woodward reagent K) and then be regenerated by N-

methylhydroxyamine, but not by glycine ethyl ester (Chang et al., 1985). The kinetic and chemical evidence indicated that a carboxylate of either glutamate or aspartate serves as a general acid-base catalyst in the enzymatic reaction. A nonessential residue, Cys99, was identified to be near the L-malate binding site by using affinity labeling with bromopyruvate and DTNB, and site-directed mutagenesis techniques (Satterlee and Hsu, 1991; Hsu et al., 1992). Selective oxidative modification using Fenton chemistry and affinity cleavage by the Fe^{2+}-Ascorbate or Cu^{2+}-ascorbate system has been carried out on the pigeon liver malic enzyme, and four aspartate residues were identified as Mn^{2+} binding ligands (Wei et al., 1994; Chou et al., 1995). Among the four, Asp258 was confirmed as a metal coordinate by site-specific mutagenesis studies (Wei, et al., 1995).

Chemical modification of the NAD-malic enzyme from *Ascaris suum* had also been conducted. The diethylpyrocarbonate inactivation of ascarid malic enzyme suggested that there are 1-2 histidines at or near the malate binding site (Rao et al. 1985). A nonessential thiol group was also suggested to be close to the malate binding site because only the modification by bulky thiol reagents, such as DTNB, inactivated the enzyme, but not small ones like cyanide (Kiick et al., 1984). An arginine residue is proposed to be essential for binding malate based on the modification of AsME with 2,3-butanedione (Rao et al, 1987).

In the human malic enzyme structure, which was recently solved, three acidic residues (E255, D256, and Asp279) and one water molecule were identified as ligands for the divalent cation that is required for catalysis (Yang et al., 2000). A tyrosine and a lysine were also identified as possible catalytic groups. Because of the high conservation of catalytic reaction mechanism, and homology among the amino acid sequences of all malic enzymes, the above information is valuable for identification of functional groups in the malic enzyme reaction. The amino acid sequence alignment of

malic enzymes showed that most of the residues mentioned above are highly conserved. Results suggest the residues may indeed play an important role in catalysis and/or binding. However, the identities of the general acid catalyst and general base catalyst, which are extremely important to an understanding of the mechanism, remained unknown. It is toward this end that the research in this dissertation was carried out.

1.4. Research Carried Out in This Dissertation and Publications.

As stated above, the identification of the general acid/base catalysts will significantly contribute to an understanding of the catalytic mechanism elucidated for the malic enzyme reaction as well as give us an opportunity to study fundamental principles of enzymatic catalysis in general. Site-directed mutagenesis studies were carried out to identify the catalytic groups in the NAD-malic enzyme from *Ascaris suum*.

1.4.1. Specific Aims.

a). When the project began four years ago, there was no crystal structure available for any malic enzyme. As a result, the first specific aim of my research was to identify potential catalytic groups based on the homology of amino acid sequences (Appendix I; Fig. 9) and information obtained from previous kinetic studies. Those ionizable residues that were highly conserved among all malic enzymes were identified from sequence alignment (Appendix I) and selected as the main targets for mutagenic studies. After the human malic enzyme structure was published in 1999, the structural information was used to aid in locating additional targets (Fig. 10).

b). Alanine-scanning mutagenesis studies were then conducted on those potential catalytic groups obtained from the above alignments. We

Figure 9. Examples of Highly Conserved Ionizable Residues. The multiple sequence alignment was done using the Clustal W program. Two major targets in the research of this dissertation, Y126 and K199 in AsME, are highlighted in yellow. Totally conserved residues are in red. Residues with strong similarity are in green. Residues with weak similarity are in blue.

Highly Conserved Y126 and K199

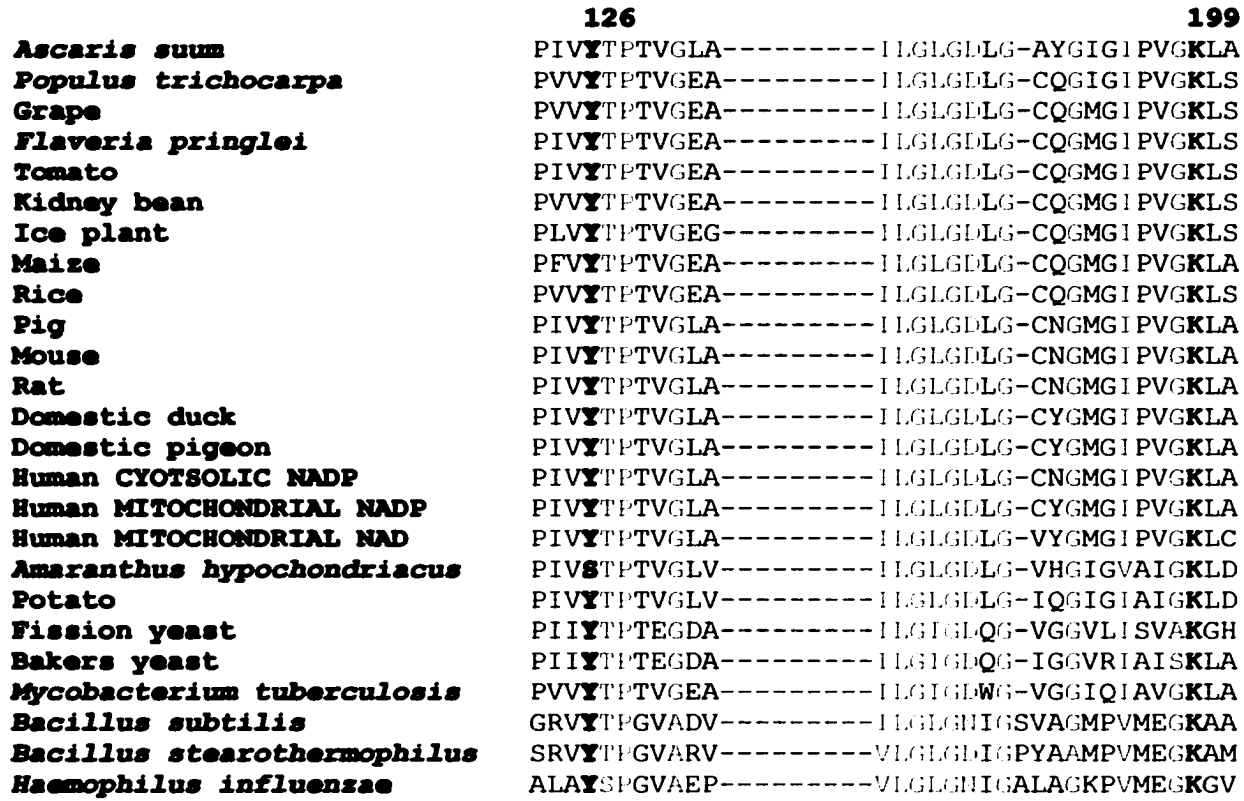

Figure 10. Key Residues in The Active Site of Malic Enzyme. A. Open Form Active Site for AsME. B. Open Form Active Site for NAD-Dependent Human Malic Enzyme. C. Closed Form Active Site for NAD-Dependent Human Malic Enzyme. The residues in both enzymes are all equivalent to each other in the sequence alignment (also see Appendix I). Bound NAD^+ is yellow. Bound tartronate is orange. Oxygen atoms are red. Nitrogen atoms are blue. Mg^{2+} is green.

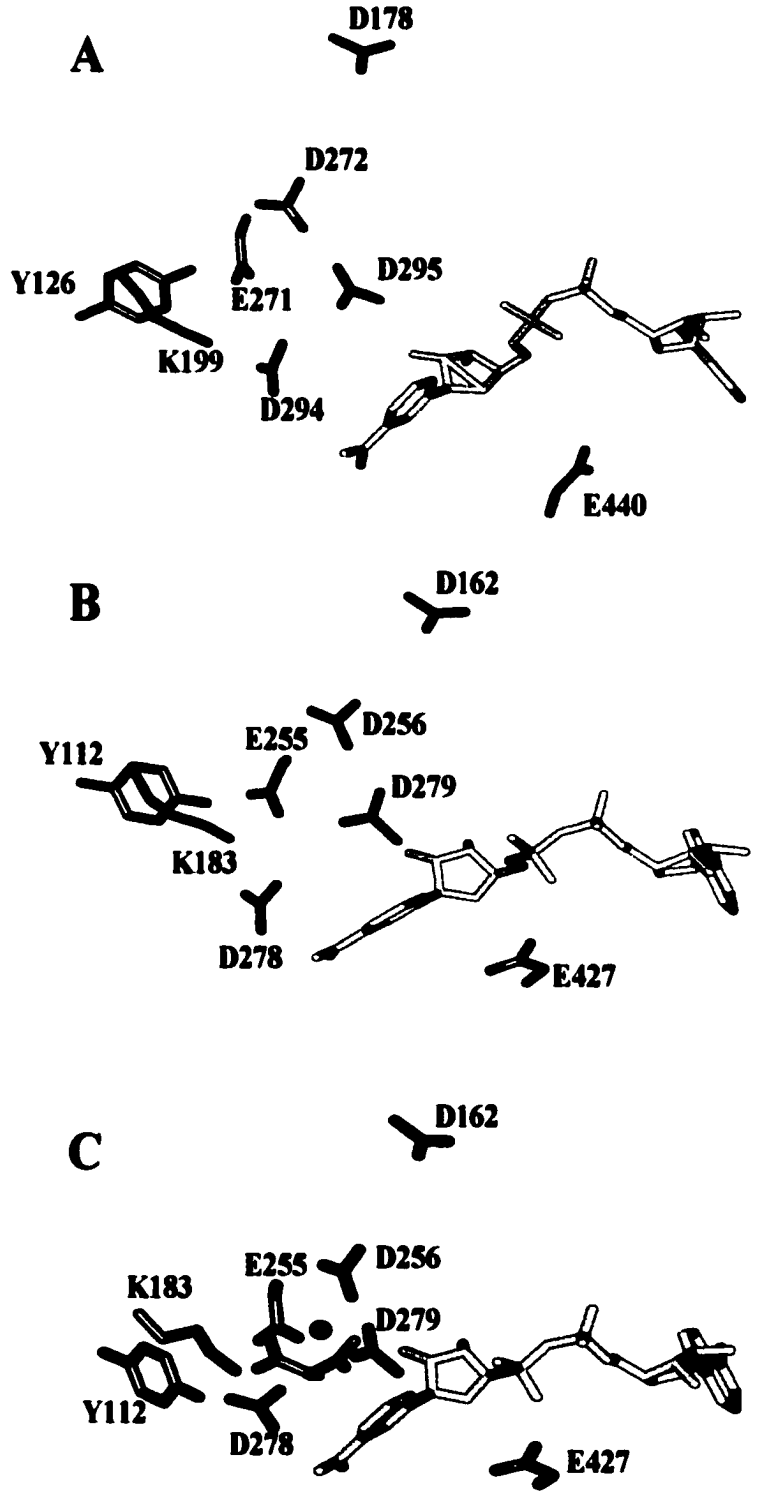
A
D178
D272
Y126
E271
D295
K199
D294
E440
B
D162
E255
D256
Y112
D279
K183
D278
E427
C
D162
E255
D256
K183
D279
Y112
D278
E427

converted the original residues to alanine residues that can eliminate the potential catalytic groups; thus severely affecting the activity of the enzyme. After purifying the mutated enzymes, initial velocity studies were carried out on the mutants. The results roughly indicated the possible roles the residues might play in the catalysis and binding.

c). Residues with a severe effect on overall activity caused by the alanine replacements were then used in further, variable mutagenesis studies to introduce other ionizable groups at those positions. Activity recovery, or elimination, due to the fact that other ionizable residues can or cannot carry out the catalytic role played by the original catalytic groups was probed.

d). Additional results on the mutants were then obtained, including those from the pH dependence of kinetic parameters, oxalacetate partitioning, tritium exchange, and isotope effects. Data provided evidence on the catalytic and/or binding role of each residue.

1.4.2. Tritium Exchange and Intermediate Partitioning

In addition to common experiments, such as circular dichroism spectroscopy, initial velocity studies and pH studies, some specialized experiments and techniques have also been used to characterize the mutant proteins, dependent on their predicted location.

The general acid catalyst assists in the tautomerization of pyruvate to enolpyruvate. It either protonates the C3 position of enolpyruvate in the forward reaction or deprotonates the C3 position of pyruvate in the reverse reaction. The tautomerization step is not a rate-determining step in either reaction direction of the malic enzyme reaction. Protonation/deprotonation at the C3 position of enolpyruvate/pyruvate is relatively fast so that equilibrium is reached rapidly in the direction of formation of enolpyruvate from pyruvate. In the reaction in which pyruvate

is reductively carboxylated in the presence of tritiated water, some of the tritium in water will be incorporated into C3 of pyruvate. The process is called tritium exchange (Fig. 11), which is exclusively assisted by the general acid catalyst of malic enzyme. The rate of the tritium exchange can be measured by monitoring the radioactivity incorporated into pyruvate and malate with time. If the general acid catalyst has been changed or eliminated, the efficiency of the tritium exchange will be severely affected. In this case, the tritium exchange experiment can effectively detect changes in general acid catalysis, thus providing exclusive evidence to identify the general acid catalyst in the malic enzyme reaction.

The malic enzyme reaction spans three catalytic steps, hydride transfer, decarboxylation and tautomerization. The general acid apparently contributes to substrate binding and the tautomerization steps. However, the question remains whether these are the only roles of the catalytic residue. The oxalacetate partitioning experiment is designed to explore this fact (Fig. 12). Oxalacetate is the intermediate formed upon hydride transfer. If the malic enzyme reaction is initiated with oxalacetate and NADH as substrates instead of malate and NAD^+, the enzyme will catalyze the reaction in both directions to give malate and NAD^+, or pyruvate and CO_2. The reaction rates in the two directions can be measured at the same time using a diode array spectrophotometer. Thus, we can probe the effect of mutation on the hydride transfer and decarboxylation steps separately, and the overall importance of the general acid catalyst in malic enzyme reaction can be disclosed.

An isotope effect is a change in the equilibrium or rate constant of a reaction consequent to the substitution of a heavy atom for a light one at (primary isotope effect) or adjacent (secondary isotope effect) to the bond that breaks in the reaction.

Figure 11. The Tritium Exchange Experiment. –B: stands for deprotonated enzyme catalytic group. Tritium is represented with "T". Rapid equilibrium steps are shown with double arrows, and slow reductive carboxylation is shown with a dashed arrow.

Pyruvate
Pyruvate-3-T
Reductive
Carboxylation
SLOW
L-Malate-3T/H

Figure 12. Oxalacetate Partitioning Experiment. The reductive hydride transfer step is shown in red. The decarboxylation of oxalacetate is shown in blue. Oxalacetate is monitored at 282 nm, and NADH is monitored at 340 nm.

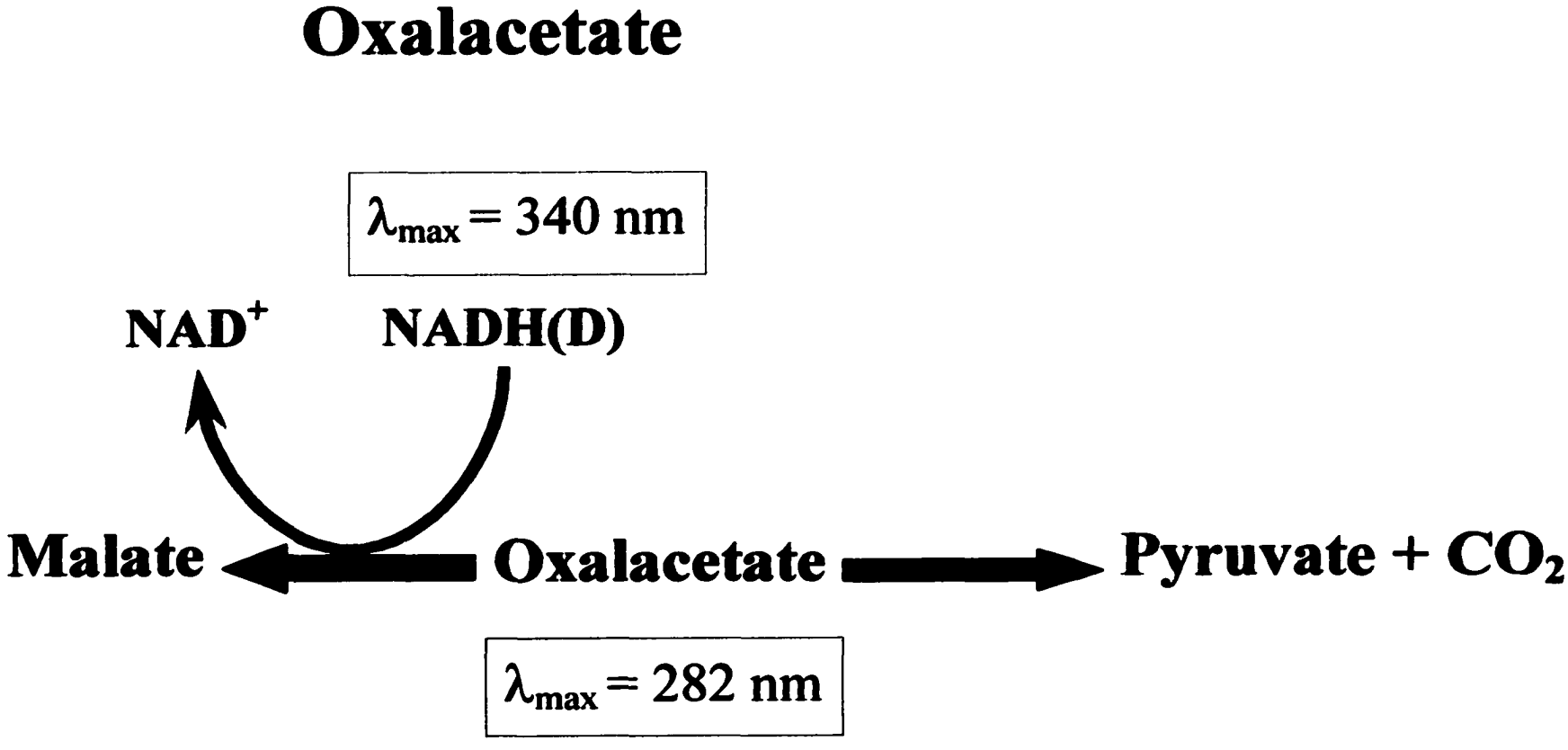
Oxalacetate
λ_{max} = 340 nm
NAD+
NADH(D)
Malate
Oxalacetate
Pyruvate + CO_2
λ_{max} = 282 nm

Isotope effects result from changes in vibrational frequencies of reactants when they are converted to products in the rate limiting steps (Cook, 1991). Isotopes are nonperturbing to the reaction because they are isoeletronic and isosteric, and this makes them a valuable tool to probe the transition state of enzymatic reactions. In this research, isotope effects of the mutant proteins are measured and compared to the same isotope effects of wild type ascarid malic enzyme. The interpretation of the results revealed mechanistic changes caused by the mutation and the catalytic roles played by the wild type residues.

1.4.3. Conclusions and Publications

In the last several years, site-directed mutagenesis studies have been carried out on the target residues chosen based on homology comparison and crystal structural information; the mutated proteins were expressed, purified and characterized. Two papers have been published based on the results.

First, in cooperation with other personnel in Dr. Cook's lab, progress in mapping the active site topography of the NAD-malic enzyme from *Ascaris suum* has been made by using alanine-scanning site-directed mutagenesis of ionizable neutral acids that are totally conserved among all malic enzymes (Karsten et al., 1999). The results suggested the following: 1). D295 and D178 are likely involved in metal ion binding; 2). D294, D361, and E440 probably play an important role in NAD binding; 3). E58 and D272 might contribute to malate binding. Moreover, the dramatic decrease in activity of D295A mutant made D295 a top candidate for the general base catalyst. My contributions to this paper were making, purifying and characterizing the glutamate mutants.

Further mutagensis studies were then carried out on K199 and Y126, which are two candidates for the general acid catalyst determined both by homology comparison

and crystal structure information (Liu et al., 2000). Data indicated that K199 is the general acid catalyst in the malic enzyme reaction, and it is in the hinge area of the structure, and thus may be intimately involved in the isomerization of the E:NADH:Mg:malate complex. On the other hand, Y126 is important to the overall reaction. It is a part of the hydrogen-bonding network and provides hydrophobic interactions in the active site. Thus Y126 might play a multiple role in maintaining the competent conformation in the active site and it may also participate in substrate binding.

CHAPTER 2

MATERIALS & METHODS

2.1. Materials

2.1.1. Chemicals and Enzymes

The ampicillin, kanamycin, tetracycline, and NADH were from Sigma, while the PERFECTprep™ Plasmid DNA Kit was from 5 prime to 3 prime, Inc. The GenecleanR II Kit was from Bio 101, Inc. The DNA molecular weight ladder was purchased from New England Biolabs. Deoxynucleotide triphosphates were from Perkin Elmer. The fmolR DNA cycle sequencing kit, T_4 DNA ligase, T_4 kinase, Taq Plus DNA polymerase, and protein molecular mass markers were from Promega. Mutagenesis and sequencing primers were purchased either from GIBCO BRL or Biosynthesis. Site-directed mutagenesis was performed using the Altered sites mutagenesis kit from Promega. Restriction endonucleases and IPTG were from GIBCO BRL. Pfu polymerase was from Stratagene. The QIAexpress System, which contained the Ni-NTA matrix was from QIAGEN. Protein concentrations were

determined according to Bradford using the Bio-Rad protein assay kit with bovine serum albumin as a standard (Bradford, 1976). Buffers, including N,N'-bis piperazine, Mes, Pipes, Hepes, Taps, Ches, and Caps, were from Research Organics. The Orange-A agarose was from Amicon, while the TAK-GEL DEAE-5W column was from TosoHaas. All other chemicals used were obtained from commercial sources, the highest quality available, and were used without further purification, unless specified.

2.1.2. Bacteria and Plasmids

The *E. coli* strain JM109 was used as a host for either pALTER-1 or pQE30 plasmids, and was purchased from Promega. The *E. coli* strain ES1301 *mut*S is a mismatch repair minus strain, which was used to host the newly mutated pATLER-1 plasmid. This strain was included in the mutagenesis kit mentioned in 2.1.1. from Promega. The M15 strain of *E. coli* is the host for both pREP4 and pQE30 plasmids, allows high level expression, and is easy to handle; it is included in the previously mentioned QIAexpress System from QIAGEN.

Phagemid pALTER-1 is included in the Altered sites mutagenesis kit from Promega. With the AsME cDNA insert, this palsmid was used to prepare a single-

stranded DNA template for the *in vivo* mutagenesis reaction. The pQE30 plasmid is a highly efficient fusion protein expression vector used to overexpress AsME mutant proteins, while pREP4 was used to control the expression of mutant proteins in strain M15 by producing the lac repressor. Both pQE30 and pREP4 are included in the QIAexpress System from QIAGEN.

2.2 Site-directed Mutagenesis

The AsME cDNA has been subcloned into the pALTER-1 vector by Karsten et al. (1999). The recombinant pALTER-1 was isolated from the JM109 host strain (Fig. 13) and used as the template in the mutagenesis reaction.

2.2.1 Preparation of the Single-stranded DNA Template, Mutagenic Oligonucleotides, and Competent Cells

Because the pALTER-1 (phagemid) has a f1 origin of replication, a very efficient production of single-stranded DNA (ssDNA) is allowed upon infection of the host cell with the proper helper phage. The preparation of the ssDNA template begins with growing 1-2 ml of overnight bacterial culture in the presence of 10 μg/ml tetracycline. Then, 0.5 ml of the above overnight culture was used to inoculate 25 ml

Figure 13. AsME cDNA in the pALTER-1 Vector. The AsME cDNA is inserted into the multiple cloning site in the *lac*Z gene that encodes for the enzyme β-galactosidase. The vector also contains the tetracycline resistant gene (Tet^r), a mutated β-lactamase gene (Amp^s), and the phage f1 origin of replication. The 1.8 kb AsME cDNA is subcloned in the 5.7 kb pALTER-1 vector using two restriction enzymes, *Bam*H I and *Hin*d III.

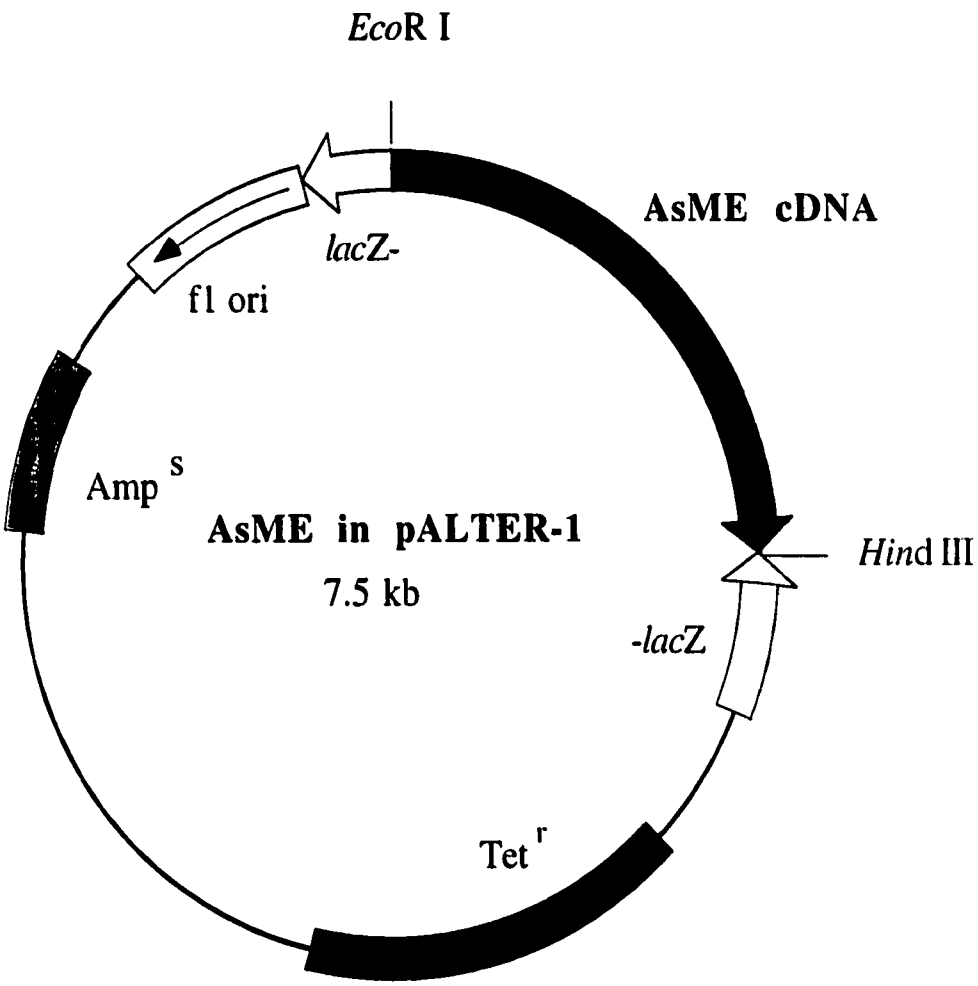
*Eco*R I
AsME cDNA
lacZ-
f1 ori
Amp s
AsME in pALTER-1
7.5 kb
*Hin*d III
-*lacZ*
Tet r

LB medium containing the same concentration of tetracycline. After shaking vigorously at 37°C for 30 minutes, the culture was infected with helper phage R408, which is included in the mutagenesis kit, and growth was for another 6 hours under the same conditions. The culture supernatant, which contains the phage particles, was harvested after pelleting the cells by centrifugation at 9,000 *g* for 15 minutes. Phage particles were then precipitated on ice by addition of 0.25 volumes of precipitation solution (3.75 M ammonium acetate, pH 8.0; 20% polyethylene glycol 8000). The ssDNA was isolated from the phage particles with TE-saturated phenol:chloroform:isoamyl alchohol, and finally suspended in 20 µl water.

Mutagenic oligonucleotides were designed to be complementary to the ssDNA template with the exception of the mutation site. Generally, a 17-20 base oligonucleotide with a single base mismatch to produce the mutation in the center of the sequence is sufficient for the specific binding to the correct position in the template. If the mutation involves two or more mismatches, oligonucleotides ≥25 bases are generated to ensure correct binding in the annealing step. All of the mutagenic oligonucleotides used in these studies are shown in Table 2, and were purchased as discussed above.

Two host strains, ES1301 *mut*S and JM109, were used in the mutagenesis

Table 2. Mutagenic Oligonucleotides.

E58A	5'-GTTCAGCCTCTACGCGCGACAATATCTCGG-3'
E271A	5'-ATACAATTCGCAGATTTTGCA-3'
E440A	5'-AGTAAAGCCGCATGTACGGCC-3'
K199A	5'-GTATCCCGGTGGGCGCGCTAGCCCTTTATG-3'
K199E	5'-GTATCCCGGTGGGCGAGCTAGCCCTTTATG-3'
K199R	5'-GTATCCCGGTGGGCAGGCTAGCCCTTTATG-3'
K199H	5'-GTATCCCGGTGGGCCACCTAGCCCTTTATG-3'
K199Q	5'-GTATCCCGGTGGGCCAGCTAGCCCTTTATG-3'
Y126F	5'-AATGCCAATTGTCTTTACGCCCACTGTTGG-3'
Y126H	5'-AATGCCAATTGTCCATACGCCCACTGTTGG-3
Y126Q	5'-AATGCCAATTGTCCAAACGCCCACTGTTGG-3'
Y126R	5'-AATGCCAATTGTCCGTACGCCCACTGTTGG-3'
Y126E	5'-AATGCCAATTGTCGAGACGCCCACTGTTGG-3'
Y126W	5'-AATGCCAATTGTCTGGACGCCCACTGTTGG-3'

Mutation sites are underlined.

experiments. Competent cells by electroporation were prepared according to the following procedure. One liter of LB is inoculated with 10 ml overnight culture, and shaken vigorously at 37°C until the OD_{600} reaches 0.5-0.7. The cells are then harvested by centrifugation. After washing the cells twice with ice-cold 10% glycerol, once with 1 liter and a second time with 20 ml, the cells are eventually suspended in 2-3 ml of ice-cold 10% glycerol and frozen at -70°C in 100 µl aliquots.

Since the purchased mutagenic oligonucleotides possess 3'- and 5'-hydroxyls, phosphorylation of the mutagenic oligonucleotides is carried out using T4 polynucleotide kinase to increase the number of mutants obtained.

2.2.2. Making and Verifying Site-directed Mutations

All site-directed mutations were prepared using the Alter Site II *in vitro* mutagenesis kit from Promega. The overall procedure is shown in Fig. 14. A typical mutagenesis reaction starts with the annealing reactions, in which 0.05 pmol ssDNA template, 1.25 pmol phosphorylated mutagenic oligonucleotide, 0.25 pmol each of the ampicillin repair oligonucleotide and tetracycline knockout oligonucleotide, and the approporate amount of 10 x annealing buffer are mixed. The annealing reaction mixture is then heated to 75°C for 5 minutes and allowed to cool down at room

Fig. 14. Mutagenesis Reaction. I. pALTER-1 phagemid with AsME cDNA insert. II. Annealing reaction *in vivo*. III. Synthesis of mutated DNA strand (red) *in vivo* using T4 polymerase. IV. DNA sample isolated from ES1301 *mut*S culture. Mutated double-strand plasmids are red. Wild type plasmids are black. V. pALTER-1 phagemid with mutated AsME insert isolated from JM109 culture.

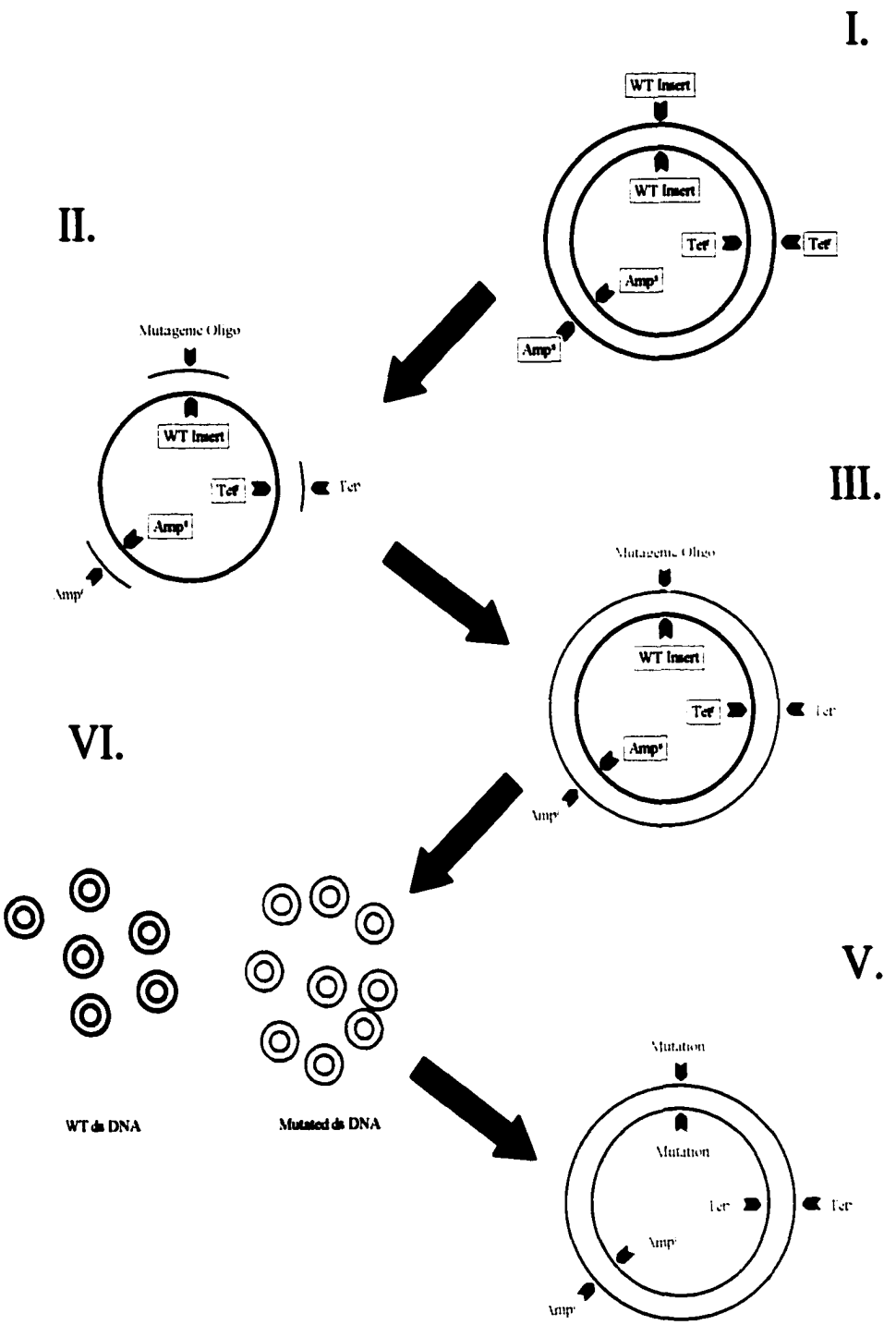
I.
WT Insert
WT Insert
Ter
Ter
Amp
Amp
II.
Mutageme Oligo
WT Insert
Ter
Ter
Amp
Amp
III.
Mutageme Oligo
WT Insert
Ter
Ter
Amp
Amp
VI.
V.
WT ds DNA
Mutated ds DNA
Mutation
Mutation
Ter
Ter
Amp
Amp

temperature to 45°C at a cooling rate about 1°C/minute. The resulting solution is then cooled to 22°C rapidly on ice. The annealing reaction allows the oligonucleotides to specifically bind to the ssDNA template.

Following the annealing reaction, T4 DNA polymerase, T4 DNA ligase, and 10 x synthesis buffer that contains the four trinucleotides are added to the annealing mixture. The reaction is then incubated at 37°C for 90 minutes to perform mutant strand synthesis and ligation.

The newly synthesized DNA strand is transfected into ES1301 *mut*S along with the template. A Bio-Rad Gene Pulser was then used, and the electroporation was conducted at a voltage of 2.5 kV. The lack of mismatch repair capability in ES1301 *mut*S cells allows plasmid amplification from both mutant and template strands. Ampicillin is then added to the culture after 40 minutes of recovery at 37°C to allow growth of the cells containing the mutated DNA. Growth is then continued for 20-24 hours with an ampicilin concentration of 125 μg/ml. The cells are then harvested, and the plasmids isolated using the PERFECTprepTM Plasmid Kit according to the manufacturer's instructions. The DNA obtained is then eletroporated into JM109 competent cells as above with the exception that ampicillin containing LB plates are used to grow single colonies after the 40 minute recovery period. Single

colonies, which contain the mutated pALTER-1 plasmid, are then picked and grown in liqiud LB medium with ampicillin. Frozen stocks of the cultures are prepared by adding 15-30% autoclaved glycerol into the ampicillin-LB culture, which is stored at -80°C.

The mutations made are then verified by restriction-endonuclease cleavage and DNA sequencing. Plasmid DNA is purified from a culture grown from frozen stock and then digested with restriction endonucleases *Eco*R I and *Hind* III. The sizes of the insert and remaining pALTER-1 fragments are determined by agarose gel electrophoresis. The DNA samples that give the expected size of the digested fragment are then sequenced using the fmol^{R} DNA Cycle Sequencing System with ^{35}S-labeled ATP. The sequencing primers used are located 150-300 base pairs upstream of the mutation site(s). Only those frozen stocks with correct mutations were kept. A typical agrose gel is shown in next chapter (Fig. 17).

2.2.3. Subcloning the Mutated AsME cDNA into the pQE30 Expression Vector

The mutated AsME cDNA in the recombinant pALTER-1 plasmid is amplified using a pair of primers 5'-GCATTGGATCCGAATGAAAGT-3', which generates a *Bam*H I site (underlined sequence), and 5'-

TAGAATACTCAAGCTTAACCATCCAT-3', which generates a *Hin*d III site (underlined sequence) at the ends of the AsME coding area. With the purified recombinant pALTER-1 plasmid DNA as the template, PCR reactions are carried out using a PTC-100 Programmable Thermal Controller from M. J. Research, Inc. The cDNA fragment produced is predicted to have a size of 1.8 kb (Fig. 15).

The double-stranded DNA produced in the PCR reaction is then digested with *Bam*H I and *Hin*d III restriction endonucleases to generate sticky ends. The pQE30 expression vector provided in the QIAexpress System from QIAGEN is also digested with the same two restriction enzymes to generate a linear plasmid with complementary sticky ends. Ligation is then performed by mixing the above two DNA fagments with complementary sticky ends, T4 ligase, ATP, and ligation buffer and incubating at 15°C for 8-10 hours. The resulting DNA is then electroporated into either the M15(pREP4) strain or the JM109 strain. Single colonies are then picked from LB/Amp/Kan plates (M15) or LB/Amp plates (JM109). The liquid cultures with appropriate antibiotic(s) are then grown from the single colonies, and frozen stocks are made by adding 15-30% autoclaved glycerol. The recombinant pQE30 plasmid DNA samples isolated from the above cultures are then digested with *Bam*H I and *Hin*d III, and the size of the digested fragments is determined by agarose gel

Figure 15. Subcloning the Mutated AsME cDNA into the pQE-30 Vector. The bold arrow represents the mutated AsME cDNA. Two smaller arrows represent the primers used in PCR reaction. Ligation is carried out using T4 DNA ligase. Transformation is by electroporation, carried out using a Bio-Rad Gene Pulser and JM109 (or M15) competent cells.

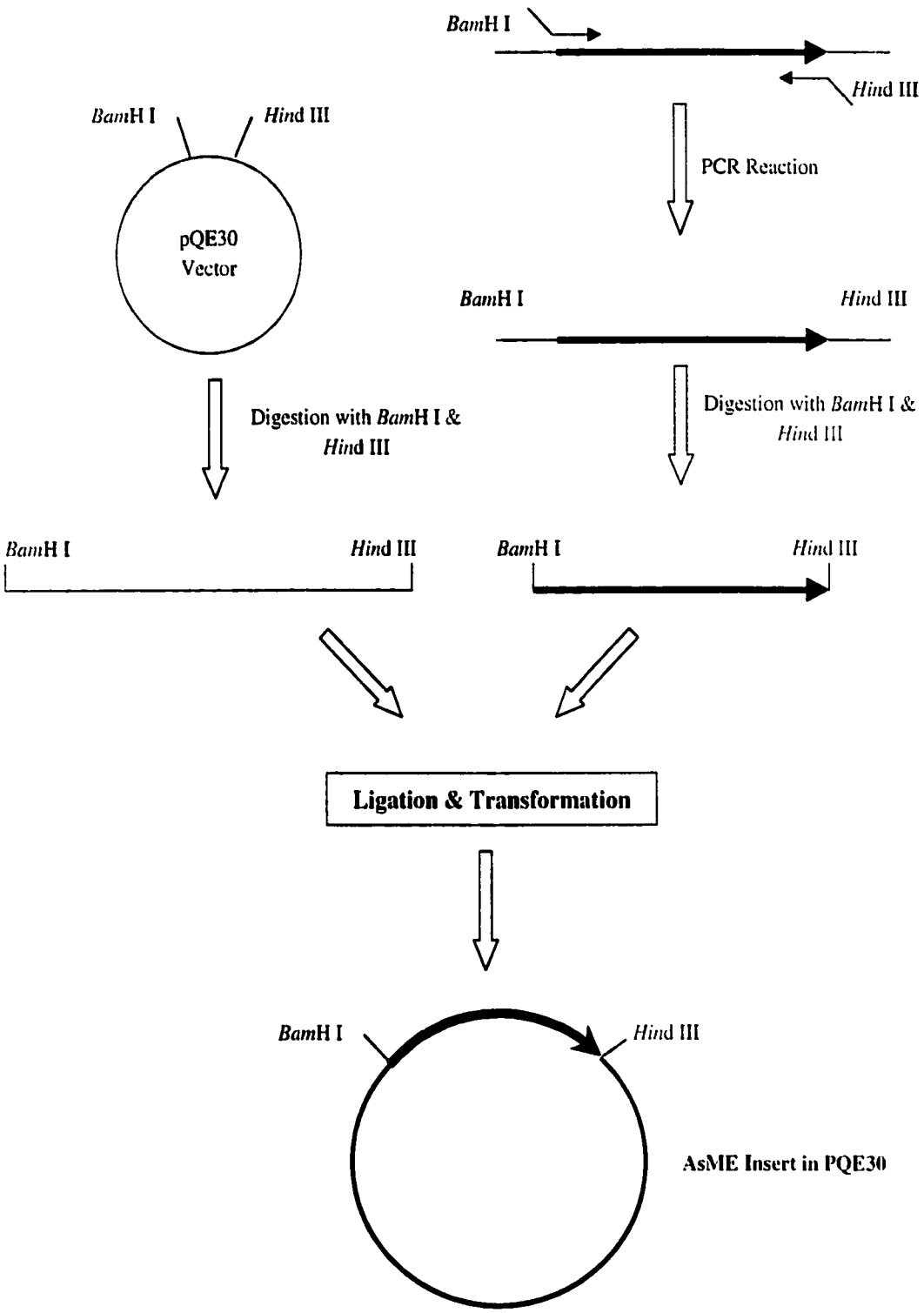
BamH I
Hind III
PCR Reaction
BamH I
Hind III
pQE30
Vector
Digestion with BamH I &
Hind III
BamH I
Hind III
Digestion with BamH I &
Hind III
BamH I
Hind III
BamH I
Hind III
Ligation & Transformation
BamH I
Hind III
AsME Insert in PQE30

eletrophoresis. The final plasmid with mutant insert is shown in Figure 16. Only the frozen stocks containing the correct plasmid size are stored at -80°C.

2.3. Expression and Purification of the AsME Mutant Enzymes

2.3.1. Growth Conditions

Two host strains are used to express the pQE30 ME proteins, M15(pREP4) and JM109. The difference in the two hosts lies in the way they produce the *lac* repressor that is the key factor in the control of expression. JM109 has the *lac* repressor gene in its genomic DNA, while M15 requires another coexisting plasmid (pREP4) to carry the lac repressor gene providing a more stringent control. The M15 culture needs kanamycin in addition to ampicillin to maintain the presence of the pREP4 plasmid. Other than this difference, the growth conditions for both hosts are the same. The M15/JM109 was inoculated in a small volume (5-10% of the expression volume) of LB liquid medium with an ampicillin concentration of 150 μg/ml from the frozen stocks; kanamycin, as well as ampicillin, is added to a concentration of 25 μg/ml for M15(pREP4) strain. After shaking vigorously at 37°C overnight, the culture is used to inoculate a 10-20 time larger volume with the same

Figure 16. Mutated AsME cDNA in pQE30. The bold arrow represents the mutated AsME cDNA. "6 x His" represents the 6 x His affinity tag encoding area. Amp represents the β-lactamase gene. "to" stands for the transcriptional terminator from phage lambda, while T5 indicates the strong promotor from T5 phage. ORI represents the origin of replication for pBR322.

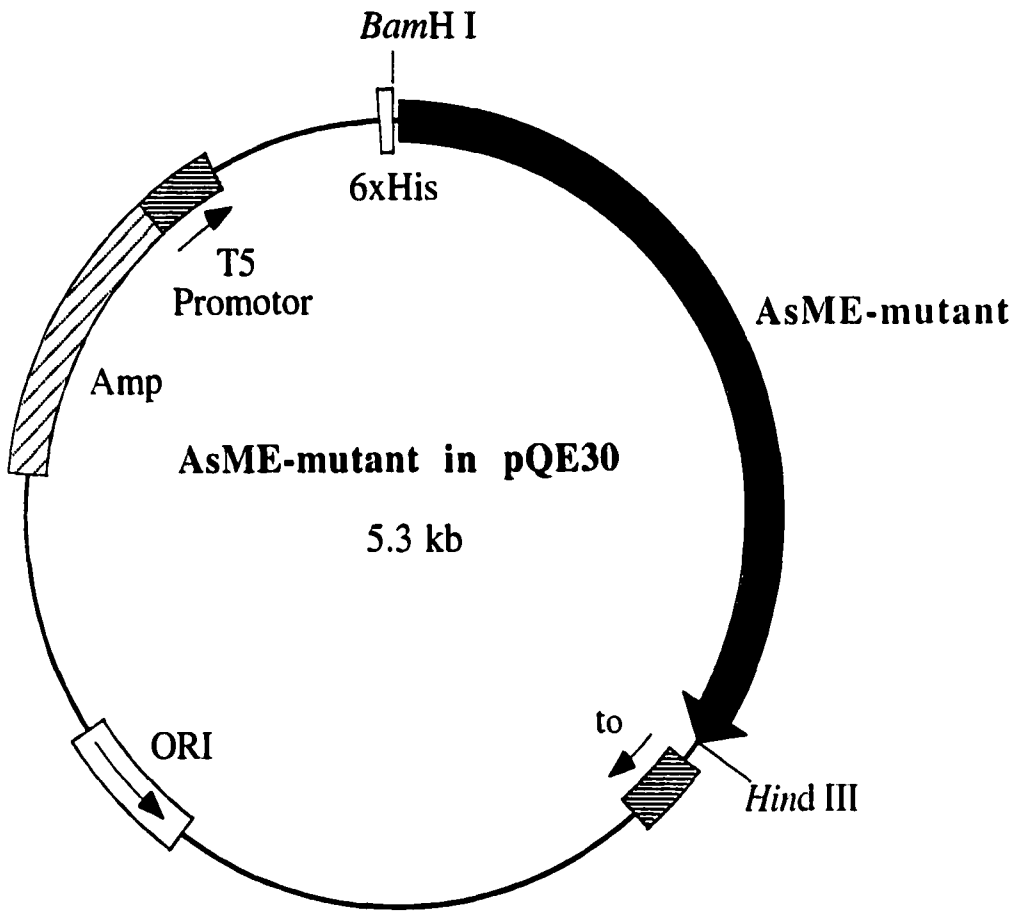
*Bam*H I
6xHis
T5
Promotor
AsME-mutant
Amp
AsME-mutant in pQE30
5.3 kb
ORI
to
*Hin*d III

ampicillin and kanamycin concentrations. Two-liter flasks containing 500 ml of culture are usually used for growth of less than a 5 liter culture, while an automated fermentation system (Bellco Glass Inc.) is used when the total volume of the desired culture is greater than 5 liters.

The culture is then grown at 30°C. When the OD_{600} reaches 0.7-0.9, IPTG is added to a concentration of 0.5 mM. The addition of IPTG induces the expression of the AsME protein. Growth is then continued at 30°C for 5 hours before the cells are harvested by centrifugation at a speed of 6,000 *g* for 15 minutes. The harvested cells are suspended in sonication buffer (50 mM Na_2HPO_4, 300 mM NaCl, and 10 mM β-mecaptoethanol, pH 8). The collected cells can be stored at –20°C or subjected to the purification procedure immediately.

2.3.2. Purification the His-tagged AsME Proteins

The pQE30 vector adds six histidines to the N-terminus of the AsME protein. The His-tag provides an affinity of the recombinant protein for the Ni-NTA resin that is provided with the QlAexpress Kit. This affinity tag makes the purification process very convenient and efficient. The capacity of this resin for a His-tagged protein is generally 5 mg/ml (of resin).

The cell suspension obtained in 2.3.1. above is sonicated for 2-4 minutes on ice using an XL Sonicator from MISONIX, Inc., and then centrifuged at 22,000 *g* for 40 minutes to pellet cell debris. The supernatant is then mixed with Ni-NTA resin preequilibated with sonication buffer, and the mixture is stirred slowly at 4 °C for about 2 hours. After that, the resin is washed thoroughly with sonication buffer to elute the unbound protein, and then packed into a column. The resin is further washed with 5 volumes of sonication buffer containing 0.025 M imidazole to remove loosely bound protein. The His-tagged AsME protein is then eluted with sonication buffer containing 0.3 M imidazole. The fractions containing AsME are collected and dialyzed against 2 liters of 100 mM Hepes, 10 mM β-mecaptoethanol, pH 7. The AsME protein is then applied to an orange A agarose column. The orange A acts as an affinity column for malic enzyme. After washing with about 5 bed-volume of buffer, the AsME protein is eluted with buffer containing 0.5 M NaCl. It has been noted that some mutant proteins lose affinity for the orange A resin. Therefore, after the dialysis against 20 mM triethyleneamine buffer at pH 7.5, these proteins are further purified on a Tak-Gel DEAE-5W column using a 5-500 mM NaCl gradient to develop the chromatogram on a Bio-Rad preparative HPLC system. The purity of the obtained protein is then determined by SDS-PAGE elecrophoresis.

2.4. Characterizations of Mutant Protiens

2.4.1. Circular Dichroism Spectroscopy

Circular dichroism spectra are recorded on an AVIV 62 HDS spectropolarimeter with an RC 6 Lauda refrigerated circulating bath to maintain a constant temperature. Enzyme is dialyzed overnight against 2 liters of 10 mM KH_2PO_4, pH 7. The final protein concentration in the cuvette is 50 μg/ml. Spectra are recorded using 0.2 cm quartz cuvettes. Far UV-CD (200-260 nm) spectra are recorded at 1 nm intervals with a dwell time of 3 seconds. The KH_2PO_4 buffer was used as a blank, and the spectrum of wild type enzyme was recorded as well as those of the mutant proteins. Each spectrum was the average of three repeats. Ellipticity values recorded in millidegrees were then converted into molar ellipticity values according to the following equation:

$$[\theta] = [\theta]_{obs}/[10(MRC)l] \qquad (1)$$

where $[\theta]$ is the molar ellipticity in degrees•cm^2/decimole, $[\theta]_{obs}$ is the ellipticity

recorded in millidegrees, MRC is the mean residue concentration of the enzyme and is equal to the number of amino acid residues times the molar concentration of protein, and l is the cuvette path length in cm. Spectra of the mutant proteins were compared to that of wild type AsME. Differences between the two reflect any global structural changes caused by the mutation.

2.4.2. Initial Velocity Studies

All data were collected using a Beckman DU 640 spectrophotometer or a Hewlett-Packard 8453 diode array spectrophotometer to monitor the appearance of NADH at 340 nm (ε = 6,220 $M^{-1}cm^{-1}$). All assays were carried out at 25 ± 0.1°C, and the temperature was maintained using a circulating water bath with the capacity to heat and cool the cell compartment. Typical assays contained 100 mM Hepes, pH 7.3, and 30 mM free Mg^{2+} (added as $MgSO_4$) and variable concentrations of free malate (0.25-10 mM) and free NAD (15 -150 mM) or 2 mM free NAD^+ and variable free Mg^{2+} (10-100 mM) and free malate (0.25-10 mM). The correction for the Mg-malate and Mg-NAD chelate complexes was according to Park et al. (1984). Initial velocity data were fitted using the appropriate rate equation and a BASIC version of the Fortran programs developed by Cleland (1979). Saturation curves for reactants

were fitted using eq. 2. Data conforming to a sequential initial velocity pattern were fitted using eq. 3,

$$v = VA/(K_a + A) \qquad (2)$$

$$v = VAB/(K_{ia}K_b + K_aB + K_bA + AB) \qquad (3)$$

where v and V represent initial and maximum velocities, A and B represent reactant concentrations, K_a and K_b are Michaelis constants for A and B, and K_{ia} is the dissociation constant for A.

2.4.3. pH Studies

The pH dependence of kinetic parameters can provide information on the optimum protonation state of functional groups on reactants and enzyme required for binding and/or catalysis. To determine whether the kinetic mechanism changes with pH, studies outlined in 2.4.2. are performed at the extremes of pH. Buffers used to obtain the pH dependence of kinetic parameters include: N,N' - bis(hydroxyehyl)piperazine, 4.0-5.5; Mes, 5.5-6.5; Pipes, 6.5-7.5; Hepes, 7.0-8.0; Taps, 8.0-9.0; Ches, 9.0-10.0; Caps, 1.0-11.0. All buffers are titrated to the

appropriate pH with KOH. Above pH 9, NAD^+ was added to the reaction mixture just prior to the addition of the enzyme to minimize the base-catalyzed degradation of NAD^+. The pH of the reaction mixture was measured before and after the reaction, and no significant change was noted. No significant effect of ionic strength was observed up to 3.5 M. The kinetic parameters V and V/K are displayed as the log parameters vs. pH. Data are fitted using the following equation:

$$\text{Log}Y = \log\{C/(1 + H/K_1 + H/K_2)\} \quad (4)$$

$$\text{Log}Y = \log\{C/(1 + H/K_2)\} \quad (5)$$

In equation (4) and (5), Y stands for V or V/K, C represents the pH independent value of Y, and H stands for proton concentration. K_1 and K_2 are the acid dissociation constants for enzyme or substrate functional groups that must be unprotonated or protonated, respectively, for activity.

2.4.4. Tritium Exchange

The enzyme-catalyzed exchange of tritium from solvent into pyruvate was measured for wild type and mutant AsME proteins. A typical tritium exchange

reaction contained 100 mM Hepes, pH 7.0, 1.3 x 10^9 cpm ^3H_2O, 100 mM pyruvate, 10 mM $MnSO_4$, 5 mM $NaHCO_3$, 1 mM NADH, and 600 μg of AsME in a volume of 1 ml. The reaction was carried out at 25°C for 2 hours, and then 0.1 ml of 1 M EDTA was added to 0.2 ml of the reaction mixture to stop the reaction.

The stopped reaction mixture was loaded onto a Dowex 1X8-200 column (0.9 x 2 cm). After washing the column extensively with water to remove unreacted ^3H_2O, the products and the remaining substrates of the reaction, pyruvate, malate, and lactate, were eluted with 0.05 N HCl, and 6 ml fractions were collected. The total radioactivity for the organic acids in each reaction was measured using a Tri-Carb 2100TR liquid Scintillation Analyzer from Packard. The amount of pyruvate in the sample was estimated by enzymatic end-point assays using lactate dehydrogenase.

2.4.5. Oxalacetate Partitioning

Oxalacetate partitioning experiments were performed according to the method of Karsten and Cook (1994), after Grissom and Cleland (1985). The partitioning reaction mixture contained 100 mM Hepes, pH 7.0, 0.4 mM NADH, 4 mM oxalacetate, 2 mM $MgSO_4$, and 1-5 units of AsME in a total volume of 1 ml. Assays were carried out using a Hewlett-Packard 8453A diode array spectrophotometer in

0.5-cm path length cuvettes. An effective extinction coefficient of oxalacetate was measured under the same condition for each experiment at 282 nm (ε_{282}= 2.78 mM^{-1} cm^{-1}) with 4 mM oxalacetate and 2 mM Mg^{2+}. Oxalacetate solutions were prepared daily and the concentration of oxalacetate was precisely determined by enzymatic end-point assays using malate dehydrogenase. In the partitioning experiments, the oxalacetate concentration was monitored at 282 nm, while the concentration of NADH was monitored at 340 nm. No significant absorbance at 282 nm caused by pyruvate is detected using this procedure.

A control reaction mixture that contained the same components with the exception of the enzyme was used to monitor the background nonenzymatic rate of oxalacetate decarboxylation caused by the metal ion. When high concentrations of enzyme were used, contaminating malate dehydrogenase activity in the malic enzyme preparations was also monitored replacing $MgSO_4$ with 2.5 mM EDTA, and carrying out the reaction as usual.

Reactions were monitored for 20 minutes, and over this time period the time courses are linear. The disappearance of oxalacetate was followed at 282 nm while the formation of malate was followed by the decrease in absorbance at 340 nm associated with the consumption of NADH. After subtraction of appropriate

background control rates, the oxalacetate partitioning ratio (r_H) was calculated according to the following equations:

$$d[\text{pyruvate}]/dt = (d[\text{oxalacetate}]/dt) - (d[\text{NADH}]/dt) \qquad (6)$$

$$r_H = (d[\text{pyruvate}]/dt)/(d[\text{NADH}]/dt) \qquad (7)$$

2.4.6. Primary Isotope Effect

Primary deuterium isotope effects were measured in both oxalacetate partitioning assays and initial velocity assays, for which the deuterated substrates used were 4*r*-NADD and L-malate-2-D, respectively. Both deuterated substrates were prepared according to Viola et al. (1979). The *4r*-NADD reaction included 28 mM ethanol-d_6, 5.6 mM NAD^+, 6 mM Taps, pH 9, 50 units equine liver alcohol dehydrogenase, and 100 units yeast aldehyde dehydrogenase. The reaction was performed at 25°C for 1 hour, and the pH of the reaction was maintained at 9 throughout the reaction by gradually adding 0.1 N KOH to the reaction mixture. The *4r*-NADD was then purified using DEAE-cellulose column chromatography and a liquid chromatography system from Isco. L-malate-2-D was provided by Dr. W.E. Karsten who prepared and purified it using the procedures of Viola et al. (1979).

Initial velocity assays for deuterium isotope effects contained 100 mM Hepes, pH 7 (or 100 Taps, pH 9), 2 mM free NAD^+, 50 mM free Mg^{2+} (added as $MgSO_4$), 2-20 mM L-malate-2-H/D, and reaction was initiated by the addition of an appropriated amount of AsME, dependent on activity. The isotope effects were estimated by direct comparison of the kinetic parameters V and V/K and data were fitted using following equation

$$v = VA/[K_a (1 + fE_{VK}) + A (1 + fE_V)] \qquad (8)$$

where f represents the present completion of reaction, and E_{VK} and E_V are the isotope effects minus 1 on V/K and V, respectively. The isotope effects are written as ^DV and $^D(V/K)$ according to Northrop (1975) and Cook and Cleland (1981).

In the oxalacetate partitioning assays, NADD replaced NADH, while other conditions remained the same. The partition ratio (r_D) was obtained as in 2.4.5. The ratio r_H/r_D, gives the isotope effect on the partition ratio.

CHAPTER 3

RESULTS

3.1. Homology Search

This research project was initiated without a three dimensional structure for a malic enzyme. The homology search became the most effective way to locate the potential catalytic residues. The AsME amino acid sequence was first used in a blast search, and unique malic enzyme sequences from different sources were chosen for alignment. A multiple sequence alignment (Appendix I.) was carried out using all of the malic enzyme sequences, and the alignment has been updated monthly to include newly submitted sequences.

Since the main goal of this project is to identify enzyme side chains that could serve as the general acid and general base in the malic enzyme reaction, highly conserved ionizable residues were selected for mutagenesis studies (Table 3.).

3.2. Site-directed Mutagenesis

Site-directed mutagenesis was performed using the Altered Site II *in vitro*

Table 3. Targets for Mutagenesis Studies

Ionizable Residue	Positions in the Amino Acid Sequence of AsME
Glutamate (E)	58, 107, 440, *271.
Aspartate (D)	178, 231, *272, 294, *295, *361.
Lysine (K)	*199.
Tyrosine (Y)	126.

All of the residues shown were totally conserved at the beginning of these studies, but only the ones with * remain so in the latest update.

mutagenesis system from Promega. After the *in vitro* mutagenesis reaction, electroporation into ES1301 *mut*S cells, and 40 minutes of recovery in LB medium, ampicillin was added to the culture as discussed in 2.2.2. It usually took the culture 20-24 hours growing in a shaker-bath at 37°C to show growth of the cells. The ampicillin resistant cells that contained mutated DNA were then collected.

The DNA was isolated from the collected ES1301 *mut*S cells, electroporated into JM109 competent cells, and plated. Usually, 20-50 single colonies were obtained on each LB-ampicillin plate. For each mutation, 6 single colonies were picked and cells were grown in LB liquid culture. The pALTER-1 plasmid with mutant AsME cDNA insert was then isolated, and digested with *Eco*R I and *Hin*d III restriction enzymes. Agarose gel electrophoresis was used to separate the digested fragments, and the size of the fragment was determined by comparison against molecular weight markers (lambda DNA-*Bst*E II Digest from Promega). Figure 17 shows the results of a digestion of the E58A mutant cDNA in pATER-1. The linear pALTER-1 plasmid appears as a 5.7 kb band, and the mutated AsME cDNA appears as a 1.8 kb band on the gel. Samples that showed the expected insert size on the gel were used as a template for DNA sequencing to verify the specifically introduced mutation. The DNA sequencing results showed that more than 80% of the randomly

Figure 17. **Agarose Gel Electrophoresis of the E58A cDNA in pALTER-1. Lane 1 and 5 are DNA markers from Promega. Lanes 2-4 and 6-8 are DNA samples isolated from single JM109 colonies on LB-ampicillin plates, that were digested with *Eco*R I and *Hin*d III before being loaded onto the gel. All six DNA samples gave two bands, a 5.7 kb linear pALTER-1 vector band and a 1.8 kb E58A(AsME) cDNA band. All six single colonies have the correct insert size in the pALTER-1 vector.**

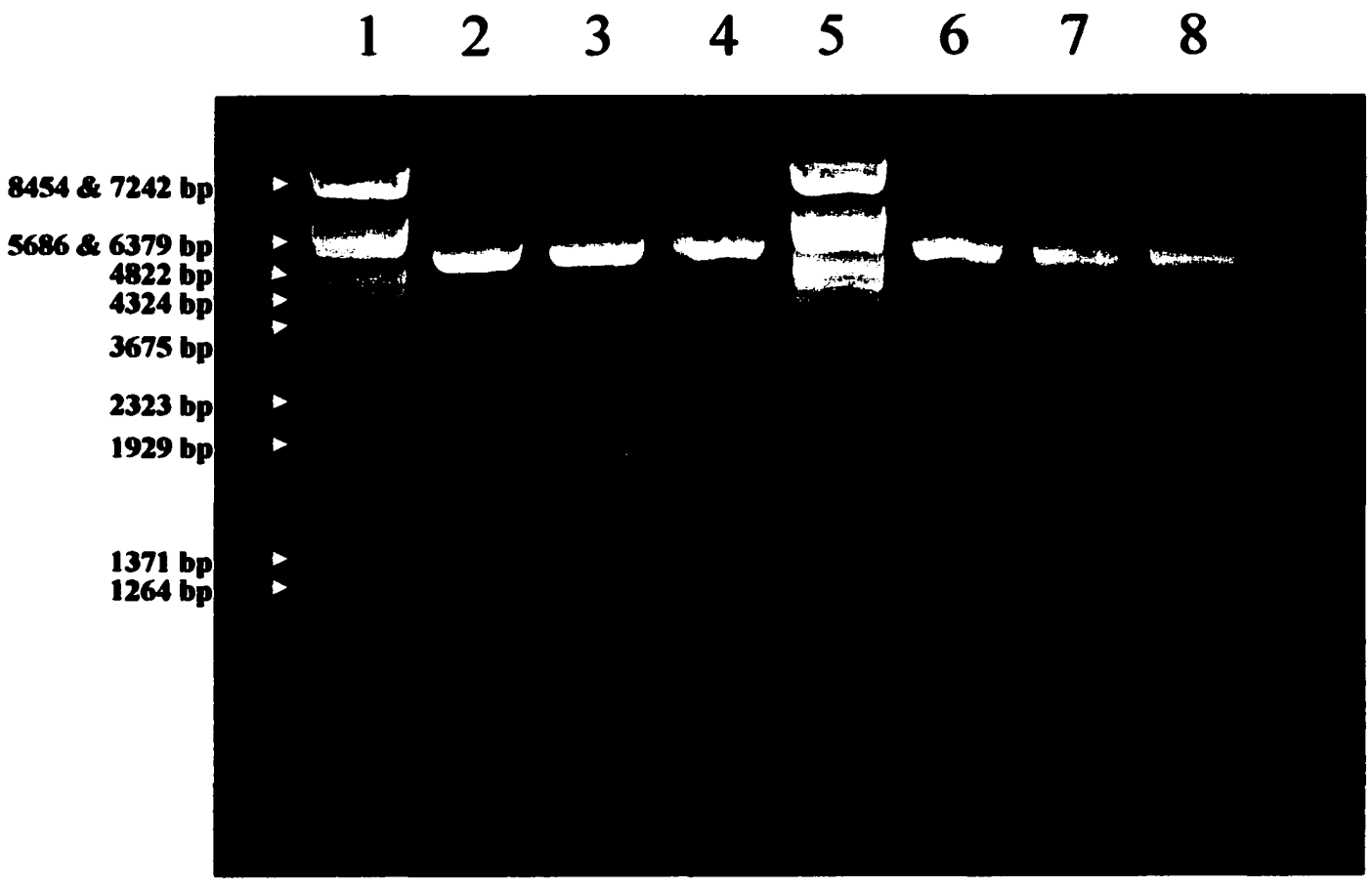
1
2
3
4
5
6
7
8
8454 & 7242 bp
5686 & 6379 bp
4822 bp
4324 bp
3675 bp
2323 bp
1929 bp
1371 bp
1264 bp

selected colonies contained the expected mutation.

3.3. Expression and Purification of the Mutant Proteins

In order to express and purify mutant proteins quickly and effectively, a fusion protein system called QIAexpress (His-tag) from Promaga was used. An extra polypeptite tail including 6 histidine (M-R-G-S-H-H-H-H-H-H-G-I-R-M) was added to the N-terminal of the recombinant protein when expressed, generating a specific affinity between the recombinant protein and the Ni-NTA resin provided with the system.

3.3.1. Subcloning the Mutants into the pQE30 Expression Vector

The mutated and wild type AsME cDNAs were subcloned into the pQE30 expression vector as discussed in 2.2.3. The pQE30 plasmid provided by the QIAexpress kit and the PCR product, which was 1.8 kb in size, were purified and both were digested with *Bam*H I and *Hind* III. The two digested fragments were then ligated, and the ligation product was transfected into either M15 (pREP4) or JM109 competent cells. Single colonies were picked and used to prepare an overnight

culture. The pQE30 plasmid with the AsME cDNA insert was then verified using agarose gel electrophoresis after being digested with *Bam*H I and *Hin*d III (Fig. 18).

3.3.2. Purification of the Mutant Proteins with His-tag

An overnight culture was grown from a frozen stock and it was used to inoculate a second culture, at a final volume of 5-10% of the total culture volume. After 5 hours of growth at 30°C, the cells were harvested, and generally 30-40 grams of wet cells were obtained from 15 liters of culture. The harvested cells were sonicated and centrifuged, and the yellowish supernatant was collected.

After binding with the His-tagged protein, the resin is washed thoroughly with sonication buffer, and then 5 column volumes of sonication buffer with 0.025 M imidazole were needed to wash off the loosely bound proteins. The His-tagged AsME is finally eluted with sonication buffer containing 0.2-0.4 M imidazole. Normally, about 30 mg of protein can be obtained from 15 liters of culture, and the AsME purity is about 60-70% at this point. The protein is then further purified using orange A or DEAE chromatography on HPLC. Figure 19 shows an example of an elution profile for the purification of Y126E (AsME). The final purity is ≥95% by SDS-PAGE, Figure 20.

Figure 18. Agarose Gel Electrophoresis Results of the K199A cDNA in pQE30. Lane 1 shows the DNA markers (Lambda DNA-*Bst*E II Digest) from Promega. Lanes 2-6 are DNA samples isolated from M15(pREP4) single colonies, digested with *Bam*H I and *Hin*d III before being loaded onto the agarose gel. All 5 samples have two very closely migrating bands, a 3.7 kb linear pQE30 vector and 3.5 kb linear pREP4 plasmid; the latter are so close to one another that they appear as one large band. Three samples, shown in lanes 2, 4 and 6, have the 1.8 kb cDNA band expected K199A(AsME), while the other two samples, lanes 3 and 5, do not.

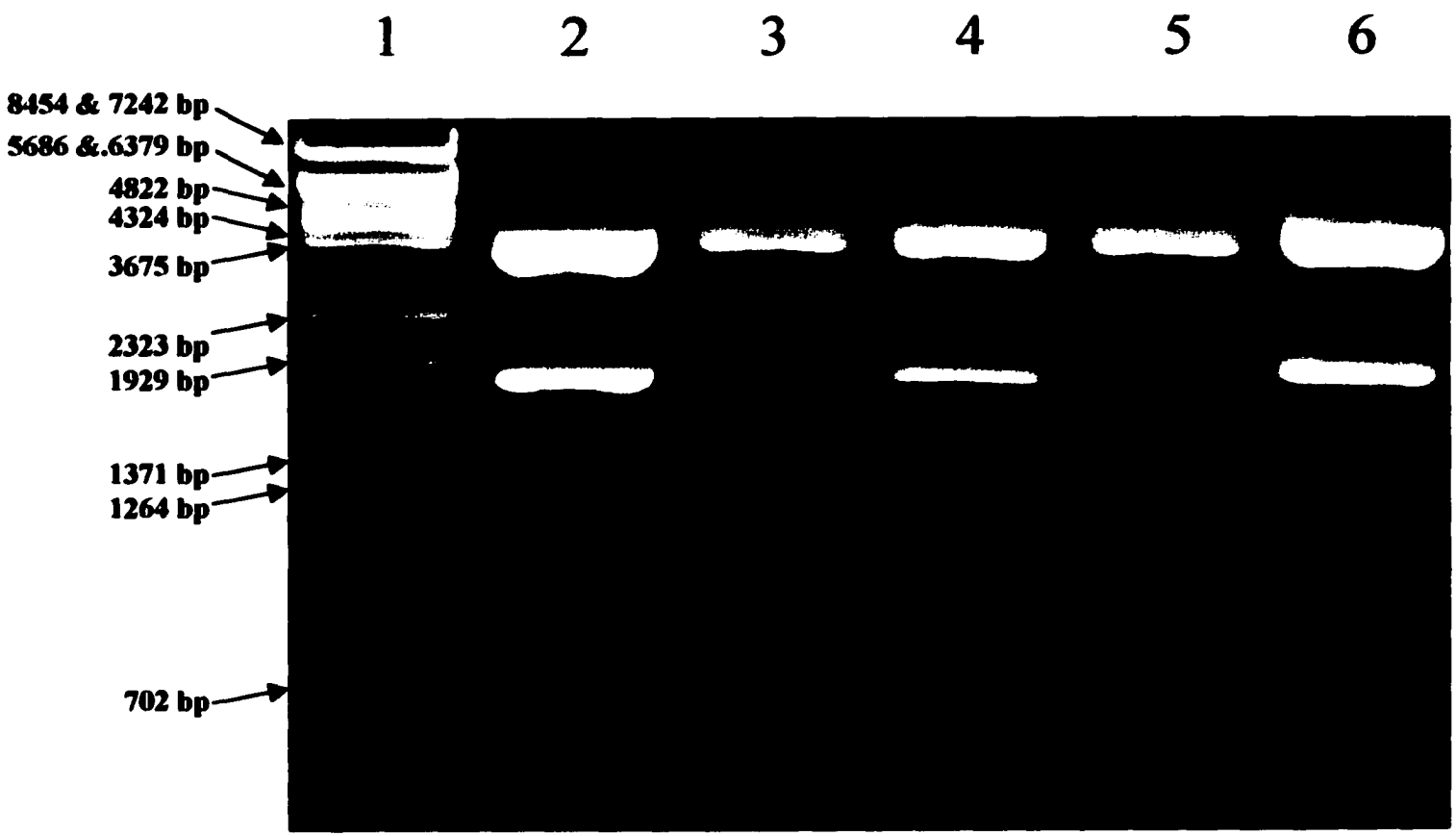
1
2
3
4
5
6
8454 & 7242 bp
5686 &.6379 bp
4822 bp
4324 bp
3675 bp
2323 bp
1929 bp
1371 bp
1264 bp
702 bp

Figure 19. **HPLC Elution Profile of Y126E AsME Mutant Enzyme. The blue line represents the absorbance at 280 nm, while the dashed black line represents the NaCl gradient (0-500 mM), and the red line represents the conductivity of the solution. Fractions 29-31 contain Y126E (AsME) protein.**

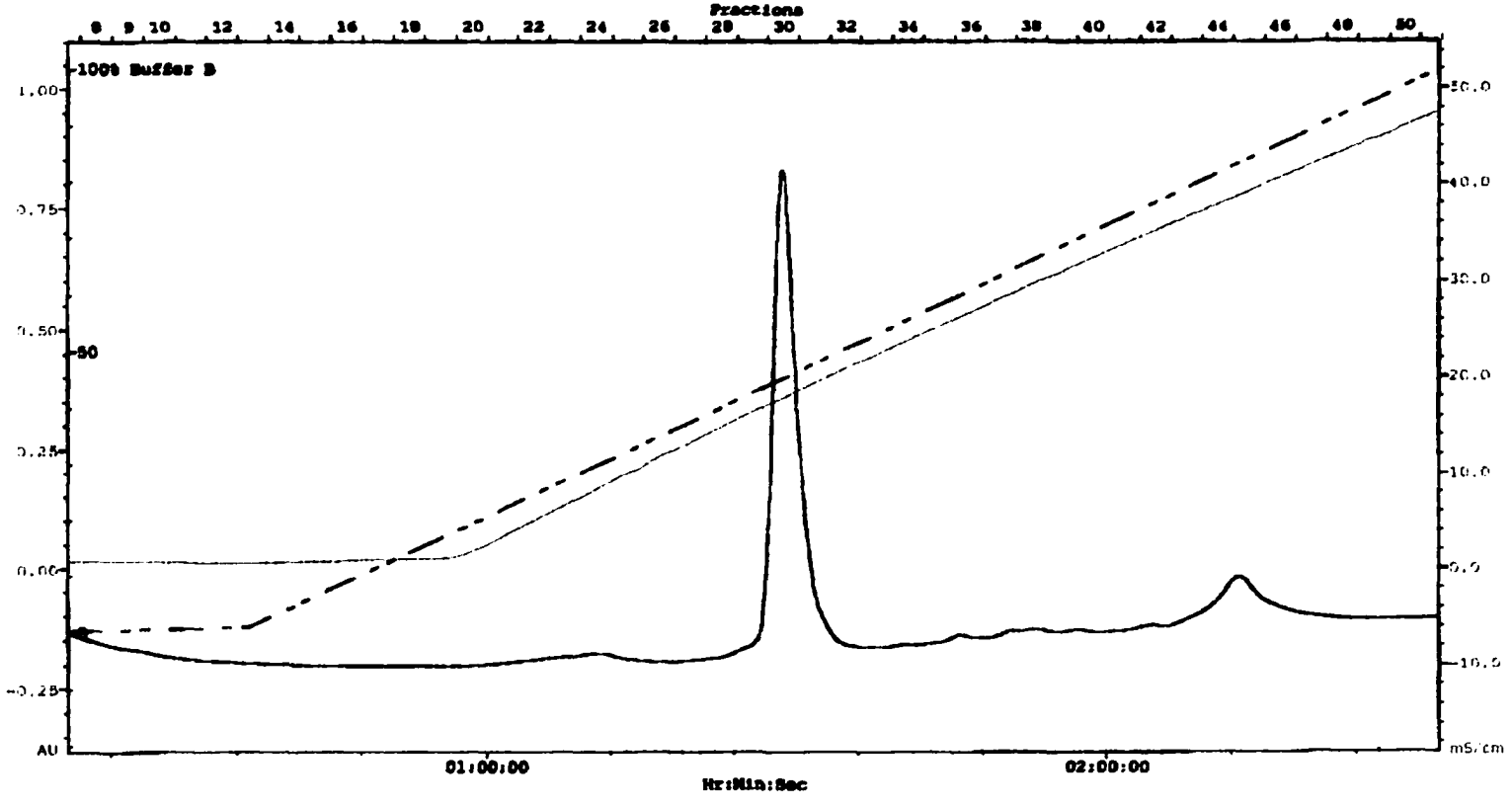
Fractions
8 9 10 12 14 16 18 20 22 24 26 28 30 32 34 36 38 40 42 44 46 48 50
100% Buffer B
1.00
0.75
0.50
50
0.25
0.00
-0.25
AU
50.0
40.0
30.0
20.0
10.0
0.0
-10.0
mS/cm
01:00:00
02:00:00
Hr:Min:Sec

Figure 20. SDS-PAGE Electrophoresis of Purified AsME Proteins. Lane 1 and 6 are protein molecular weight markers from Sigma. Lane 2, wild type AsME purified after Orange A Agarose chromatography. Lane 3, wild type AsME after DEAE column chromatography (HPLC). Lane 4, K199A mutant enzyme after DEAE column chromatography (HPLC). Lane 5, Y126F mutant enzyme after DEAE column chromatography (HPLC). All protein samples have a major band with a molecular mass of 68 kd, and a purity of ≥95%. 30 μg of enzyme were loaded for lane 2 & 5; 60 μg of enzyme were loaded for lane 3 & 4.


1
2
3
4
5
6
205 kD
116 kD
97 kD
66 kD
45 kD
29 kD
205 kD
116 kD
97 kD
66 kD
45 kD
29 kD

3.4. Alanine-Scanning of the Conserved Glutamate Residues

Since the crystal structure was not available when the project was started, all of the targets chosen based upon the homology search were first mutated to alanine to eliminate their functional group. Four mutations, E58A, E107A, E271A, and E440A were made as discussed in Chapter 2. The glutamate at position 107 was later found not to be totally conserved, and characterization was discontinued. On the other hand, E58A, E440A and E271A were subcloned into the pQE30 vector, and mutant proteins were expressed. The E271A mutant protein was very poorly expressed, and thus, it was not further characterized, while E58A and E440A mutant proteins were purified. Initial velocity studies were carried out with the E58A and E440A mutant enzymes. Figure 21 shows an example of a double reciprocal plot obtained for E58A, varying the concentration of NAD^+. The kinetic parameters measured for E58A and E440A are shown in Table 4, with data obtained for the wild type enzyme for comparison. Mutations caused a decrease in the turnover number by 75-fold and 590-fold for E58A and E440A, respectively. The Michealis constants for malate and NAD^+ are also affected by the changes.

3.5. Characterization of Y126 and K199 Mutants

Figure 21. Double Reciprocal Plot for the E58A Mutant Enzyme. The variable reactant is NAD^+, while Mg^{2+} (added as $MgSO_4$) and L-malate are maintained at a saturating concentration. Squares represent measured initial rates, while the straight line is obtained by fitting equation 2 to the data. The enzyme concentration is about 1 µg/ml, and the assays are performed at pH 7, and 25 °C.

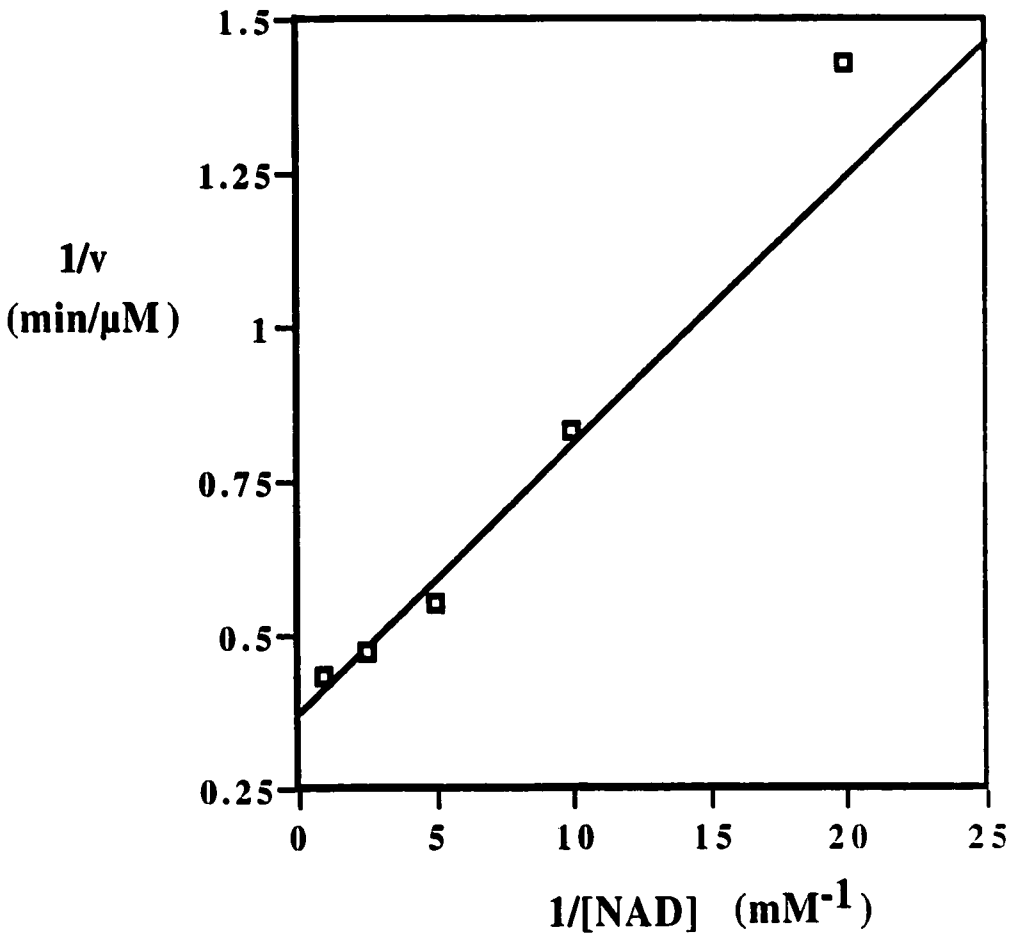
1.5
1.25
1
0.75
0.5
0.25
1/v
(min/μM)
0
5
10
15
20
25
1/[NAD] (mM-1)

Table 4. Kinetic Data for the E58A and E440A Mutant Enzymes

Wild Type AsME	V/E_t (s^{-1})		36 ± 1	
	K_{malate} (mM)	0.73 ± 0.07	$V/K_{malate}E_t$ ($M^{-1}s^{-1}$)	(4.9 ± 0.5) x 10^4
	K_{NAD} (μM)	25 ± 4	$V/K_{NAD}E_t$ ($M^{-1}s^{-1}$)	(1.4 ± 0.2) x 10^6
	K_{Mg} (mM)	11 ± 4	$V/K_{Mg}E_t$ ($M^{-1}s^{-1}$)	(3 ± 1) x 10^5
E58A	V/E_t (s^{-1})		0.48 ± 0.05 (75)[a]	
	K_{malate} (mM)	10 ± 2 (13)	$V/K_{malate}E_t$ ($M^{-1}s^{-1}$)	49 ± 11 (1000)
	K_{NAD} (μM)	120 ± 20 (5)	$V/K_{NAD}E_t$ ($M^{-1}s^{-1}$)	(4.2 ± 0.8) x 10^3 (333)
	K_{Mg} (mM)	9 ± 2 (-)	$V/K_{Mg}E_t$ ($M^{-1}s^{-1}$)	50 ± 10 (60)
E440A	V/E_t (s^{-1})		0.061 ± 0.007 (590)	
	K_{malate} (mM)	0.7 ± 0.1 (-)	$V/K_{malate}E_t$ ($M^{-1}s^{-1}$)	80 ± 15 (810)
	K_{NAD} (μM)	140 ± 20 (5.6)	$V/K_{NAD}E_t$ ($M^{-1}s^{-1}$)	440 ± 80 (3211)
	K_{Mg} (mM)	10 ± 3 (-)	$V/K_{Mg}E_t$ ($M^{-1}s^{-1}$)	6 ± 2 (550)

[a] Values in parentheses are fold-decrease for rate constants and fold-increase for K_m values.

Two other highly conserved residues, Y126 and K199, were targeted because of their location in the active site, based on the three dimensional structure, Figure 9. The K199A and Y126F mutants were prepared first to eliminate the functional groups. After confirming that the activity decreased dramatically for these mutants, other amino acid replacements were introduced at the two positions.

3.5.1. Circular Dichroism Spectroscopy

The purified mutant proteins were first subjected to circular dichroism spectroscopic studies. The CD spectrum of a protein is a sum of the protein secondary structural elements of the specific protein, and can be used as an indicator of its structural integrity. The CD spectra of mutant proteins were measured along with that of the wild type *Ascaris suum* malic enzyme. Spectra are shown in Figure 22. All spectra are superimposable within error with that of the wild type enzyme. Therefore, the global structures of the mutant proteins have not been changed by the mutations, and the decrease in activity is thus likely caused by changes at the active site.

3.5.2. Kinetic Parameters of K199 Mutants

Figure 22. **Circular Dichroism Spectra of Mutant Enzymes. The Y axis is ellipticity, while the X axis is wavelength. Measurements were performed with 50 μg protein in KH_2PO_4, pH 7. Data at wavelengths lower than 200 nm were not used as a result of low signal to noise at the high dynode voltages observed.**

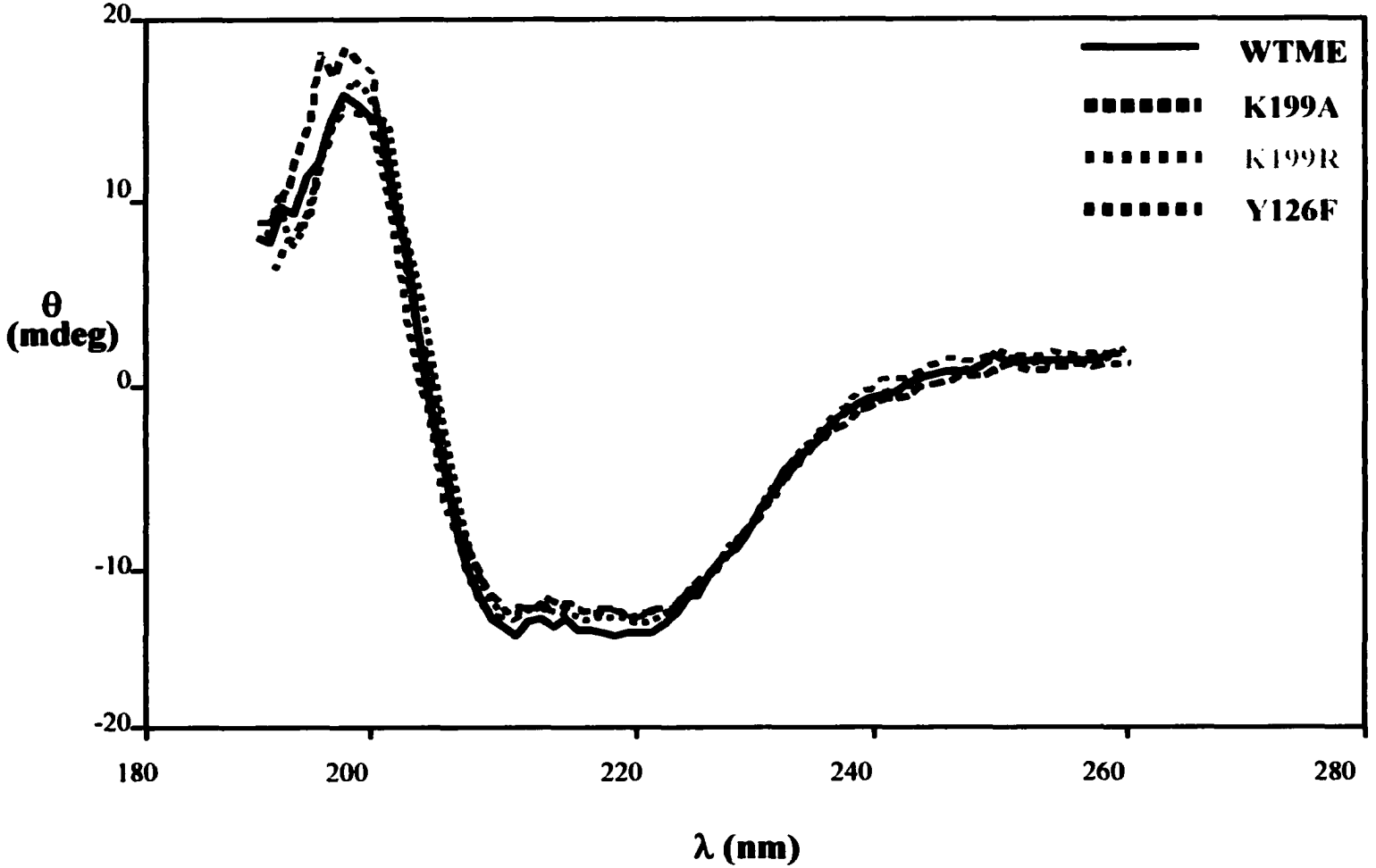
20
10
0
-10
-20
θ
(mdeg)
180
200
220
240
260
280
λ (nm)
WTME
K199A
K199R
Y126F

Lysine199 is the only totally conserved lysine residue in the malic enzyme sequence, Figure 11. In previous studies, the general acid was shown to have a pK of 8.9 based on the pH dependence of kinetic parameters (Kiick et al. 1986). The crystal structures of the human and *Ascaris* mitochondrial NAD-malic enzyme indicate that K199 is in the active site, and in a position to be a candidate for the general acid catalyst.

Lysine199 was replaced with alanine, arginine, aspartate, histidine, and asparagine. Mutant proteins were expressed and purified as discussed above. Among the mutants made, only K199H was unstable and was not isolated. Initial velocity studies were performed on the remainder of the mutant enzymes. Figure 23 shows an example of initial velocity data measured for K199R. Kinetic data for the K199 mutant enzymes are summarized in Table 5, along with those of the wild type enzyme.

Elimination of the ε-amine of K199 resulted in a dramatic decrease in malic enzyme activity. The turnover number of K199A is decreased 1.3 x 10^5 fold compared to the wild type enzyme, while K_{malate} increases 7-fold, and K_{NAD} is unchanged. Replacing the lysine with arginine results in a decrease of only 10-fold in k_{cat}, so that R can largely replace K functionally. The K199E and K199Q mutant

Figure 23. **Initial Velocity Pattern Obtained for K199R. The initial rates were measured at different NAD^+ and L-malate concentrations, as shown, while Mg^{2+} was maintained saturating. Points represent the initial rates measured, while the lines are theoretical based on a fit of equation 3 to the data.**

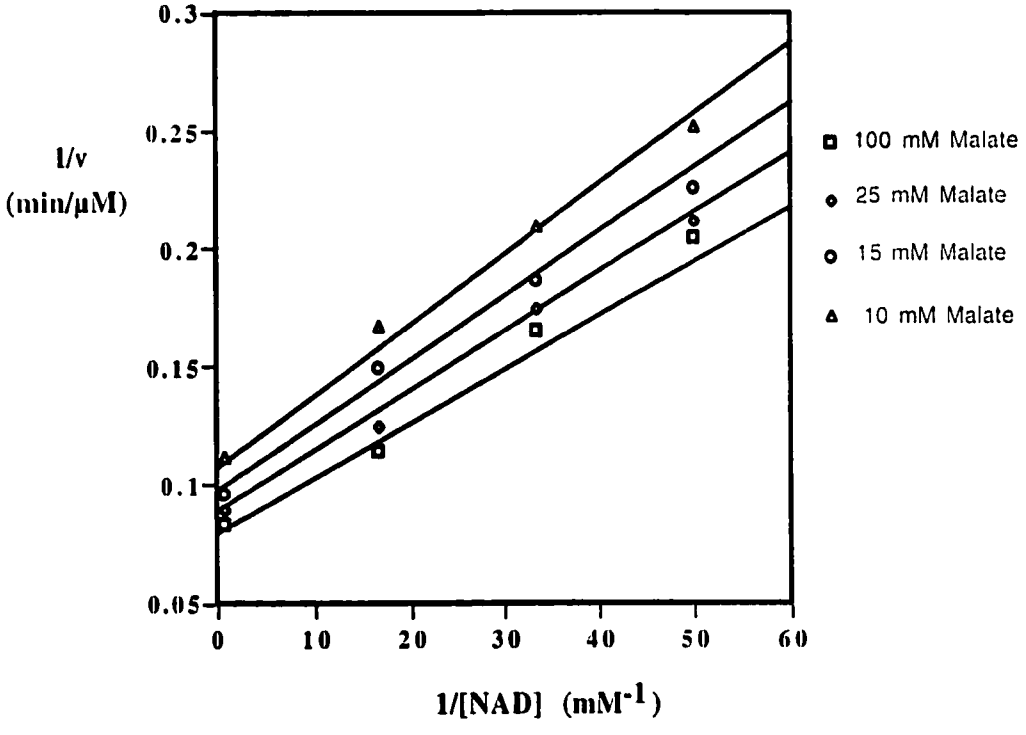
0.3
0.25
0.2
0.15
0.1
0.05
1/v
(min/µM)
0
10
20
30
40
50
60
1/[NAD] (mM-1)
100 mM Malate
25 mM Malate
15 mM Malate
10 mM Malate

Table 5. Kinetic Parameters Obtained for the K199 Mutant Enzymes

	V/E_t (s^{-1})	K_{malate} (mM)	K_{NAD} (mM)	K_{Mg} (mM)	$V/K_{malate}E_t$ ($M^{-1}s^{-1}$)	$V/K_{NAD}E_t$ ($M^{-1}s^{-1}$)	$V/K_{Mg}E_t$ ($M^{-1}s^{-1}$)
WT	36 ± 1	0.73 ± 0.07	0.025 ± 0.004	11 ± 4	(4.9 ± 0.5) x 10^4	(1.4 ± 0.2)x 10^6	(3 ± 1) x 10^3
K199A	(2.7 ± 0.4) x 10^{-4} (1.3 x 10^5)[a]	3 ± 1 (4)	0.034 ± 0.003 (-)	80 ± 30 (7)	0.08 ± 0.03 (6 x 10^5)	8 ± 1 (1.8x 10^5)	0.04 ± 0.01 (9.4x 10^4)
K199R	3.5 ± 0.1 (10)	3.8 ± 0.4 (5)	0.032 ± 0.003 (-)	60 ± 20 (5)	900 ± 100 (53)	(1.0 ± 0.1) x 10^5 (14)	60 ± 20 (50)
K199E	(3.7 ± 0.2) x 10^{-3} (10^4)	0.27 ± 0.08 (3)	1.4 ± 0.2 (55)	N.D.[b]	14 ± 4 (3.5 x 10^3)	2.7 ± 0.4 (5 x 10^5)	N.D.
K199Q	(9 ± 2) x10^{-4} (4 x 10^5)	5 ± 2 (7)	0.020 ± 0.001 (-)	800 ± 300 (76)	0.18 ± 0.08 (3 x 10^5)	40 ± 10 (3.5 x 10^4)	(1.1 ± 0.5) x 10^{-3} (3 x 10^6)

[a]Values in parentheses are folds changed from the same parameters of the wild type enzyme.

[b]N.D. stands for Not Determined.

enzymes have turnover numbers slightly higher than that of K199A mutant, indicating that if K199 is the general acid, it likely also has other functions, given the lack of significant general acid behavior expected for Q and E. On the other hand, K199E gives a 40-fold increase in K_{NAD}, and K199Q increases the Michaelis constants for Mg^{2+} and L-malate by a factor of 76.

3.5.3. Kinetic Parameters of Y126

Tyrosine126 is highly conserved, with only one of the 26 malic enzyme sequences exhibiting a replacement by serine, Figure 11. Tyrosine 126 is also found in the active site area and in proximity to K199. Thus, Y126 has been mutated to a number of other residues, including F, E, W, R, and H. All of the Y126 mutants have been expressed and purified.

Initial velocity data are summarized in Table 6. Elimination of the hydroxyl group of Y126, by substituting with F gives a significant decrease in activity, 1500-fold, but not as large a change as observed for K199A. All of the other mutations, Y126E, Y126W, Y126R, and Y126H, gave enzymes with lower activity than Y126F. The Y126E and Y126R mutant enzymes decreased the turnover number from that of wild type by 3.1×10^4 and 2.2×10^5 fold respectively, whereas K_{malate} increased by 15-

Table 6. Kinetic Parameters Obtained for the Y126 Mutant Enzymes

	V/E_t (s^{-1})	K_{malate} (mM)	K_{NAD} (mM)	K_{Mg} (mM)	$V_{max}/ K_{malate} E_t$ ($M^{-1} s^{-1}$)	$V_{max}/ K_{NAD} E_t$ ($M^{-1} s^{-1}$)	$V_{max}/ K_{Mg} E_t$ ($M^{-1} s^{-1}$)
WT	36 ± 1	0.73 ± 0.07	0.025 ± 0.004	11 ± 4	(4.9 ± 0.5) x 10^4	(1.4 ± 0.2) x 10^6	(3 ± 1) x 10^3
Y126F	0.023 ± 0.001 (1.5 x 10^3)[a]	5.1 ± 0.9 (7)	0.09 ± 0.02 (3.6)	21 ± 8 (2)	4.5 ± 0.8 (1.1 x 10^4)	260 ± 60 (5.4 x 10^3)	1.1 ± 0.4 (3 x 10^3)
Y126E	(1.2 0 ± 0.02) x 10^{-3} (3.1 x 10^4)	10.4 ± 0.7 (15)	0.038 ± 0.002 (-)	9.3 ± 0.2 (-)	0.110 ± 0.008 (4.4 x 10^5)	31 ± 2 (4.5 x 10^4)	0.130 ± 0.004 (2.5 x 10^4)
Y126W	(2.30 ± 0.02) x 10^{-4} (1.6 x 10^5)	1.9 ± 0.4 (3)	0.047 ± 0.004 (2)	160 ± 50 (14)	0.12 ± 0.02 (4.0 x 10^5)	4.8 ± 0.4 (2.9 x 10^5)	(1.4 ± 0.4) x 10^{-3} (2.4 x 10^6)
Y126R	(1.6 ± 0.1) x 10^{-4} (2.2 x 10^5)	12 ± 2 (16)	0.055 ± 0.003 (2)	58 ± 3 (5)	(1.3 ± 0.2) x 10^{-2} (3.8 x 10^6)	2.9 ± 0.2 (4.8 x 10^5)	(2.8 ± 0.2) x 10^{-3} (1.2 x 10^6)

[a] Values in the parentheses are fold changes of the kinetic parameters compared to those of the wild type enzyme.

and 16-fold, respectively. The Y126W mutant enzyme gave a decrease in the turnover number by 1.6 x 10^5 fold, while kinetic parameters for Y126H were not defined.

As to the Michaelis constant for Mg^{2+}, Y126F, Y126R, and Y126W increased the K_{Mg} by 2-, 5-, and 14-fold, respectively, while Y126E gives only a slight change. On the other hand, none of the Y126 mutants exhibited a significant effect on the Michaelis constant for NAD^+.

3.5.4. pH profiles of K199R and Y126F

A general acid/base mechanism for the *Asscaris suum* malic enzyme reaction was proposed previously based on pH studies (Kiick et al., 1986). The pKs of the general acid and base were defined as 9 and 5, respectively (Fig. 24). The pH studies on the mutant enzymes provide information on their role as catalytic groups in the malic enzyme reaction. Of the mutant enzymes made, K199R and Y126F retained the most activity. Therefore, pH studies were carried out with K199R and Y126F, and pH profiles are shown in Figures 25 and 26.

The pH dependence of V and V/K_{malate} for wild type AsME is shown in Figure 24 (reproduced from the data of Kiick et al., 1986). The V is pH independent over

Figurre 24. pH Dependence of the Kinetic Parameters for Wild Type AsME (Kiick et al., 1986).

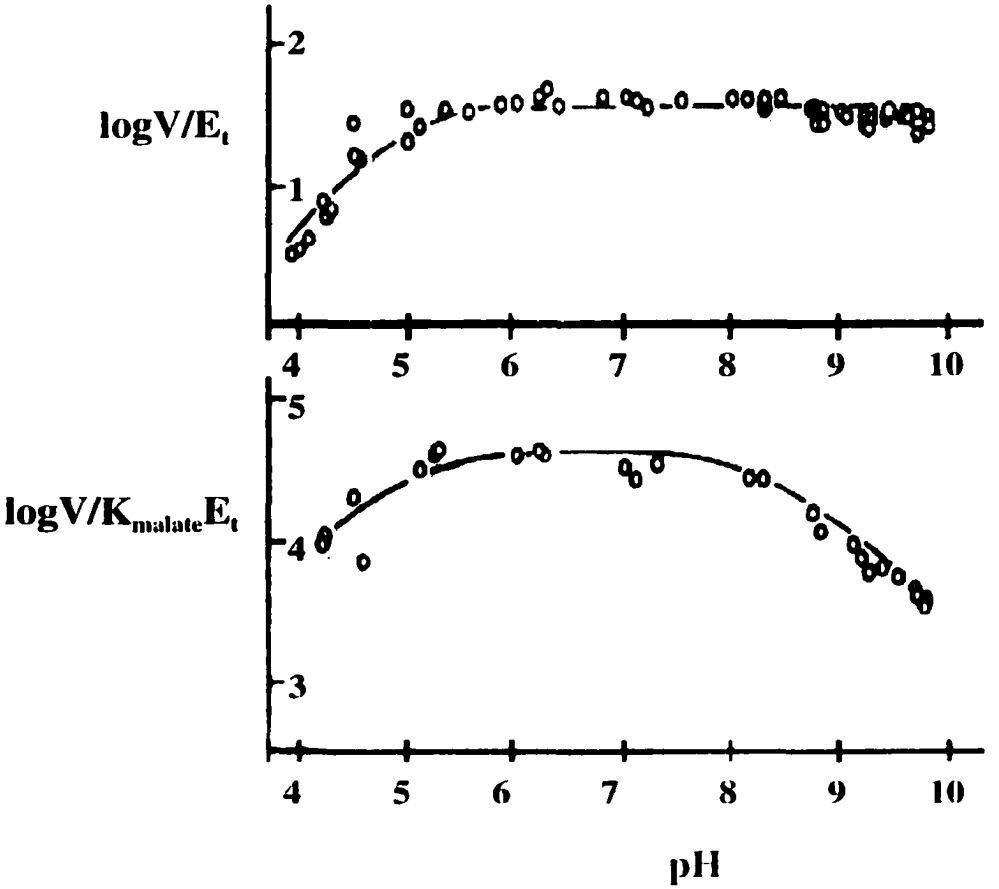
logV/E$_t$
2
1
4
5
6
7
8
9
10
logV/K$_{malate}$E$_t$
5
4
3
4
5
6
7
8
9
10
pH

Figure 25. pH Dependence Kinetic Parameters for K199R. Rates were measured at saturating concentrations of NAD^+ (2 mM) and Mg^{2+} (100 mM). The malate concentration varied from 0.5 to 50 mM. The concentration of K199R is 53 nM. Points are the experimental values, while curves are theoretical based on a fit of the data for V to equation 4, and for V/K_{malate} to equations 5 and 6.

logV/K$_{malate}$E$_t$
logV/E$_t$
pH
4
5
6
7
8
9
10
2
2.5
3
3.5
4
0.1
0.3
0.5
0.7
0.9

Figure 26. pH Dependence of Kinetic Parameters for Y126F. Rates were measured at saturating concentrations of NAD^+ (2 mM) and Mg^{2+} (100 mM). The malate concentration varied from 0.5 mM to 50 mM. The concentration of Y126F is 2.1 μM. Points are experimental, while curves are theoretical based on a fit of the data for V to equation 4, and for V/K_{malate} to equation 5.

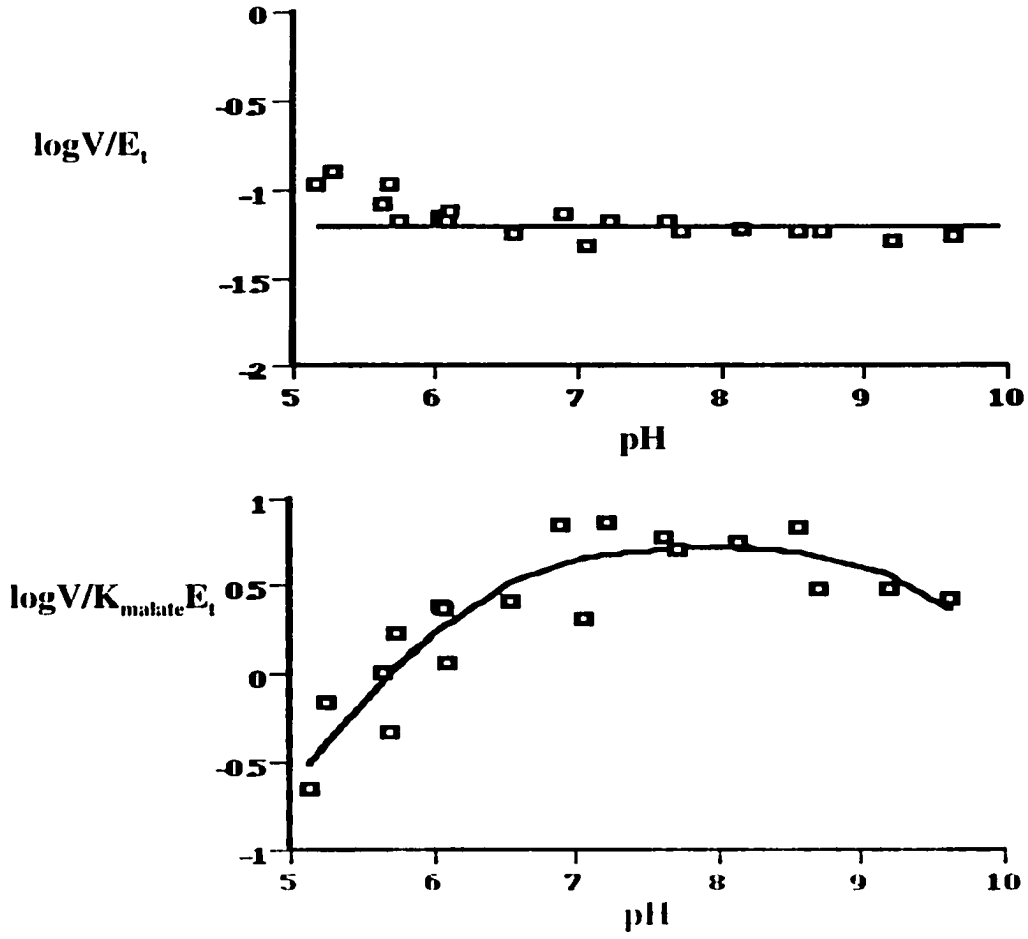
0
-05
-1
-15
-2
logV/E$_t$
5
6
7
8
9
10
pH
1
05
0
-05
-1
logV/K$_{malate}$E$_t$
5
6
7
8
9
10
pH

the range of 4-10 with a constant value of 36 s^{-1}, and decreases below a pK of 4.7, while the V/K_{malate} profile decreases at low pH with a limiting slope of 2, and at high pH, with a limiting slope of –1. The curve for V/K_{malate} has been corrected for a pK of 4.7, attributed to the β-carboxyl of malate (Kiick et al., 1986). pK values of 4.7 ± 0.3 and 9.0 ± 0.2 are obtained at low and high pH, respectively, reflecting a general base (4.7) and general acid (9). The V/K_{malate} has a pH independent value of 4.9 x 10^4 M^{-1} s^{-1} between pH 6 and 8.

In the case of K199R, Figure 25, the pH dependence of the V is very similar to that of wild type AsME; the V is pH independent in the pH range of 6.5-10 with a constant value of 3.5 s^{-1} and decreases at lower pH giving a pK of 4.9. The V/K_{malate} is pH dependent and exhibits complex behavior. The V/K_{malate} profile decreases at low pH with a limiting slope of 2, and gives two identical pKs. After subtracting the effect of the β-carboxyl of malate as for wild type enzyme, a pK of 5.3 ± 0.4 is obtained similar to that of WT AsME. As the pH increases, V/K_{malate} attains a maximum value of about 4 x 10^3 M^{-1} s^{-1}, and then decreases giving a pK of 6.3 ± 0.3, reaching a new pH independent value of 355 M^{-1} s^{-1} as the pH increases above 7, giving a pK of 7.1 ± 0.3 for the parameter leveling off at a new constant value. The partial change at high pH will be interpreted in the Discussion.

In the case of Y126F Fig. 26, V is pH independent over the range of 5-10 with a constant value of 0.023 s^{-1}, while the V/K_{malate} profile is pH dependent with limiting slopes of 1 and −1 at low pH and high pH, respectively. Estimated pK values are 6.3 ± 0.4 and 9.3 ± 0.3, respectively. Even though the pK for malate is below the pH range considered and not observed in the plot, the data at pH value lower than 7 have been corrected for the effect of a pK of 4.7. The V/K_{malate} has a constant value of 4.5 M^{-1} s^{-1} over the range of pH 7-8.5.

3.5.5. Tritium Exchange

The general acid catalyzes the final tautomerization step in the malic enzyme reaction (Fig. 8). Tritium exchange experiments were performed to obtain evidence on the identity of the general acid group. Wild type AsME, the K199A mutant enzyme, along with a variety of control proteins, including denatured K199A, denatured WT AsME, and BSA, were used in tritium exchange experiments. A negative control reaction without any protein was also carried out at the same time. The results are shown in Table 7.

The reaction was carried out for 2 hours, after which the reaction was stopped, pyruvate was reduced to lactate and isolated. The concentration of pyruvate

Table 7. Tritium Exchange Results

Reaction	Sample Volume	Total Counts	Pyruvate Concentration
ASME WT	1 ml	395,070 CPM[a]	90 mM
Control	1 ml	86,880 CPM	96 mM
K199A	1 ml	84,210 CPM	96 mM
Denatured WT	1 ml	82, 290 CPM	97 mM
Denatured K199A	1 ml	86, 400 CPM	97 mM
BSA	1 ml	87, 180 CPM	96 mM

[a] CPM stands for counts per minute.

remaining was determined, and the percentage remaining was ≥90% in every reaction. The total radioactivity, which represents the tritium exchange rate, was measured using a scintillation counter. The total radioactivity of the wild type AsME was about 5 times higher than that of the K199A mutant and any of the controls.

3.5.6. Oxalacetate Partitioning

To investigate the effects on the two rate-limiting steps, hydride transfer and decarboxylation, oxalacetate partitioning experiments were carried out using K199A, Y126F, and wild type enzymes. Oxalacetate was added to the enzyme in the presence of NADH and Mg^{2+}, and the spectrum was recorded as a function of time using a diode array spectrophotometer. An example of spectra is shown in Figure 27. The partition ratio r_H, which represents the rate ratio between the decarboxylation and reductive hydride transfer steps, was determined as discussed in Methods, and results are shown in Table 8. The partition ratio for K199A increased by a factor of 4 compared to that of the wild type enzyme, while that obtained for Y126F remained the same as that of the wild type within error.

4r-NADD was used in the oxalacetate partitioning experiments with K199A and K199R to determine the isotope effects on the partition ratio, and results

Figure 27. **Difference Spectra for Oxalacetate Partitioning Experiments. Data shown are the results measuring the absorbance from 260-400 nm every 30 seconds. A. The spectrum of the nonenzymatic control. The reaction contains all components with the exception of the enzyme. The change in A_{280} in the control reaction results from the metal ion-catalyzed decarboxylation of oxalacetate. B. Data for the AsME wild type reaction. The absorbance at 282 and 340 nm disappears depending on time. The initial rates for oxalacetate reduction and decarboxylation are calculated by substracting the nonenzymatic rates from the rates of the enzymatic reaction.**

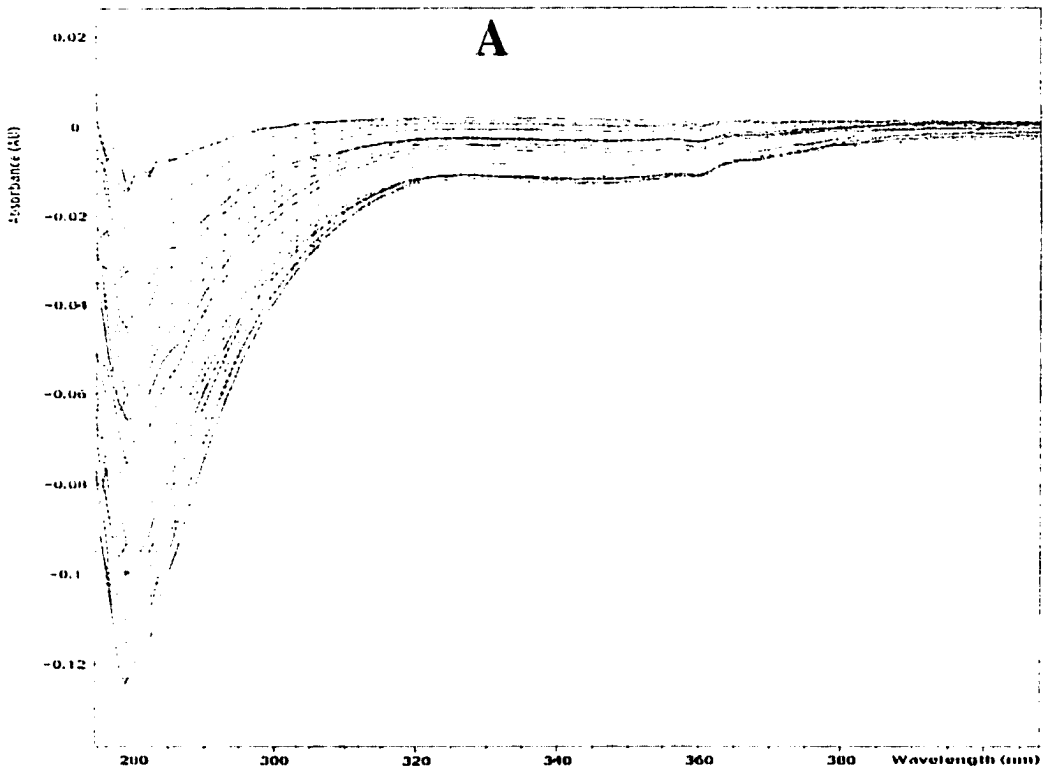
A
0.02
0
-0.02
-0.04
-0.06
-0.08
-0.1
-0.12
200
300
320
340
360
380
Wavelength (nm)

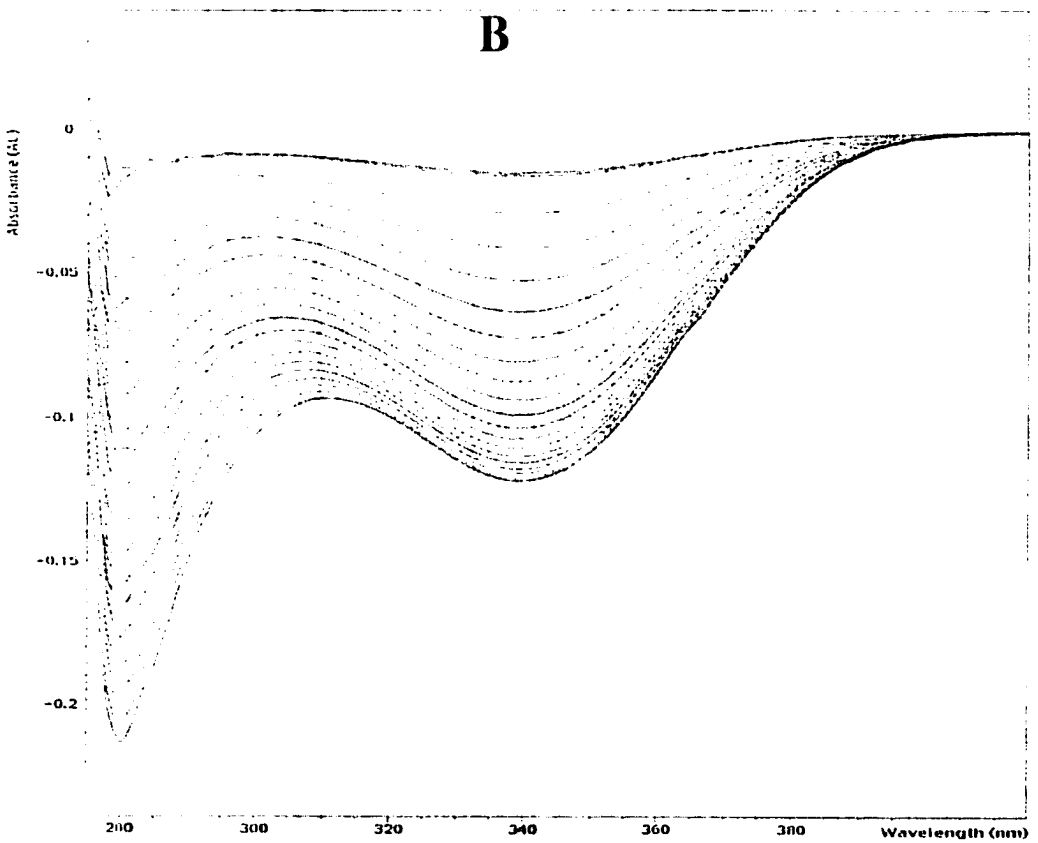
B
0
-0.05
-0.1
-0.15
-0.2
200
300
320
340
360
380
Wavelength (nm)

Table 8. Oxalacetate Partition Ratio and Primary Isotope Effects on the Partition Ratio

	r_H	r_D	r_H/r_D
Wild-type	**0.4 ± 0.1**	**1.2 ± 0.1**	**0.33 ± 0.08**
K199A	**1.6 ± 0.2**	**1.6 ± 0.4**	**1.0 ± 0.3**
Y126F	**0.30 ± 0.15**	**1.0 ± 0.2**	**0.30 ± 0.17**

Each ratio has been measured at least eight times, and the average value is shown in the table.

are also summarized in Table 8. In the oxalacetate partitioning reaction, K199A shows no isotope effects on the reductive hydride transfer step while that obtained with Y126 remains the same as that of the wild type enzymes.

3.5.7. Primary Deuterium Isotope Effects

Primary deuterium isotope effects were measured for wild type AsME as well as for the Y126F, K199A, and K199R mutant enzymes to further investigate the importance of K199 and Y126. L-Malate-2-D was used in the oxidative decarboxylation reaction, and the kinetic isotope effects were determined by direct comparison of initial rates. Figure 28 gives an example of the comparison of the double reciprocal plots for the K199R mutant enzyme using L-malate-2-H/D as reactants. The ratio of slopes and intercepts represent isotope effects on V/K and V, respectively. Data are summarized in Table 9.

In the oxidative decarboxylation reaction, $^{D}(V)$ and $^{D}(V/K_{malate})$ for Y126F are slightly larger than those obtained for the wild type enzyme. Isotope effects for the K199R mutant enzyme were measured at two pH values. $^{D}(V)$ and $^{D}(V/K_{malate})$ for both K199R and Y12F are slightly increased compared to that of wild type.

Figure 28. Primary Isotope Effect Determination for K199R at pH 8.9. Rates were determined at saturating concentrations of NAD^+ (2 mM) and Mg^{2+} (50 mM). L-Malate-2-H/D was varied from 0.1-10 mM. Points are experimental, while lines are based on a fit of the data using equation 9.

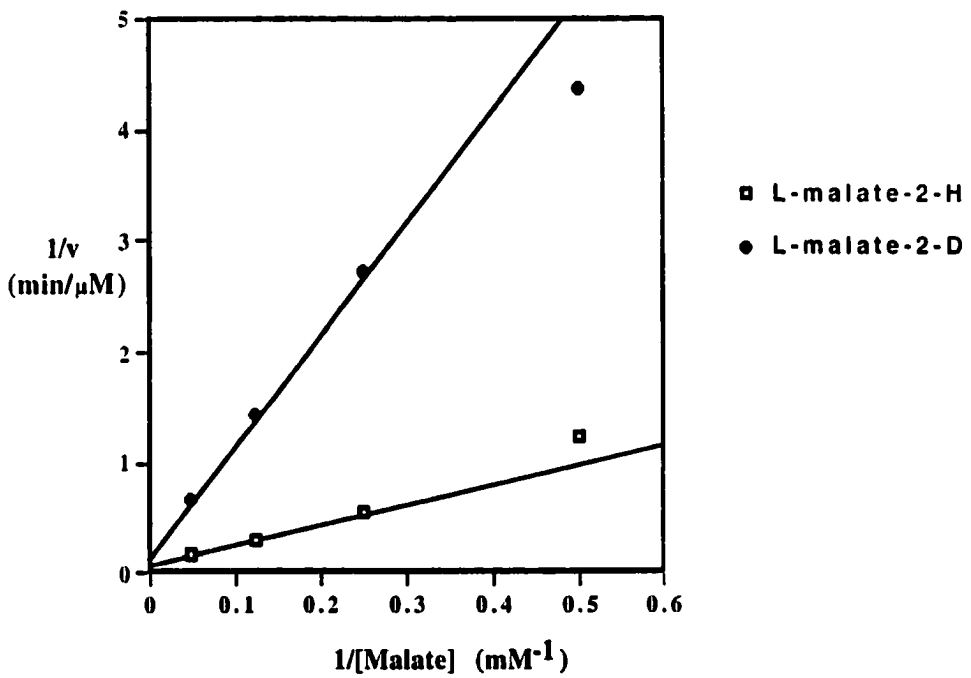
5
4
3
2
1
0
1/v
(min/μM)
0
0.1
0.2
0.3
0.4
0.5
0.6
1/[Malate] (mM-1)
L-malate-2-H
L-malate-2-D

Table 9. Primary Isotope Effects with L-Malate-2-h/d

	$^{D}(V)$	$^{D}(V/K_{malate})$
WT	**2.0 ± 0.2**	**1.6 ± 0.3**
Y126F	**2.5 ± 0.2**	**1.6 ± 0.3**
K199R (pH = 5.8)	**2.2 ± 0.2**	**2.2 ± 0.4**
K199R (pH = 8.9)	**2.3 ± 0.4**	**2.2 ± 0.5**

Each result is the average value of at least three measurements.

CHAPTER 4

DISCUSSION

4.1. Identifying Potential Functional Groups

The potential catalytic and/or binding groups in the malic enzyme reaction, particularly the possible general acid and general base groups, were identified based upon previous studies of the mechanism of the malic enzyme reaction, homology search, and the crystal structures of the human and *Ascaris suum* malic enzymes. Site-directed mutagenesis making use of alanine-scanning was then carried out on the residues selected to verify their catalytic importance.

4.1.1. Homology Search

All malic enzymes studied thus far are shown to have the same catalytic mechanism. Thus, it would not be a surprise if all malic enzymes had the same functional groups to bind reactants and facilitate catalysis. A multiple sequence alignment using the Clustal W program (Appendix I) shows that the homology among all malic enzymes is high. Moreover, functional groups that had been identified by

chemical modification in previous studies, such as a metal ion binding ligand D258 in the pigeon liver malic enzyme (Wei, et al., 1995), are highly conserved.

Based on the alignment, twelve highly conserved ionizable groups, shown in Table 3. were selected as candidates for catalytic and/or binding groups in the malic enzyme reaction. When the three-dimensional structure of malic enzyme became available (Xu et al., 1999; Yang et al., 2000; Colemen et al., 2000), the location of the residues selected was pinpointed; most of them are in the active site area (Fig. 29). Eventually, the general acid and general base catalysts, along with other important functional groups in the malic enzyme reaction were identified among those targeted based on the homology results. Homology searching mechanistically important enzyme residues is thus effective in locating potential catalytic and/or binding groups.

4.1.2. Alanine-Scanning Mutagenesis: an Overview

The targets selected based on homology search and three-dimensional structural information, were first replaced with alanine to eliminate the potential functional groups, with one exception of replacing a tyrosine with a phenylalanine.

Making and subcloning of site-directed mutations have been verified using agarose gel electrophoresis and DNA sequencing. The mutant proteins have been

Figure 29. Locations of the Mutated Residues. The active sites are indicated with *. The bound NAD^+ is in red stick-and-ball form. The mutated residues involved in NAD^+ binding, including E440 and D361, are in yellow space filling form. The mutated residues involved in malate and metal ion binding, including D178, Y126, K199, E271, D272, D294, and D295, are in green space filling form. The residues proposed to be involved in fumarate binding, including R105, R142, and K143, are in blue space filling form. The mutated residues involved in fumarate binding, directly or indirectly, including E58, E107, and D231, are in cyan space filling form.

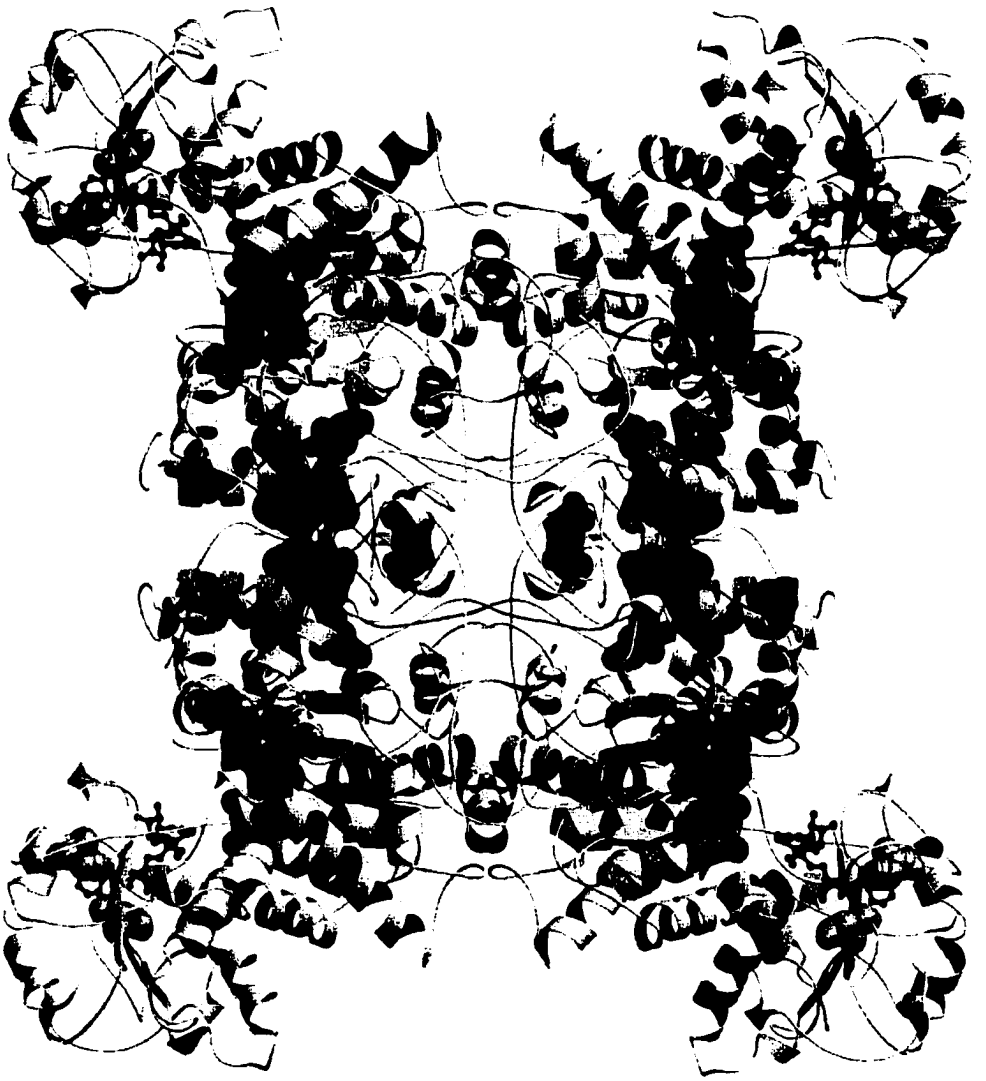

expressed and purified efficiently using a His-tagged system, along with a DEAE ion-exchange chromatography on HPLC. The pure mutant malic enzymes (purity ≥ 95%) were obtained in amounts sufficient to carry out the proposed studies.

Kinetic data for alanine mutants of conserved glutamates are shown in Table 4, and kinetic data for K199A and Y126F are shown in Tables 5 and 6, respectively. Six aspartate residues were studied by others in the lab, and are thus not included in this dissertation (Karsten et al., 1999).

Kinetic data for only the E58A and E440A mutant enzymes were obtained and are summarized in Table 4. The turnover numbers of the E58A and E440A mutant enzymes decrease 75-fold and 590-fold, respectively, compared to the wild type enzyme. The decreases are not as significant as expected for a crucial catalytic group, e.g. the general acid or general base. Neither E58 nor E440 is thus likely to be the general acid or general base, but they do contribute to overall catalysis in some less significant manner.

The K_{malate} and K_{Mg} of the E440A mutant enzyme remain the same as that of the wild type AsME, while K_{NAD} increases by 6-fold. Therefore, the E440 likely contributes to binding NAD^+. The three-dimensional structure of AsME shows that E440 is indeed in the NAD^+ binding site area but not in hydrogen-bonding distance

with NAD^+. So E440 likely contributes to NAD^+ binding as a second-sphere group, that helps maintain the structure of the NAD^+ binding site.

The K_{Mg} for the E58A mutant enzyme remains the same as that of the wild type enzyme, while its K_{malate} and K_{NAD} increase by 13- and 5-fold, respectively. However, the position of E58 is nowhere near the active site but at the tetramer interface of malic enzyme and the effect of its mutation is thus likely general. The mutation could also reflect a decrease in the stablility of the tetrameric form of AsME. Studies of this aspect will be carried out in the future.

As discussed in Chapter 1, fumarate is an allosteric regulator of AsME: it activates the AsME at low concentrations while it inhibits the enzyme at high concentrations. A fumarate binding site area, including arginine 97, 128 and 129, was proposed in human NAD-malic enzyme (Yang et al., 2000). According to the three-dimensional-structure of the *Ascaris* malic enzyme, E107 is not in the active site area but in the vicinity of the area that is equivalent to the putative fumarate binding site in the human NAD-malic enzyme, and it is also close to the tetrameric interface (Fig. 29). However, studies of E107A were discontinued, since it appeared not to be totally conserved in an update of the alignment soon after the project had begun. The characterization of the E271A mutant enzyme was also not carried out

since it appeared to be poorly expressed. In the AsME structure, E271 is in the active site area and may contribute to the substrate binding. The reason for its instability is not clear at this point, but it is now in the process of being studied further.

Elimination of the functional groups at positions 126 (Y) and 199 (K) cause a significant decrease in the enzyme activity (Tables 5 and 6). Compared to the wild type enzyme, the turnover numbers of the K199A and Y126F mutant enzymes are decreased about 10^5- and 10^3-fold, respectively. Thus, K199 and Y126 are candidates for the general acid catalyst. Moreover, three-dimensional structure of malic enzyme reveals that Y126 and K199 could be in a position to donate a proton to C3 of L-malate (Yang et al., 2000), although K199 is the best candidate of the two.

4.2. Circular Dichroism Spectroscopy: A Measurement of Global Structural Integrity

The circular dichroism spectrum of each mutant enzyme purified was determined. The CD spectrum represents a sum of the secondary structural components of the protein, and thus reflects the structural integrity of the mutant proteins. Figure 22 shows the spectra of some important mutant enzymes along with that of the wild type enzyme. There is little difference between all of the spectra,

indicating that the global structure of the mutant enzymes is intact. Therefore, the change in activity of mutant enzymes is not due to the loss of structural integrity, but reflects changes within the active site. Catalytic groups usually participate in local conformational changes during the process of substrate binding and catalysis, and it is therefore reasonable to assume that changes in these groups will likely be tolerated structurally.

4.3. K199 Mutants

Since K199 was a major candidate for the general acid based on the alanine-scanning data, other mutations including K199R, K199H, K199E, and K199Q were made to determine their effect on activity and reactant binding. The K199H mutant enzyme was poorly expressed and could not be purified, while the others were well expressed and purified to near homogeneity.

4.3.1. Kinetic Data of K199 Mutant Enzymes

Kinetic data for the K199 mutant enzymes are consistent with the idea that K199 may serve as the general acid in the malic enzyme reaction. First, the K199A mutant enzyme, which eliminated the possible general acid functional group, suffers a

severe decrease in activity. The turnover number of the K199A mutant enzyme decreases 1.3 x 10^5-fold, and V/K_{malate} decreases 6 x 10^5-fold, compared to that of the WT AsME. Replacing lysine with arginine gives only about 10-fold decrease in k_{cat}, or in another way of looking at the data, replacing alanine with arginine gives a 10^4-fold recovery of activity. This behavior is expected if K199 is the general acid catalyst in the malic enzyme reaction, since the arginine can serve in the same capacity as lysine as a general acid. On the other hand, the turnover number of the K199E mutant enzyme is just 10-fold higher than that of the K199A mutant enzyme, while the K199Q mutation improves the turnover number by only a factor of 3. In both cases, the side chains are shorter than that of lysine and should easily be accommodated in the site. However, their potential interactions with substrates will be affected because of the decreased chain length. In addition, the glutamine side chain can only donate a hydrogen bond to malate, but cannot act as a general acid. A protonated γ-carboxyl group of glutamate is capable of being a proton donor to facilitate tautomerization, but its proton affinity is much lower than that of lysine, and it also will not function well to donate a proton.

Based on previous studies, the protonated general acid catalyst contributes to malate binding (Park et al., 1984). Elimination of the ε-amino group by replacing

lysine with alanine caused a 4-fold increase in K_{malate}, suggesting that the protonated amino group is not the main determinant in malate binding, but may contribute as much as 0.8 kcal/mol in binding energy. One might expect that the K199R mutant would have WT affinity for malate. At the pH optimum for the mutant, K_{malate} is identical to that obtained for the wild type enzyme. (The pH-rate profiles for the K199R mutant enzyme will be discussed below.) Replacing K199 with Q results in a 7-fold increase in K_{malate}, and thus, the positive charge of K199 may be contribute to maintaining the correct conformation of bound malate. The K199E mutant enzyme introduces an opposite charge at the 199 position, and surprisingly decreases K_{malate} by 3-fold. The explanation could be that the negative charge causes a change in the active site, as a result of hydrogen-bonding with other residues in its vicinity, such as D294. This may result in a slightly more effective binding of malate but with a geometry that is not favored for catalysis. The above explanation is supported by the fact that the K199E mutant enzyme is the only one that causes an increase in K_{NAD}. Based on the structure, the NAD^+ binding site is away from K199; NAD^+ binding would thus only be affected by the changes in the overall active site.

The metal ion is surrounded by a cluster of negative charges, including E271, D272, D294, and D295 (Fig 9). Lysine 199 is close to this cluster, and it might play a

role in stabilizing the negative charge and maintaining the correct conformation to bind the metal ion. The K199A mutant enzyme exhibits a 7-fold increase in K_{Mg}, suggesting a possible second-sphere effect on Mg^{2+} binding, likely a result of maintaining an optimum active site structure (see 4.3.3. below). In agreement with this hypothesis, K_{Mg} also increases by about 5-fold for the K199R mutant enzyme. The increase in this case likely reflects the bulkier guanidino side chain of R compared to the ε-amino group of K. Replacing the lysine with a neutral Q gives a 76-fold increase in the K_{Mg}, again indicating the importance of a positive charge at this position in maintaining active site structure. The smaller change in K_{Mg} observed for the K199A mutant enzyme may result from an increased flexibility in the active site, recruiting other residues nearby to compensate for the loss in charge.

4.3.2. pH Profile of K199R

The K199R mutant enzyme is the most active among all K199 mutant enzymes prepared. Thus, the pH dependence of the kinetic parameters for the K199R mutant enzyme was determined and compared to that of the wild type enzyme. As a point of reference, the proposed mechanism is provided in Figure 8 (Kiick et al., 1986). The pH dependence of V for the K199R mutant is identical to that of the WT

enzyme, and reflects the binding of L-malate to the correctly protonated form of the enzyme, that is with the general base unprotonated and the general acid protonated, but with a pH dependent conformational change of the E:NAD complex that gives a pK of 5 (Park et al., 1989; Rajapaksa et al., 1993). The pH dependent conformational change in the E:NAD complex is not shown in Figure 8 since we begin with all reactants bound. The V/K_{malate} profile of the WT enzyme gives a pK of 9 for the general acid that protonates C3 of enolpyruvate to give pyruvate, and a pK of 4.7 for the general base that accepts the hydroxyl proton of malate in the hydride transfer step. The V/K_{malate} profile of the K199R mutant enzyme also shows a pK of 5.3 for the general base, which is virtually the same as that of the wild type enzyme within error. This fact indicates the general base catalyst in the mutant enzyme is intact, and thus, eliminates the possibility that K199 is the general base. On the other hand, V/K_{malate} is pH independent over the range of 7-10, as expected if R now functions as the general acid. The newly introduced arginine provides a functional group with a pK higher than that of the original lysine, and the pK of the general acid is higher and out of the accessible range of this pH study. In other words, the pK of the general acid for the K199R mutant enzyme is higher than 10 and cannot be observed. This

predicted change, along with the results from tritium exchange experiments, provide good evidence that K199 is the general acid catalyst in the malic enzyme reaction.

However, a glimpse at the pH-rate profile for K199R (Fig.25), shows some unexpected changes in the V/K_{malate} profile for the K199R mutant enzyme over the pH range 6-7. Note that the $\log V/K_{malate}$ decreases with a limiting slope of one and comes to a constant value at higher pH. This partial activity loss indicates that another ionizable residue in the K199R mutant enzyme is also important in its protonated form for optimum binding of malate. The same residue is not as important in the wild type enzyme since its ionization is not observed. The V/K_{malate} profile gives a pK of 6.3 for this group in the E:NAD:Mg enzyme form and a pK of 7.1 in the E:NAD:Mg:malate complex. Based on the observed pK values and the active site structure, the new enzymic group is suggestive of a carboxyl group. In the active site, there is a cluster of four carboxyl groups in the malate and metal ion binding sites. Two of them, E271 and D294 are very close to K199; the side chain of K199 is 3.4 Å and 2.4 Å away from that of E271 and D294, respectively. When the lysine is replaced with arginine, the slightly larger guadininium group could closely approach one of the carboxyl groups and cause it to move closer to the β-carboxylate of malate. Thus, the carboxyl group would be required protonated to maintain the competent

conformation of bound malate. Glutamate 271 directly interacts with both malate and metal ion, based on the human enzyme tartronate structure, and any effect on E271 would be expected to result in significant decrease in k_{cat}. Since the V pH-rate profile of the K199R mutant enzyme is identical to that of the WT enzyme, and the turnover number is only decreased by a factor of 10, E271 is unlikely to be the residue observed. On the other hand, D294 is closer to K199 than E271, and it does not directly interact with either malate or metal ion, Figure 10. Thus, D294 is likely the new group that is observed in the pH dependence of V/K_{malate} for the K199R mutant enzyme and is required protonated for optimum binding of malate.

The rate equation for a bell-shape pH profile is given in equation 4: $LogY = logC/(1 + H/K_1 + K_2/H)$, where Y is the value of V/K observed at any pH, C is the pH independent value of Y, and K_1 and K_2 are the acid dissociation constants for the general base (pK = 5) and general acid (pK = 9), respectively. In the case of the K199 mutant enzyme, the bell-shape profile has a partial change superimposed on it that exhibites a decrease in the value of the parameter as the pH is increased above 6. Based on the two pH dependencies, the rate equation for the pH dependence of V/K_{malate} is thus given by equation 9:

$$\log Y = \log[Y_L + (Y_H)(K_3/H)]/(1 + K_3/H)(1 + H/K_1 + K_2/H) \qquad (9)$$

where Y, K_1 and K_2 have the same meaning as above, while Y_L is the low pH independent value of V/K, Y_H is the high pH independent value of V/K and K_3 is the pK for the group that affects the binding of malate. (From a thermodynamic analysis of the pH dependence of malate binding on the protonation state of the group with pK_3, it follows that the acid dissociation constant of the group on enzyme, when malate is bound, is obtained from $Y_H K_3/H$.). Since the pK for arginine, the general acid, is not observed in Figure 25, equation 9 reduce to:

$$\log Y = \log[Y_L + (Y_H)(K_3/H)]/(1 + K_3/H)(1 + H/K_1) \qquad (10)$$

It is informative to determine the limits of equation 10, as applied to Figure 25, and they are given below:

$H > K_1, K_3 \qquad Y = Y_L K_1/H$

$K_1 > H > K_3 \qquad Y = Y_L$

$K_1, K_3 > H \qquad Y = Y_H$

Thus, at low pH, V/K will decrease by a factor of 10 per pH unit as observed in Figure 25. As the pH increases, such that H^+ is lower compared to K_1, but still higher than K_3, the V/K value reaches a maximum value, while the value decreases to a constant value at high pH.

One might ask why there is a decrease in V at all since R is a proton donor over an even broader pH range than K. There are two possibilities. First, for proton transfer reaction, the rate will be optimum when there is a thermodynamic match between the proton affinities of the donor and acceptor. However, in order that net proton transfer occurs to pyruvate from the general acid, the proton affinity of pyruvate (proton acceptor) should be somewhat greater than that of K199 (proton donor). When the proton affinity of the donor is increased by 2 orders of magnitude, the driving force for protonation of pyruvate is not as high. The rate of protonation and thus the overall rate of the malic enzyme reaction will decrease as the protonation step begins to limit. Although this phenomenon will occur, it is unlikely it contributes substantially to the observed decrease in rate since the primary deuterium isotope effect indicates hydride transfer still limits significantly. Tritium exchange and solvent deuterium isotope effect experiments will be carried out to see if the increased pK of R has had an effect on the rate limitation of the tautomerization step. A second and more likely possibility in this case is that the presence of the side-chain guanidinium causes a change in geometry of the bound reactants in the site and as a result gives a decrease in the rates of a number of steps along the reaction pathway.

Attempts to determine the 3D-structure of the K199R mutant enzyme are currently in progress.

4.3.3. Kinetic Mechanism for the K199R Mutant Enzyme

The partition ratio for the oxalacetate intermediate (Table 8) increases in favor of pyruvate by a factor of 4 for the K199A mutant enzyme compared to the WT enzyme. that is decarboxylation is favored with respect to reverse hydride transfer. This result is unexpected for a change in the general acid, which should decrease the decarboxylation of oxalacetate and tautomerization of enolpyruvate to give pyruvate. It is very likely that K199 donates a hydrogen bond to the 4-carboxyl of malate and thus contributes to its binding affinity. The proposed interaction with malate would place positive charge in the vicinity of the β-carboxyl, and this would certainly hinder decarboxylation. The latter hydrogen-bonding scheme is observed in the 6-phosphogluconate dehydrogenase reaction with the general acid (E190) hydrogen-bonded to the 1-carboxyl of 6PG in the E:NADP:6PG complex (Adams et al., 1994). The hydrogen bond has been eliminated in the E:NADPH:3-keto-6PG complex (Adams et al., 1994), thus favoring decarboxylation. The same may be true in the case of the malic enzyme reaction, and this is corroborated by the recent structure of

the E:NAD:Mn:tartronate complex of the human mitochondrial enzyme, which shows K183 (homologous to K199 of the *Ascaris* enzyme) within hydrogen-bonding distance (3.3 Å) to an oxygen of tartronate that would be equivalent to C3 of malate (Yang et al., 2000). The lack of a deuterium isotope effect on the reduction of oxalacetate suggests that the hydride transfer step no longer limits the overall rate. Rather, a step after hydride transfer, probably an isomerization of the E:NAD:Mg:malate complex to release reactants, likely limits. The presence of such an isomerization is documented by the difference in structure of the E:NAD (Xu et al., 1999) and E:NAD:Mn:tartronate (Yang et al., 2000) complexes, respectively. That the effect of mutating K to A is more pronounced on the isomerization than on the catalytic step(s), is suggestive of a dual role of the lysine. There are a number of examples from the literature for catalytic residues that are found in the hinge region of loops that close to generate the catalytic conformation. Enzymes in this category include loops in triosephosphate isomerase [TIM (Sampson and Knowles, 1992)], the α-subunit of tryptophan synthase (Rhee et al., 1997), enolase (Reed et al., 1996), ribulose bisphosphate carboxylase (Larson et al., 1995), and *Yersenia* protein tyrosine phosphatase (Jia et al., 1995; Keng et al., 1998; Wang et al., 1998). The best-documented example is that of TIM (Sampson and Knowles, 1992), which has a

catalytic loop (residues 166-176) comprised of a 3 amino acid N-terminal hinge, a 5 amino acid hydrophobic lid, and a 3 amino acid N-terminal hinge. Sampson and Knowles (1992) originally suggested that the loop closed upon fromation of the Michaelis complex and closure is linked to orientation of active site residues and substrate functional groups, with the concomitant deprotonation of C1 of dihydroxyacetone phosphate by E165.

A similar arrangement may be true in the case of the *Ascaris* malic enzyme. Indeed, K183 (the human NAD-malic enzyme equivalent of K199) is found toward the C-terminal end of helix αB2 (Xu et al., 1999). The B-domain is comprised of two subdomains that include residues 131-277 and 467-538. The catalytic lysine is in the vicinity of the subdomain interface of the B-domain and at the juncture of the B- and C-domains. Closure of the open form to generate the catalytic conformation will be centered on the juncture of B- and C-domains. The small effect on K_{malate} may indicate a nearly equal affinity for opened and closed (catalytic) forms of the enzyme.

The primary deuterium isotope effects using L-malate-2D/H of the K199R mutant enzyme have been determined at two pH values, pH 5.8 (the maximum in the V/K_{malate} pH-rate profile) and pH 8.9 (a pH in the range where V/K_{malate} is constant at high pH). In the malic enzyme reaction, the value of $^{D}(V)$ is determined by the rate of

the chemical steps and the rate of isomerization of E:NAD, while the value of $^{D}(V/K_{malate})$ is determined by the rate of chemical steps and the off-rate of malate (Karsten and Cook, 1994).

At pH 5.8, slight increases in both $^{D}(V)$ and $^{D}(V/K_{malate})$ are observed, compared to those obtained for the wild type enzyme, and like the isotope effects with the wild type enzyme, $^{D}(V)$ equals $^{D}(V/K_{malate})$. The arginine at position 199 is not a perfect mimic for the lysine, and the overall rate of the malic enzyme reaction is decreased by a factor of 10. Thus, the primary isotope effects obtained for K199R are somewhat higher than those of the wild type enzyme. On the other hand, arginine is able to fulfill the role that the lysine plays in the hinge area. In this case, the isomerization step discussed above is not as rate-limiting as it is in the reaction catalyzed by the K199A mutant enzyme. Based on the initial velocity data, binding of malate and NAD^+ are unchanged due to the mutation. The increase in the deuterium isotope effect is thus likely caused by a decrease in the rate of the chemical step.

The $^{D}(V)$ of the K199R mutant enzyme is pH independent, indicating that, once bound, the overall rate of the malic enzyme reaction is limited by oxidative decarboxylation and isomerization of E:NAD at pH values $\geq$ 5.5. The value of

$^{D}(V/K_{malate})$ at pH 8.9 is increased by a factor of about 2 compared to its value at pH 5.8. Since V is pH independent over this pH range, it is the binding affinity for malate that is decreased by a factor of 10 as the pH is increased from 5.8 to 7. The lower affinity can be directly translated into a higher off-rate for malate, and therefore, a larger isotope effect on $^{D}(V/K_{malate})$.

Comparing the WT and mutant enzymes, an analysis of the isotope effect data can be carried out. For the wild type malic enzyme the following mechanism holds (Karsten and Cook, 1994).

$$\text{E:MA} \underset{k_6}{\overset{k_5B}{\rightleftharpoons}} \text{E:MAB} \underset{k_8}{\overset{k_7}{\rightleftharpoons}} \text{(E:MAB)} \underset{k_{10}}{\overset{k_9}{\rightleftharpoons}} \text{E:MXR} \xrightarrow{k_{11}} \qquad (12)$$

Where M is Mg^{2+}, A is NAD^+, B is malate, and X is oxalacetate. In mechanism 12, k_5 and k_6 represent binding and desorption of malate, k_7 and k_8 reflect a conformational change, k_9 and k_{10} reflect hydride transfer to NAD^+ and oxalacetate, respectively, and k_{11} reflects decarboxylation.

Isotope effect equations based on the above are:

$$^{D}V = \frac{^{D}k_9 + (k_9/k_7 + k_9/k_{11})/(1 + k_8/k_7) + {}^{D}K_{eq}(k_{10}/k_{11})}{1 + (k_9/k_7 + k_9/k_{11})/(1 + k_8/k_7) + (k_{10}/k_{11})} \quad (13)$$

$$^{D}(V/K_{malate}) = \frac{^{D}k_9 + (k_9/k_8)(1 + k_7/k_6) + {}^{D}K_{eq}(k_{10}/k_{11})}{1 + (k_9/k_8)(1 + k_7/k_6) + (k_{10}/k_{11})} \quad (14)$$

The difference in the isotope effects reflect differences in C_f $[(k_9/k_8)(1 + k_7/k_6)]$ and C_{Vf} $[(k_9/k_7 + k_9/k_{11})/(1 + k_8/k_7)]$ since all other parameters are common to both equations. Value of ^{D}V and $^{D}(V/K_{malate})$ are 2.0 and 1.6 for the wild type enzyme suggesting that C_f is slightly larger than C_{Vf}, that is the net off-rate constant for malate is greater than the net rate constant for the chemical step.

The K199R mutant enzyme has a decreased rate of about 10-fold reflected in V and V/K_{malate} at both pH 5.8 and 8.9. The slight increase in $^{D}(V/K_{malate})$ must reflect an increase in k_6 (that is, K_{malate}). Considering that a 10-fold increase in k_6 is observed based on the pH-rate profile, one would expect a significant increase in $^{D}(V/K_{malate})$ as the pH is increased from 5.8-9. The slight increase in $^{D}(V/K_{malate})$ to 2.2 at pH 9 must then reflect a decrease in the isomerization step (k_7 and k_8) prior to the hydride transfer in addition to an increase in k_6. These data are consistent with the

oxalacetate-partitioning results on the K199A mutant enzyme. Base on the(V/K_{malate}) pH-rate profile of the K199R mutant enzyme, the new group involved in the optimum binding of malate has a pK around 6. Therefore, the new group is likely a carboxyl group. If that is ture, the group will be negtively charged at pH 9, and thus capable of repulsing the negatively charged carboxyl of malate and slowing down the isomerization step.

4.4. Y126 Mutants

The tyrosine at position 126 is a highly conserved residue in all of the malic enzymes sequenced to date with one exception, Appendix I. The malic enzyme from *Amaranthus hypochondriacus* has a serine (a semiconservative substitution) in the place of the tyrosine. Tyrosine126 is at the active site and very close to K199. An equivalent pair of tyrosine and lysine is also found in isocitrate dehydrogenase (Hurley et al., 1991). Structurally, Y126, which has a pK of 10.5 in solution, could also be a catalytic group such as the general base, but its lack of conservation and data discussed below argues against this.

4.4.1. Kinetic Data of Y126 Mutant Enzymes

The decrease in activity observed when Y126 is replaced with F is significant, but not as substantial as that observed for the K199A mutant enzyme. Although the tyrosine is obviously important to the overall reaction, it is unlikely that the tyrosine serves as the general base because of the following two reasons: 1) Y126 is too far away from the position of the C2 hydroxyl [>4 Å (Yang et al., 1999)]; 2) the general base has an intrinsic pK of 5 (Kiick et al., 1986), and it is thus unlikely, given the hydrophobic nature of the active site, that the tyrosine pK could be perturbed by 5.5 pH units from its solution pK of 10.5. Moreover, the effect of replacing Y126 with F seems to spread over the whole active site area; the Michaelis constants for malate, NAD^+, and Mg increase 7-, 4-, and 2-fold, respectively. Thus, Y126 likely has some effect on the localized structure and/or environment of the malic enzyme active site. Based on the three-dimensional structure (Fig 30), the hydroxyl group of the tyrosine is involved in a hydrogen-bonding network including malate, metal ion, N478, N479, Y126, K199, E271, D272, D294, and D295 (Fig. 30). The equivalent hydrogen-bonding network was first proposed in the human NAD-malic enzyme by Yang et al. (2000). Of the above residues, only Y126 belongs to domain A (Fig. 30). In fact, Y126 is a part of a long helix, which is the only portion of domain A in the active site area. The hydroxyl group of the tyrosine likely acts as an anchor to the long helix,

Figure 30. **The Local Structure and Environment in the Active Site. Residues from domain A are red. Residues from domain B are blue. Residues from domain C are yellow. Residues involved in the hydrogen-bonding network at the acitive site are in stick-and-ball form.**

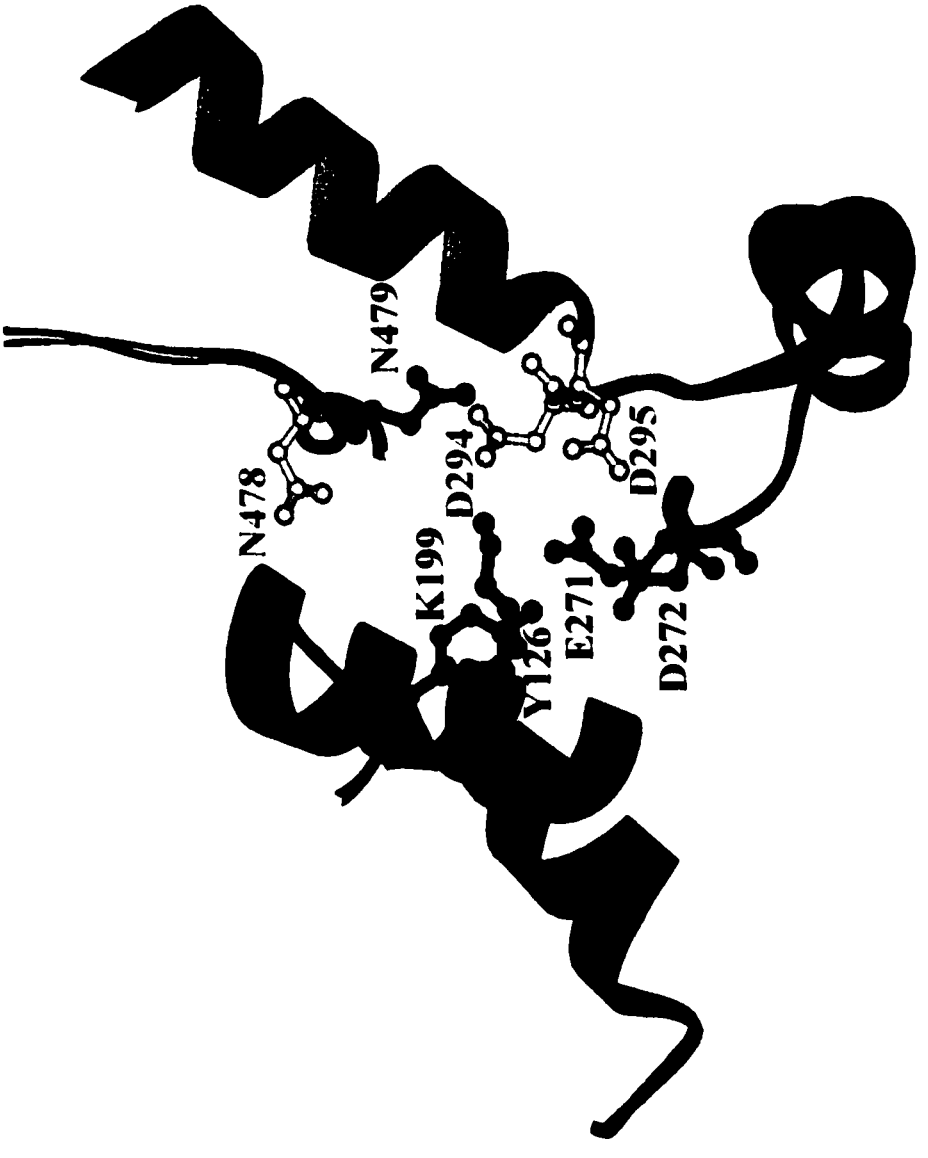
N479
N478
D294
D295
K199
Y126
E271
D272

holding it in a position between domains B and C, thus effectively burying the bound reactants deep in the active site cavity. The elimination of the tyrosine hydroxyl group likely makes the long helix loose and disrupts the overall active site conformation

Glutamate was also used to replace Y126, since its γ-carboxyl might be expected to participate in the hydrogen-bonding network as the hydroxyl group replaced. The change might be able to provide an anchor to the long helix, substituting for tyrosine. Although the Y126E mutant enzyme does maintain the binding affinity for NAD^+ and Mg, k_{cat} is decreased and K_{malate} is increased. So the aromatic ring of the tyrosine likely also plays an important role in malate binding and overall catalysis, helping to regulate active site topology.

The Y126W mutation provides an appropriate replacement for the aromatic ring of the tyrosine, and the mutant enzyme does retain some of the malate-binding affinity of the wild type enzyme. However, there is a slight increase in K_{NAD} as observed for the Y126F enzyme, likely because W cannot participate in the hydrogen-bonding network as can Y. Moreover, the bulky side chain of W may interfere with the nearby metal ion binding site. In addition, the turnover number of the Y126W mutant enzyme is lower than that of the Y126F enzyme and close to that

of the Y126E mutant enzyme. Substitution with the oppositely charged R gives the most severe effect, as might be expected since R cannot participate in the hydrogen-bonding network as can Y.

Overall, initial velocity data obtained for the Y126 mutant enzymes support the importance of both the aromatic ring and hydroxyl group of Y126 in maintaining a competent conformation of the active site of AsME.

4.4.2. pH Profile of Y126F

The Y126F mutant enzyme is the only one among the Y126 mutant enzymes purified that is active enough to perform pH studies. The kinetic parameters become undefined at pH values lower than 5 due to the dramatic increase in K_{malate}. The pH profile of the Y126F mutant enzyme was only determined over the range of pH 5-10.

The V of the Y126F mutant enzyme becomes pH independent, while that of the WT enzyme decreases below a pK of about 4.9 (Park et al., 1984). The pK observed in the pH profile of the WT enzyme reflects an ionizable group involved in the isomerization of the E:NAD complex. It is likely that the decrease in the turnover number of the Y126F mutant enzyme by 1.5 x 10^3-fold reflects a decrease in the rate

of the chemical steps, and the isomerization step is no longer rate-limiting. Thus, the pK visible in the WT profile disappears in the V profile of the Y126F mutant enzyme.

The V/K_{malate} profile of the Y126F mutant enzyme is very similar to that of the wild type, it decreases above a pK of 9.3 and below a pK of 6.3. Within error, the pK of the general acid in the Y126 enzyme is similar to that of the wild type enzyme. This rules out the possibility that Y126 could be the general acid. Otherwise, the pK of the general acid would be expected to disappear over the pH range measured. However, the Y126F mutation seems to make the pK of the general base become about a pH unit higher, likely a result of a change in the local environment around the general base group (see above).

When substrates bind to the malic enzyme active site, domains B and C move closer to each other (Yang et al., 2000). These two domains, along with the long helix from domain A, bury the substrates deep into the active site cavity and give the closed form of malic enzyme (Fig. 30). When Y126 is replaced with F, the long helix loses one of the anchors that hold it between domains C and B. Therefore, the movement of the domains B and C will result in a novel position for the long helix of domain A. The rearrangement could easily result in a tighter interaction between domains B and C and bury the general base, D295, deeper into the protein. The

increased hydrophobicity around the aspartate would result in an increased pK for its carboxyl group. Alternatively, the tighter interaction between domains B and C in the active site area could bring D295 closer to other carboxylate side chains, such as E271 or D272, resulting in an increase in the pK for the general base. Which of these possibilities is correct will have to await further study.

Nonetheless, the pH-rate data for the Y126F mutant enzyme indicate the tyrosine side chain plays an important role in maintaining an integral localized structure in the active site.

4.4.3. Kinetic Mechanism for the Y126F Mutant Enzyme

The oxalacetate partioning ratio and the isotope effect on oxalacetate reduction are identical for the WT and the Y126F mutant enzymes. Data suggest that the kinetic mechanism does not change upon mutating Y126, that is although the overall rate decreases, the relative rate of oxalacetate reduction and decarboxylation remain the same. In agreement with this suggestion, the primary deuterium isotope effects measured for the Y126F mutant enzyme and the isotope effect on the partition ratio are very similar to those obtained for the WT enzyme. These again suggest that Y126 is not the general acid in the malic enzyme reaction.

4.5. Conclusions

Overall, the following conclusions on the mechanism of the malic enzyme reaction can be drawn from the research in this dissertation: (1) Glutamate 58 likely plays a role in maintaining the subunit-subunit interface and a second-sphere role in the allosteric regulation region of AsME. (2) Glutamate 440 contributes to NAD^+ binding although it is not within hydrogen-bonding distance with the NAD^+ molecule. (3) Lysine 199 is the general acid catalyst in the malic enzyme reaction: the ε-amino group of the lysine acts as a proton donor facilitating the tautomerization step during catalysis and contributing to malate binding. (4) Lysine199 exists in a "hinge area" in the active site of AsME and is involved in an important conformational change during the catalysis. The positive charge of the lysine likely contributes to this role. (5) Tyrosine 126 plays a role in maintaining the localized structure and environment in the active site area. Both the aromatic ring and the hydroxyl of the tyrosine contribute to its role. (6) A hydrogen-bonding network, including malate, metal ion, N478, N479, Y126, K199, E271, D272, D294, and D295, plays an important role in maintaining conformation of the active site of AsME. Any change that disturbs this network can cause an effect on catalysis of the malic enzyme reaction. (7) New

group important for optimum binding of malate has been observed in the K199R pH-rate profile for V/K_{malate}.

LITERATURES CITED

Adams, M. J., Ellis, G. H., Gover, S., Naylor, C. E., and Philips, C. (1994) Crystallographic Study of Coenzyme Analogue and Substrate Binding in 6-Phosphogluconate Dehydrogenase: Implication for NADP Specificity and the Enzyme Mechanism. *Structure* **2**, 651-668.

Allen, B. L. and Harris, B. G. (1981) Purification of Malic Enzyme from *Ascaris suum* Using NAD^+-Agarose. *Mol. Biochem. Parasitol.* **2**, 367-372.

Baggetto, L. G. (1992) Deviant Energetic Metabolism of Glycolytic Cancer Cells. *Biochimie* **74**, 959-974.

Bradford, M. M. (1976) A Rapid and Sensitive Method for the Quantitation of Microgram Quantities of Protein Utilizing the Principle of Protein-Dye Binding. *Anal. Biochem.* **72**, 248-254.

Chang, G-G. and Hsu, R-Y. (1977) Mechanism of Pigeon Liver Malic Enzyme Modification of Histidyl Residues by Ethoxyformic anhydride. *Biochim. Biophys. Acta 483*, 228-235.

Chang, G-G, Shiao, M-S. Liaw, J-G., and Lee, H-J. (1989) Periodate-oxidized 3-Aminopyridine Adenine Dinucleotide Phosphate as a Fluorescent Affinity Label for Pigeon Liver Malic Enzyme. *J. Biol. Chem. 264*, 280-287.

Chang, G-G. and Huang T-M. (1980) Involvement of Tyrosyl Residues in the Substrate Binding of Pigeon Liver Malic Enzyme. *Biochim. Biophys. Acta. 611*, 217-226.

Chang, G-G. and Huang, T-M. (1981) Modification of Essential Arginine Residues of Pigeon Liver Malic Enzyme. *Biochim. Biophys. Acta 660*, 341-347.

Chang, G-G., Huang, T-M., and Wu, J-A. (1985) Mechanism of Pigeon Liver Malic Enzyme: Modification of Essential Carboxyl Groups. *Proc. Natl. Sci. Counc. Repub. China. B 9*, 56-66.

Chang, G-G., Huang, T-M., Huang, S-M., and Chou, W-Y. (1994) Dissociation of Pigeon-Liver Malic Enzyme in Reverse Micelles. *Eur. J. Biochem. 225,* 1021-1027.

Chen, C-X., Harris, B. G., and Cook, P. F. (1988) Isotope Partitioning for NAD-Malic Enzyme from *Ascaris suum* Confirms a Steady-State Random Kinetic Mechanism. *Biochemistry 27,* 212-219.

Chooback, L., Karsten, W. E., Kulkarni, G., Nalabolu, S. R., Harris, B. G., and Cook, P. F. (1997) Expression, Purification, and Characterization of the Recombinant NAD-Malic Enzyme from *Ascaris suum. Protein Expression and Purification 10,* 51-54.

Chou, W-Y., Tsai, W-P., Lin, C-C., and Chang, G-G. (1995) Selective Oxidative Modification and Affinity Cleavage of Pigeon Liver Malic Enzyme by the Cu^{2+}-Ascorbate System. *J. Biol. Chem. 270,* 25935-25941.

Clancy, L. L., Rao, G. S. J., Finzel, B. C., Muchmore, S. W., Holland, D. R., Watenpaugh, K. D., Krishnamurthy, H. M., Sweet, P. F., Cook, P. F., Harris, B. G., and Einspahr, H. M (1992) Crystallization of the NAD-Dependent Malic Enzyme from the Parasitic Nemantode *Ascaris suum. J. Mol. Biol. 226,* 565-569.

Cleland, W.W. (1979) Statistical Analysis of Enzyme Kinetic Data. *Methods. Enzymol. 63,* 103-138.

Coleman, D., Rao, G. S. J., Cook, P. F., and Harris, B. G. (2001) Crystal Structure of the Malic Enzyme from Ascaris suum Complexed with NAD^+ at 2.3 Å Resolution. (Submitted).

Cook, P. F. (1991) *Enzyme Mechanism from Isotope Effects.* Boca Raton, Florida, *CRC press.*

Cook, P. F. and Cleland, W. W. (1981) Mechanistic Deductions from Isotope Effects in Multireactant Enzyme Mechanisms. *Biochemistry 20,* 1790-1796.

Dozin, B., Magnuson, M. A., and Nikodem, V. M. (1985) Tissue-Specific Regulation of Two Functional Malic Enzyme mRNAs by Triiodothyronine. *Biochemistry 24,* 5581-5586.

Edens, W. A., Urbauer, J. L., and Cleland, W. W., (1997) Determination of the Chemical Mechanism of Malic Enzyme by Isotope Effects. *Biochemistry 36,* 1141-1147.

Frankel, R. (1975) Regulation and Phsiological Function of Malic Enzyme. *Curr. Top. Cell. Regul. 9,* 157-181.

Fodge, D. W., Gray, R. W., and Harris, B. G. (1972) Studies on Enzymes from Parasitic Helminths. I. Purification and Physical Properties of Malic Enzyme from the Muscle Tissue of *Ascaris suum. Biochim. Biophys. Acta 268,* 271-284.

Gornall, A. G., Bradwall, C. J., and David, M. M., (1949) Determination of Serum Proteins by Means of the Biuret Reaction. *J. Biol. Chem. 177,* 751-766.

Grissom, C. B. and Cleland, W. W. (1985) Use of Intermediate Partitioning to Calculate Intrinsic Isotope Effects for the Reaction Catalyzed by Malic Enzyme. *Biochemistry 24,* 944-948.

Hermes, J. D., Roeske, C. A., O'Leary, M .H., and Cleland, W. W. (1982) Use of Multiple Isotope Effects to Determine Enzyme Mechanism and Intrinsic Isotope Effects. Malic Enzyme and Glucose-6-Phosphate Dehydrogenase. *Biochemistry 21*, 5106-5114.

Hsu, R. Y., Glynias, M. J., Satterlee, J., Feeney, R., Clarke, A. R., Emery, D. C., Roe, B. A., Wilson, R. K., Goodridge, A. G., and Holbrook, J. J. (1992) Duck Liver Malic Enzyme. Expression in *Escherichia coli* and Characterization of the Wild-Type Enzyme and Site-Directed Mutants. *Biochem. J. 284*, 869-876.

Hurley, J. H., Antony, M., Dean, D. E., Koshland, D. E. Jr., and Robert, M. S., (1991) Catalytic Mechanism of $NADP^+$-Dependent Isocitrate Dehydrogenase: Implication from Structure of Magnesium-Isocitrate and $NADP^+$ Complexes. *Biochemistry. 30*, 8671-8678.

Jia, Z., Barford, D., Flint, A. J., and Tonks, N. K. (1995) Structural Basis for Phosphotyrosine Peptide Recognition by Protein Tyrosine Phosphatase 1B. *Science. 268*, 1754-1757.

Karsten, W. E. and Cook, P. F. (1994) Stepwise versus Concerted Oxidative Decarboxylation Catalyzed by Malic Enzyme: A Reinvestigation. *Biochemistry 33*, 2096-2103.

Karsten, W. E., Gavva, S. R., Park, S-H., and Cook, P. F. (1995) Metal Ion Activator Effects on Intrinsic Isotope Effects for Hydride Transfer and Decarboxylation in the Reaction Catalyzed by the NAD-Malic Enzyme from *Ascaris suum*. *Biochemistry 34*, 3253-3260.

Karsten, W. E., Chooback, L., Liu, D., Hwang, C-C., Lynch, C., and Cook, P. F. (1999) Mapping the Active Site Topography of the NAD-Malic Enzyme via Alanine-Scanning Site-Directed Mutagenesis. *Biochemistry. 38*, 10527-10532.

Karsten, W. E. and Cook, P. F. (2000) Pyridine Nucleotide-Dependent β-Hydrooxyacid Oxidative Decarboxylases: An Overview. *Pr. Pep. Lett. 7*, 281-286.

Keng, Y. F., Wu, L., and Zhang, Y. Z. (1999) Probing the Function of the Conserved Tryptophan in the Flexible Loop of the *Yersinia* Protein-Tyrosine Phosphate. *Eur. J. Biochem. 259*, 809-814.

Kiick, D. M., Allen, B. L., Rao, J. G. S., Harris, B. G., and Cook, P. F. (1984) Determination of Dissociation Constants for Enzyme-Reactant Complexes for NAD-Malic Enzyme by Modulation of the Thiol Inactivation Rate. *Biochemistry 23*, 5454-5459.

Kiick, D. M., Harris, B. G., and Cook, P. F. (1986) Protonation Mechanism and Location of Rate-Determining Steps for the *Ascaris suum* Nicotinamide Adenine Dinucleotide-Malic Enzyme Reaction from Isotope Effects and pH Studies. *Biochemistry 25*, 227-236.

Kohler, P and Bachmann, R., (1980) Mechanism of Respiration and Phosphorylation in *Ascaris* Muscle Mitochondria. ***Mol. Biochem. Parasitol.*** *1*, 75-90.

Kulkarni, G., Cook, P.F., and Harris, B.G. (1993) Cloning and Nucleotide Sequence of a Full-length cDNA Encoding *Ascaris suum* Malic Enzyme. *Arch. Biochem. Biophys. 300*, 231-237.

Lai, C-J., Harris, B. G., and Cook, P. F. (1992) Mechanism of Activation of the NAD-Malic Enzyme form *Ascaris suum* by Fumarate. *Arch. Biochem. Biophys. 299*, 214-219.

Landsperger, W. J. and Harris, B. G. (1976) NAD^+-Malic Enzyme Regulatory Properties of the Enzyme from *Ascaris suum*. *J. Biol. Chem. 251*, 3599-3602.

Landsperger, W. J., Fodge, D. W., and Harris, B. G. (1978) Kinetic and Isotope Partitioning Studies on the NAD^+-Malic Enzyme from *Ascaris suum*. *J. Biol. Chem. 253*, 1868-1873.

Lardy, H. A., Foster, D. O., Shrago, E., and Ray, P. D. (1964) Metabolic and Hormonal Regulation of Phosphopyruvate Synthesis. *Adv. Enzyme. Regul. 2*, 39-47.

Larson, E. M., Larimer, F. W., and Hartman F. C. (1995) Mechanistic Insights Provided by Deletion of A Flexible Loop at the Active Site of Ribulose-1, 5-Bisphosphate Carboxylase/Oxygenase. *Biochemistry. 31*, 4531-4537.

Liu, D., Karsten, W. E., and Cook, P. F. (2000) Lysine 199 Is the General Acid in the NAD-Malic Enzyme Reaction. *Biochemistry. 39*, 11955-11960.

Loeber, G., Maurer-Fogy, I., and Schwendenwen, R. (1994) Purification, cDNA Cloning and Heterologous Expression of the Human Mitochondrial $NADP^{(+)}$-Dependent Malic Enzyme. *Biochem. J. 304*, 687-692.

Mallick, S., Harris, B. G., and Cook, P. F. (1991) Kinetic Mechanism of NAD-Malic Enzyme from *Ascaris suum* in the Direction of Reductive Carboxylation. *J. Biol. Chem. 266*, 2732-2738.

Mckeehan, W. L. (1982) Glycolysis, Glutaminolysis, and Cell Proliferation. *Cell Biol. Int. Rep. 6*, 635-650.

Moulder, J. W., Vennesland, B., and Evans, E. A. Jr. (1945) A Study of Enzymatic Reactions Catalyzed by Pigeon Liver Extracts. *J. Biol. Chem., 160*, 305-325.

Northrop, D. B. (1975) Steady-State Analysis of Kinetic Isotope Effects in Enzyme Reactions. *Biochemistry 14*, 2644-2651.

Ochoa, S., Mehler,. A. H., and Kornberg, A. (1947) Reversible Oxidative Decarboxylation of Malic Acid. *J. Biol. Chem.. 167*, 871-872.

Olsen, O.W. (1974) Animal Parasites: Their Life Cycles and Ecology. *Baltimore, University Park Press.*

Park, S-H., Kiick, D. M., Harris, B. G., and Cook, P. F. (1984) Kinetic Mechanism in the Direction of Oxidative Decarboxylation for NAD-Malic Enzyme from *Ascaris suum. Biochemistry 23,* 5446-5453.

Park, S-H., Harris, B. G., and Cook, P. F. (1986) pH Dependence of Kinetic Parameters for Oxalacetate Decarboxylation and Pyruvate Reduction Reactions Catalyzed by Malic Enzyme. *Biochemistry 25,* 3752-3759.

Rajapaksa, R., Abu-Doud, H., Raushel, F. M., Harris, B. G., and Cook, P. F. (1993) Pre-Steady-State Kinetics Reveal a Slow Isomerization of the Enzyme-NAD Complex in the NAD-Malic Enzyme Reaction. *Biochemistry 32,* 1928-1934.

Rao, J. G. S., Harris, B. G., and Cook, P. F. (1985) Diethylpyrocarbonate Inactivation of NAD-Malic Enzyme from *Ascaris suum. Arch. Biochem. Biophys. 241,* 67-74.

Rao, J. G. S., Kong, C-T., Benjamin, R. C., Harris, B. G., and Cook, P. F. (1987) Modification of an Arginine Residue Essential for the Activity of NAD-Malic Enzyme from *Ascaris suum*. *Arch. Biochem. Biophys. 255*, 8-13.

Reed, G. H., Poyner, R. R., Larsen, T. M., Wedekind, J. E., and Rayment, I. (1996) Structural and Mechanistic Studies of Enolase. *Curr. Opin. Struct. Biol. 6*, 736-743.

Rhee, S., Parris, K. D., Hyde, C. C., Ahmed, S. A., Miles, E. W., and Davies, D. R. (1997) Crystal Structures of A Mutant (βK87T) Trytophan Synthase $\alpha_2\beta_2$ Complex with Ligands Bound to the Active Sites of the α- and β-Subunits Reveal Ligand-Induced Conformational Changes. *Biochemistry. 36*, 7664-7680.

Rutter, W., and Lardy, H. A., (1958) Purification and Properties of Pigeon Liver Malic Enzyme. *J. Biol. Chem., 233*, 374-382.

Sampson, N. S. and Knowles, J. R. (1992) Segmental Motion in Catalysis: Investigation of A Hydrogen Bond Critical for Loop Closure in the Reaction of Triosephosphate Isomerase. *Biochemistry. 31*, 8488-8494.

Sanz, N., Diez-Fernandez, C., Valverde, A. M., Lorenzo, M., Benito, M., and Cascales, M. (1997) Malic Enzyme and Glucose 6-Phosphate Dehydrogenase Gene Expression Increase in Rate Liver Cirrhogenesis. *Br. J. Cancer 75*, 487-492.

Satterlee, J. and Hsu, R. Y. (1991) Duck Liver Malic Enzyme: Sequence of a Tryptic Peptide Containing the Cysteine Residue Labeled by the Substrate Analog Bromopyruvate. *Biochim. Biophys. Acta. 1079*, 247-252.

Saz, H. J. and Hubbard, J. A. (1957) The Oxidative Decarboxylation of Malate by *Ascaris lumbericoides*. *J. Biol. Chem. 225*, 921-933.

Saz, H. J., (1971) Anaerobic Phosphorylation in *Ascaris suum* Mitochondria and the Effects of Anthelmintics. *Comp. Biochem. Physiol. B Comp. Biochem. 39*, 627-637.

Saz, H. J., (1971) Facultative Anaerobiosis in the Invertebrates: Pathways and Control Systems. *AM. Zoologist. 11*, 125-133.

Saz, H. J. (1981) Energy Metabolism of Parasitic Helminths: Adaptation to Parasitism. *Annu. Rev. Physiol. 43*, 323-341.

Schimerlik, M. I., and Cleland, W. W., (1977) pH Variation of the Kinetic Parameters and the Catalytic Mechanism of Malic Enzyme. *Biochemistry 16*, 576-583.

Schimerlik, M. I., Grimshaw, C. E., and Cleland, W. W., (1977) Determination of the Rate-limiting Step for Malic Enzyme by the Use of Isotope Effects and Other Kinetic Studies. *Biochemistry 16*, 571-576.

Seidman, I. and Entner, N. (1961) Oxidative Enzymes and Their Role in Phosphorylation in Sarcosomes of Adult *Ascaris lumbricoides*. *J. Biol. Chem. 236*, 915-919.

Shifrin, R. Y., and Kaplan, N. O. (1960) Coenzyme Binding. *Adv. Enzymol., 22*, 337-415.

Shrago, E., Lardy, H. A., Nordlie, R. C., and Foster, D. O. (1963) Metabolic and Hormonal Control of Phosphoenolpyruvate Carboxykinase and Malic Enzyme in Rat Liver. *J. Biol. Chem. 238*, 3188-3192.

Stryer, L., (1995) *Biochemistry. 4th editon.* WH Freeman & Company, New York, NY. 678-679.

Tipton, P. A. (1993) Intermediate Partitioning in the Tartrate Dehydrogenase-Catalyzed Oxidative Decarboxylation of D-Malate. *Biochemistry 32*, 2822-2827.

Tipton, P. A. and Peisach, J. (1990) Characterization of the Multiple Catalytic Activities of Tartrate Dehydrogenase. *Biochemistry 29*, 1749-1756.

Tipton, P. A., Quinn, T. P., Peisach, J. and Cook, P. F. 1996 Role of the Divalent Metal Ion in the NAD-Malic Enzyme Reaction: an ESEEM Determination of the Ground State Conformation of Malate in the E:Mn:Malate Complex. *Protein Sci. 5*, 1648-1654.

Viola, R. E., Cook P. F., and Cleland, W. W. (1979) Stereoselective Preparation of Deuterated Reduced Nicotinamide Adenine Nucleotides and Substrates by Enzymatic Synthesis. *Anal. Biochem. 96*, 334-340.

Wang, F., Li, W., Emmett, M. R., Hendrickson, C. L., Marshall, A. G., Zhang, Y. L., Wu, L., and Zhang, Z. Y. (1998) Conformational and Dynamic Changes of *Yersinia* Protein

Tyrosine Phosphate Inudced by Ligand Binding and Active Site Mutation and Revealed by H/D Exchange and Electrospray Ionization Fourier Transform Ion Cyclotron Mass Spectrometry. *Biochemistry 37*, 15289-15299.

Ward, C. W. and Fairbain, D. (1970) Enzymes of Beta-Oxidation and the Tricarboxylic Acid Cycle in Adult *Hymenolepis Diminuta (Cestoda) and Ascaris suum (Nematoda)*. *J. Parasitol. 56*, 1009-1012.

Wei, C-H., Chou, W-Y., Huang, S-M., Lin, C-C., and Chang, G-G. (1994) Affinity Cleavage at the Putative Metal-Binding Site of Pigeon Liver Malic Enzyme by the Fe^{2+}-Ascorbate System. *Biochemistry 33*, 7931-7936.

Wei, C-H., Chou, W-Y., and Chang, G-G. (1995) Identification of Asp^{258} as the Metal Coordinate of Pigeon Liver Malic Enzyme by Site-Specific Mutagenesis. *Biochemistry 34*, 7949-7954.

Weiss, P. M., Gava, S. R., Harris, B. G., Urbauer, J. L., Cleland, W. W., and Cook, P. F. (1991) Multiple Isotope Effects with Alternative Dinucleotide Substrates as a Probe of the Malic Enzyme Reaction. *Biochemistry 30*, 5755-5763.

Xu, Y., Bhargava, G., Wu, H., Loeber, G., and Tong, L. (1999) Crystal Structure of Human Mitochondrial NAD(P)$^+$-Dependent Malic Enzyme: a New Class of Oxidative Decarboxylases. *Structure 7*, 877-889.

Yang, Z., Floyd, D., Loeber, G., and Tong, L. (2000) Structure of a Closed Form of Human Malic Enzyme and Implications for Catalytic Mechanism. *Nature Structure Biology 7*, 251-257.

Zhang, L. and Cook, P.F. (2000) Chemical Mechanism of 6-Phosphogluconate Dehydrogenase Via Kinetic Studies and Site-Directed Mutagenesis *Pr. Pep. Lett. 7*, 313-322.

APPENDIX

SEQUENCE ALIGNMENT OF MALIC ENZYMES

```
Populus_trichocarpa          ----------------------------------------------------MESTLKEMR
Grape                        ----------------------------------------------------MESTLKDIR
Flaveria_pringlei            MMSLNSSSVVKSSISGVSWTQSQSVRLSVRRPMVVAMVNSNGRPERSVGVSVDGAVKDVN
Tomato                       ------------------------------------------------------------
Kidney                       ----------------------------------------------------MSSISLKEN
ice_plant                    ----------------------------------------------------MGGSNALN
Maize                        MLSTRTAAVAASASPASPWKLG--------GRSEGGASCDGCRTYRNTLRRRAAPAKVRA
Rice                         MLSARAAATAAAAAASPLWKRGEG------GSSGSGSGCTSCREVR--RR---AAVRVRT
Human_CYOT_NADP              ------------------------------------------------------------
Pig                          ------------------------------------------------------------
Mouse                        ------------------------------------------------------------
Rat                          ------------------------------------------------------------
Domestic_duck                ------------------------------------------------------------
Domestic_pigeon              ------------------------------------------------------------
Human_MITOCHONDRIAL_NADP     ----------------------------------------------MGAALGTGTRLAPWP
Human_MITOCHONDRIAL_NAD      ------------------------------------------------------------
Ascaris_suum                 ---------------------------------------PRVRSFIAHQSGITSVIRRSP
Amaranthus_hypochondriacus   ----------------------------------------------------MLVLCSRSR
Potato                       ----------------------------------------------------MAIFSNQMR
Fission_yeast                ------------------------------------------------------------
Bakers_yeast                 -MLRT----RLSVSVAARSQLTRSLT-ASRTAPLRRWPIQQSRLYSSNTRSHKATTTREN
Mycobacterium_tuberculosis   -MVESGTGIPLPASCWSRTRSRRCMPKDSSPHWIWHSSAARAALYVRGKRRPDGQGRRSC
Bacillus_subtilis            ------------------------------------------------------------
Bacillus_stearothermophilus  ------------------------------------------------------------
Haemophilus_influenzae       ------------------------------------------------------------
```

```
Populus_trichocarpa             --------------DGASVLDMDPKSTVGGGVEDVYG--------EDRATEDQLVTPWTI
Grape                           --------------DGASVLDLDPKATVGGGVEDLYG--------EDFATEDQLVTPWTV
Flaveria_pringlei               APVAV---------EVADSESKKPTAVVGGGVEDVYG--------EDSATEDHFITPWSV
Tomato                          ---------------------IRHESTVTGGVQDVYG--------EDSATEDQSITPWTL
Kidney                          ----------------GGEVSVKKDYSNGGGVRDLYG--------EDSATEDHLITPWTF
ice_plant                       -------------------EMTNGSDGITGGVADVYG--------EEFATQDQLVTPWSF
Maize                           LPPRR---------VDAVAMVSNAETETEKEQEEAAA-----------ASEELPVMPWAT
Ricexx4                         PVPRR---------VEAVAMESAAETEKKEEVAAAGGG------VEDMATEEVPVTPWAF
Human_CYOT_NADP                 ------------------------------------------------MEPEAPRRRH
Pig                             ------------------------------------------------------------
Mouse                           ------------------------------------------------MEPRAPRRRH
Rat                             ------------------------------------------------MDPRAPRRRH
Domestic_duck                   ------------------------------------------------------------
Domestic_pigeon                 ------------------------------------------------------------
Human_MITOCHONDRIAL_NADP        GRACG---------ALPRWTPTAPA--------------------QGCHSKPGPARPVP
Human_MITOCHONDRIAL_NAD         -------------------MLSRLR--------------------VVSTTCTLACRHLH
Ascaris_suum                    DIAHR---------MVRSLSVSSQRNKSVAHHEDVYSHNLPPMDEKEMALYKLYRPERVT
Amaranthus_hypochondriacus      ---------------LTSSLIRRLKDQIANVSN-------------HRSFATSEGHRLAI
Potato                          ---------------LSSTLLKRLHQRVAAAVNSSS----------SRNFTTTEGHRPTI
Fission_yeast                   -------------------MPAGTKEQ-----------------------IECPLKGV
Bakers_yeast                    TFQKP------YSDEEVTKTPVGSRARKIFEAPHPHAT-------RLTVEGAIECPLESF
Mycobacterium_tuberculosis      ALRNRGRTPATGPGPGQSPSPVGARQPALPSRRPLNPA-------R----SRTEVVMSDA
Bacillus_subtilis               ------------------------MIAKH-----------------MIRTLMIETPSV
Bacillus_stearothermophilus     --------------------MALPGGAAMN-----------------ITIRLQFEKDIV
Haemophilus_influenzae          ------------------------------------------------------------
```

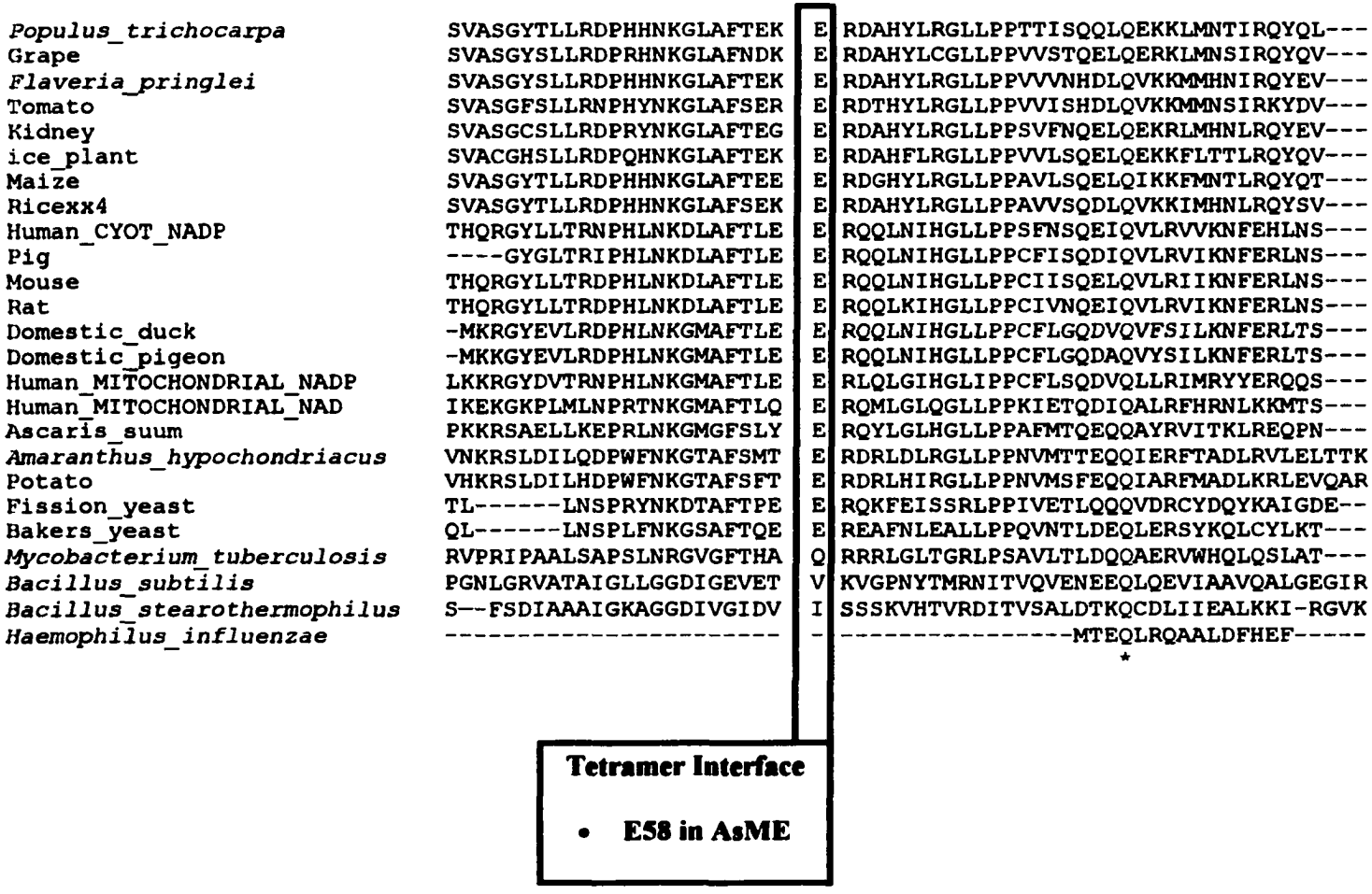
Populus_trichocarpa SVASGYTLLRDPHHNKGLAFTEK E RDAHYLRGLLPPTTISQQLQEKKLMNTIRQYQL---
Grape SVASGYSLLRDPRHNKGLAFNDK E RDAHYLCGLLPPVVSTQELQERKLMNSIRQYQV---
Flaveria_pringlei SVASGYSLLRDPHHNKGLAFTEK E RDAHYLRGLLPPVVVNHDLQVKKMMHNIRQYEV---
Tomato SVASGFSLLRNPHYNKGLAFSER E RDTHYLRGLLPPVVISHDLQVKKMMNSIRKYDV---
Kidney SVASGCSLLRDPRYNKGLAFTEG E RDAHYLRGLLPPSVFNQELQEKRLMHNLRQYEV---
ice_plant SVACGHSLLRDPQHNKGLAFTEK E RDAHFLRGLLPPVVLSQELQEKKFLTTLRQYQV---
Maize SVASGYTLLRDPHHNKGLAFTEE E RDGHYLRGLLPPAVLSQELQIKKFMNTLRQYQT---
Ricexx4 SVASGYTLLRDPHHNKGLAFSEK E RDAHYLRGLLPPAVVSQDLQVKKIMHNLRQYSV---
Human_CYOT_NADP THQRGYLLTRNPHLNKDLAFTLE E RQQLNIHGLLPPSFNSQEIQVLRVVKNFEHLNS---
Pig ----GYGLTRIPHLNKDLAFTLE E RQQLNIHGLLPPCFISQDIQVLRVIKNFERLNS---
Mouse THQRGYLLTRDPHLNKDLAFTLE E RQQLNIHGLLPPCIISQELQVLRIIKNFERLNS---
Rat THQRGYLLTRDPHLNKDLAFTLE E RQQLKIHGLLPPCIVNQEIQVLRVIKNFERLNS---
Domestic_duck -MKRGYEVLRDPHLNKGMAFTLE E RQQLNIHGLLPPCFLGQDVQVFSILKNFERLTS---
Domestic_pigeon -MKKGYEVLRDPHLNKGMAFTLE E RQQLNIHGLLPPCFLGQDAQVYSILKNFERLTS---
Human_MITOCHONDRIAL_NADP LKKRGYDVTRNPHLNKGMAFTLE E RLQLGIHGLIPPCFLSQDVQLLRIMRYYERQQS---
Human_MITOCHONDRIAL_NAD IKEKGKPLMLNPRTNKGMAFTLQ E RQMLGLQGLLPPKIETQDIQALRFHRNLKKMTS---
Ascaris_suum PKKRSAELLKEPRLNKGMGFSLY E RQYLGLHGLLPPAFMTQEQQAYRVITKLREQPN---
Amaranthus_hypochondriacus VNKRSLDILQDPWFNKGTAFSMT E RDRLDLRGLLPPNVMTTEQQIERFTADLRVLELTTK
Potato VHKRSLDILHDPWFNKGTAFSFT E RDRLHIRGLLPPNVMSFEQQIARFMADLKRLEVQAR
Fission_yeast TL------LNSPRYNKDTAFTPE E RQKFEISSRLPPIVETLQQQVDRCYDQYKAIGDE--
Bakers_yeast QL------LNSPLFNKGSAFTQE E REAFNLEALLPPQVNTLDEQLERSYKQLCYLKT---
Mycobacterium_tuberculosis RVPRIPAALSAPSLNRGVGFTHA Q RRRLGLTGRLPSAVLTLDQQAERVWHQLQSLAT---
Bacillus_subtilis PGNLGRVATAIGLLGGDIGEVET V KVGPNYTMRNITVQVENEEQLQEVIAAVQALGEGIR
Bacillus_stearothermophilus S--FSDIAAAIGKAGGDIVGIDV I SSSKVHTVRDITVSALDTKQCDLIIEALKKI-RGVK
Haemophilus_influenzae ---------- - ----------MTEQLRQAALDFHEF-----
*
Tetramer Interface
• E58 in AsME

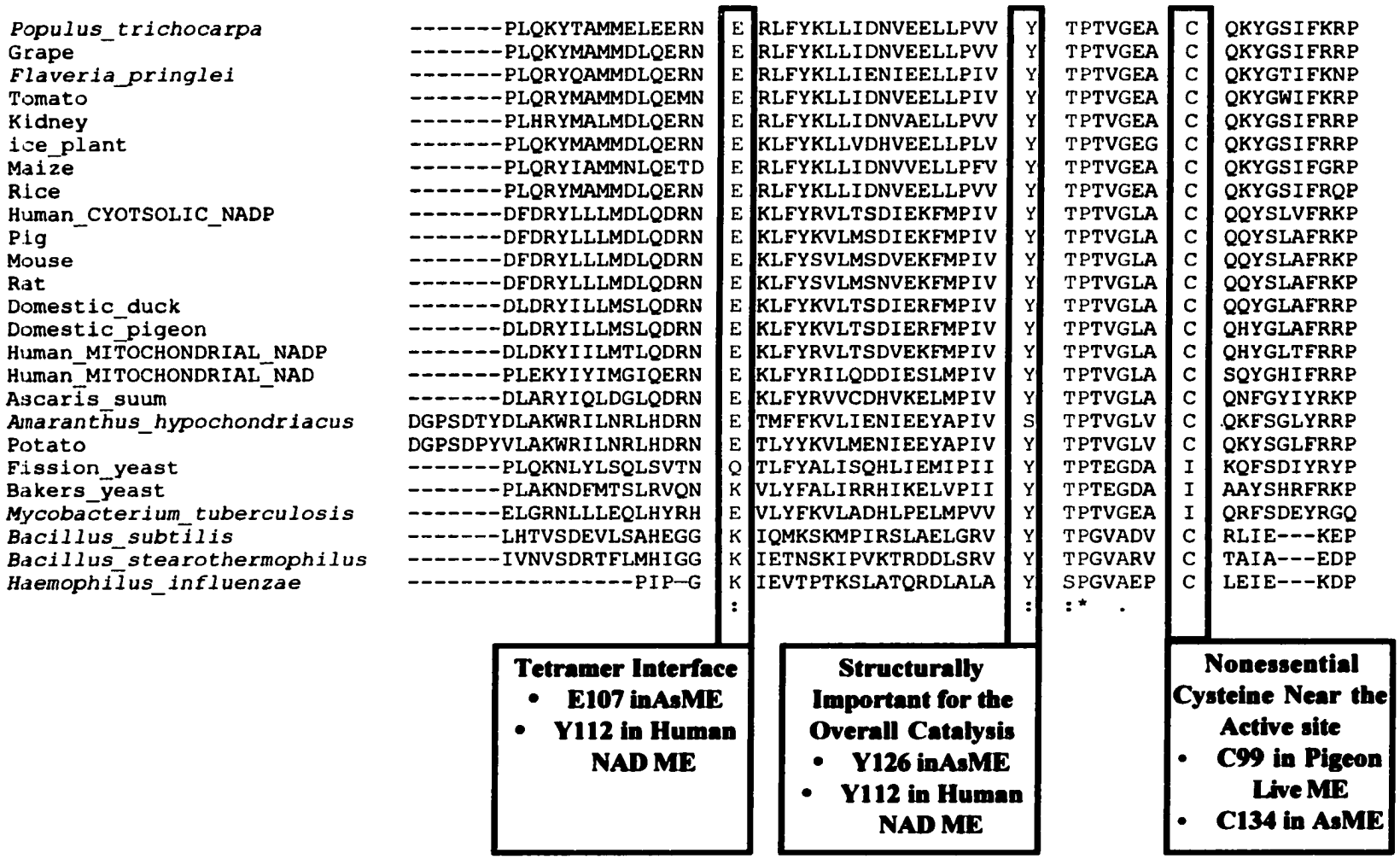
Populus_trichocarpa -------PLQKYTAMMELEERN E RLFYKLLIDNVEELLPVV Y TPTVGEA C QKYGSIFKRP
Grape -------PLQKYMAMMDLQERN E RLFYKLLIDNVEELLPVV Y TPTVGEA C QKYGSIFRRP
Flaveria_pringlei -------PLQRYQAMMDLQERN E RLFYKLLIENIEELLPIV Y TPTVGEA C QKYGTIFKNP
Tomato -------PLQRYMAMMDLQEMN E RLFYKLLIDNVEELLPIV Y TPTVGEA C QKYGWIFKRP
Kidney -------PLHRYMALMDLQERN E RLFYKLLIDNVAELLPVV Y TPTVGEA C QKYGSIFRRP
ice_plant -------PLQKYMAMMDLQERN E KLFYKLLVDHVEELLPLV Y TPTVGEG C QKYGSIFRRP
Maize -------PLQRYIAMMNLQETD E RLFYKLLIDNVVELLPFV Y TPTVGEA C QKYGSIFGRP
Rice -------PLQRYMAMMDLQERN E RLFYKLLIDNVEELLPVV Y TPTVGEA C QKYGSIFRQP
Human_CYOTSOLIC_NADP -------DFDRYLLLMDLQDRN E KLFYRVLTSDIEKFMPIV Y TPTVGLA C QQYSLVFRKP
Pig -------DFDRYLLLMDLQDRN E KLFYKVLMSDIEKFMPIV Y TPTVGLA C QQYSLAFRKP
Mouse -------DFDRYLLLMDLQDRN E KLFYSVLMSDVEKFMPIV Y TPTVGLA C QQYSLAFRKP
Rat -------DFDRYLLLMDLQDRN E KLFYSVLMSNVEKFMPIV Y TPTVGLA C QQYSLAFRKP
Domestic_duck -------DLDRYILLMSLQDRN E KLFYKVLTSDIERFMPIV Y TPTVGLA C QQYGLAFRRP
Domestic_pigeon -------DLDRYILLMSLQDRN E KLFYKVLTSDIERFMPIV Y TPTVGLA C QHYGLAFRRP
Human_MITOCHONDRIAL_NADP -------DLDKYIILMTLQDRN E KLFYRVLTSDVEKFMPIV Y TPTVGLA C QHYGLTFRRP
Human_MITOCHONDRIAL_NAD -------PLEKYIYIMGIQERN E KLFYRILQDDIESLMPIV Y TPTVGLA C SQYGHIFRRP
Ascaris_suum -------DLARYIQLDGLQDRN E KLFYRVVCDHVKELMPIV Y TPTVGLA C QNFGYIYRKP
Amaranthus_hypochondriacus DGPSDTYDLAKWRILNRLHDRN E TMFFKVLIENIEEYAPIV S TPTVGLV C QKFSGLYRRP
Potato DGPSDPYVLAKWRILNRLHDRN E TLYYKVLMENIEEYAPIV Y TPTVGLV C QKYSGLFRRP
Fission_yeast -------PLQKNLYLSQLSVTN Q TLFYALISQHLIEMIPII Y TPTEGDA I KQFSDIYRYP
Bakers_yeast -------PLAKNDFMTSLRVQN K VLYFALIRRHIKELVPII Y TPTEGDA I AAYSHRFRKP
Mycobacterium_tuberculosis -------ELGRNLLLEQLHYRH E VLYFKVLADHLPELMPVV Y TPTVGEA I QRFSDEYRGQ
Bacillus_subtilis -------LHTVSDEVLSAHEGG K IQMKSKMPIRSLAELGRV Y TPGVADV C RLIE---KEP
Bacillus_stearothermophilus -------IVNVSDRTFLMHIGG K IETNSKIPVKTRDDLSRV Y TPGVARV C TAIA---EDP
Haemophilus_influenzae ----------PIP-G K IEVTPTKSLATQRDLALA Y SPGVAEP C LEIE---KDP
: : :* .
Tetramer Interface
• E107 inAsME
• Y112 in Human NAD ME
Structurally Important for the Overall Catalysis
• Y126 inAsME
• Y112 in Human NAD ME
Nonessential Cysteine Near the Active site
• C99 in Pigeon Live ME
• C134 in AsME

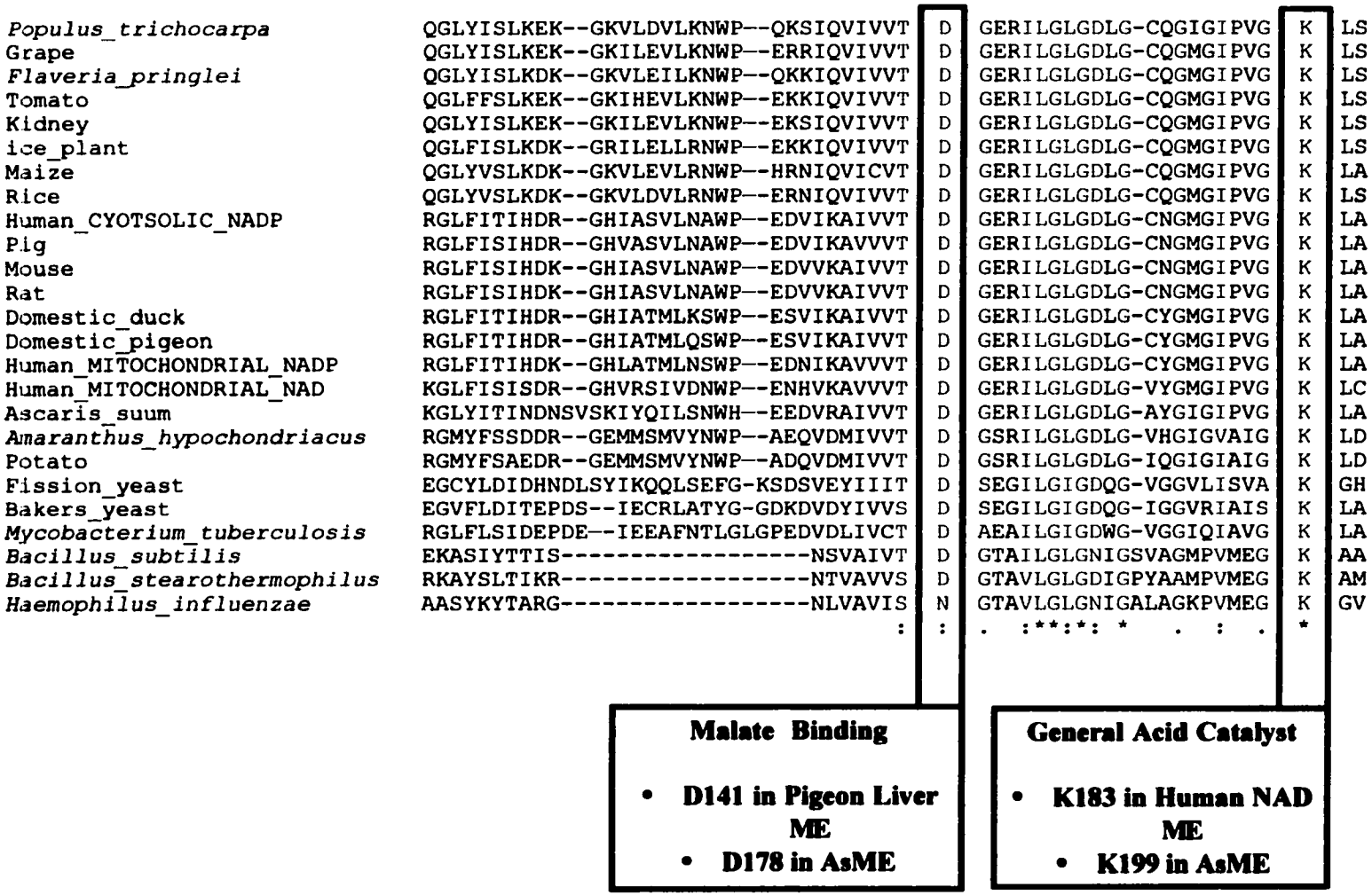
Populus_trichocarpa QGLYISLKEK--GKVLDVLKNWP--QKSIQVIVVT D GERILGLGDLG-CQGIGIPVG K LS
Grape QGLYISLKEK--GKILEVLKNWP--ERRIQVIVVT D GERILGLGDLG-CQGMGIPVG K LS
Flaveria_pringlei QGLYISLKDK--GKVLEILKNWP--QKKIQVIVVT D GERILGLGDLG-CQGMGIPVG K LS
Tomato QGLFFSLKEK--GKIHEVLKNWP--EKKIQVIVVT D GERILGLGDLG-CQGMGIPVG K LS
Kidney QGLYISLKEK--GKILEVLKNWP--EKSIQVIVVT D GERILGLGDLG-CQGMGIPVG K LS
ice_plant QGLFISLKDK--GRILELLRNWP--EKKIQVIVVT D GERILGLGDLG-CQGMGIPVG K LS
Maize QGLYVSLKDK--GKVLEVLRNWP--HRNIQVICVT D GERILGLGDLG-CQGMGIPVG K LA
Rice QGLYVSLKDK--GKVLDVLRNWP--ERNIQVIVVT D GERILGLGDLG-CQGMGIPVG K LS
Human_CYOTSOLIC_NADP RGLFITIHDR--GHIASVLNAWP--EDVIKAIVVT D GERILGLGDLG-CNGMGIPVG K LA
Pig RGLFISIHDR--GHVASVLNAWP--EDVIKAVVVT D GERILGLGDLG-CNGMGIPVG K LA
Mouse RGLFISIHDK--GHIASVLNAWP--EDVVKAIVVT D GERILGLGDLG-CNGMGIPVG K LA
Rat RGLFISIHDK--GHIASVLNAWP--EDVVKAIVVT D GERILGLGDLG-CNGMGIPVG K LA
Domestic_duck RGLFITIHDR--GHIATMLKSWP--ESVIKAIVVT D GERILGLGDLG-CYGMGIPVG K LA
Domestic_pigeon RGLFITIHDR--GHIATMLQSWP--ESVIKAIVVT D GERILGLGDLG-CYGMGIPVG K LA
Human_MITOCHONDRIAL_NADP RGLFITIHDK--GHLATMLNSWP--EDNIKAVVVT D GERILGLGDLG-CYGMGIPVG K LA
Human_MITOCHONDRIAL_NAD KGLFISISDR--GHVRSIVDNWP--ENHVKAVVVT D GERILGLGDLG-VYGMGIPVG K LC
Ascaris_suum KGLYITINDNSVSKIYQILSNWH--EEDVRAIVVT D GERILGLGDLG-AYGIGIPVG K LA
Amaranthus_hypochondriacus RGMYFSSDDR--GEMMSMVYNWP--AEQVDMIVVT D GSRILGLGDLG-VHGIGVAIG K LD
Potato RGMYFSAEDR--GEMMSMVYNWP--ADQVDMIVVT D GSRILGLGDLG-IQGIGIAIG K LD
Fission_yeast EGCYLDIDHNDLSYIKQQLSEFG-KSDSVEYIIIT D SEGILGIGDQG-VGGVLISVA K GH
Bakers_yeast EGVFLDITEPDS--IECRLATYG-GDKDVDYIVVS D SEGILGIGDQG-IGGVRIAIS K LA
Mycobacterium_tuberculosis RGLFLSIDEPDE--IEEAFNTLGLGPEDVDLIVCT D AEAILGIGDWG-VGGIQIAVG K LA
Bacillus_subtilis EKASIYTTIS----------NSVAIVT D GTAILGLGNIGSVAGMPVMEG K AA
Bacillus_stearothermophilus RKAYSLTIKR----------NTVAVVS D GTAVLGLGDIGPYAAMPVMEG K AM
Haemophilus_influenzae AASYKYTARG----------NLVAVIS N GTAVLGLGNIGALAGKPVMEG K GV
: : . :**:*: * . : . *
Malate Binding
• D141 in Pigeon Liver ME
• D178 in AsME
General Acid Catalyst
• K183 in Human NAD ME
• K199 in AsME

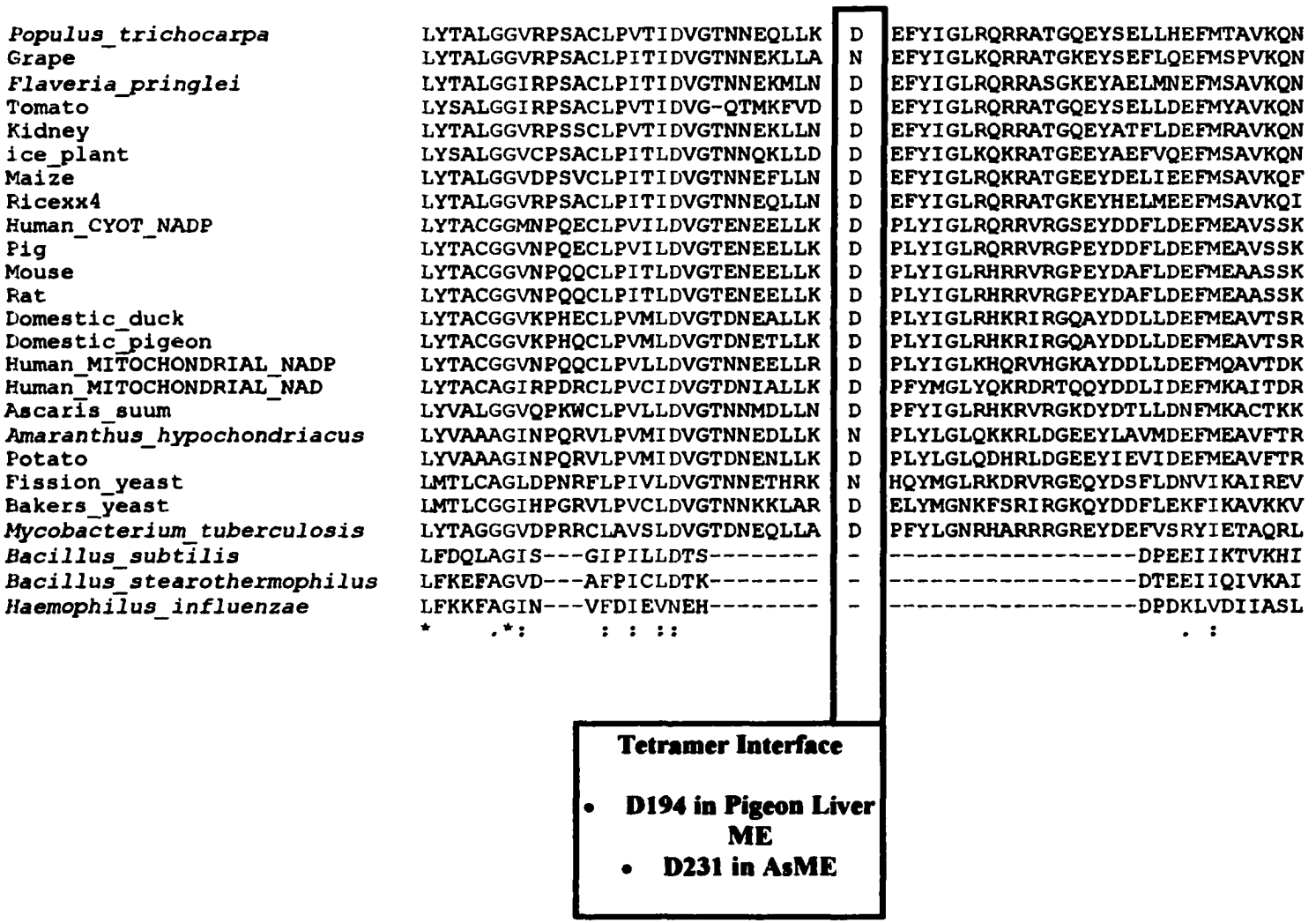
Populus_trichocarpa LYTALGGVRPSACLPVTIDVGTNNEQLLK D EFYIGLRQRRATGQEYSELLHEFMTAVKQN
Grape LYTALGGVRPSACLPITIDVGTNNEKLLA N EFYIGLKQRRATGKEYSEFLQEFMSPVKQN
Flaveria_pringlei LYTALGGIRPSACLPITIDVGTNNEKMLN D EFYIGLRQRRASGKEYAELMNEFMSAVKQN
Tomato LYSALGGIRPSACLPVTIDVG-QTMKFVD D EFYIGLRQRRATGQEYSELLDEFMYAVKQN
Kidney LYTALGGVRPSSCLPVTIDVGTNNEKLLN D EFYIGLRQRRATGQEYATFLDEFMRAVKQN
ice_plant LYSALGGVCPSACLPITLDVGTNNQKLLD D EFYIGLKQKRATGEEYAEFVQEFMSAVKQN
Maize LYTALGGVDPSVCLPITIDVGTNNEFLLN D EFYIGLRQKRATGEEYDELIEEFMSAVKQF
Ricexx4 LYTALGGVRPSACLPITIDVGTNNEQLLN D EFYIGLRQRRATGKEYHELMEEFMSAVKQI
Human_CYOT_NADP LYTACGGMNPQECLPVILDVGTENEELLK D PLYIGLRQRRVRGSEYDDFLDEFMEAVSSK
Pig LYTACGGVNPQECLPVILDVGTENEELLK D PLYIGLRQRRVRGPEYDDFLDEFMEAVSSK
Mouse LYTACGGVNPQQCLPITLDVGTENEELLK D PLYIGLRHRRVRGPEYDAFLDEFMEAASSK
Rat LYTACGGVNPQQCLPITLDVGTENEELLK D PLYIGLRHRRVRGPEYDAFLDEFMEAASSK
Domestic_duck LYTACGGVKPHECLPVMLDVGTDNEALLK D PLYIGLRHKRIRGQAYDDLLDEFMEAVTSR
Domestic_pigeon LYTACGGVKPHQCLPVMLDVGTDNETLLK D PLYIGLRHKRIRGQAYDDLLDEFMEAVTSR
Human_MITOCHONDRIAL_NADP LYTACGGVNPQQCLPVLLDVGTNNEELLR D PLYIGLKHQRVHGKAYDDLLDEFMQAVTDK
Human_MITOCHONDRIAL_NAD LYTACAGIRPDRCLPVCIDVGTDNIALLK D PFYMGLYQKRDRTQQYDDLIDEFMKAITDR
Ascaris_suum LYVALGGVQPKWCLPVLLDVGTNNMDLLN D PFYIGLRHKRVRGKDYDTLLDNFMKACTKK
Amaranthus_hypochondriacus LYVAAAGINPQRVLPVMIDVGTNNEDLLK N PLYLGLQKKRLDGEEYLAVMDEFMEAVFTR
Potato LYVAAAGINPQRVLPVMIDVGTDNENLLK D PLYLGLQDHRLDGEEYIEVIDEFMEAVFTR
Fission_yeast LMTLCAGLDPNRFLPIVLDVGTNNETHRK N HQYMGLRKDRVRGEQYDSFLDNVIKAIREV
Bakers_yeast LMTLCGGIHPGRVLPVCLDVGTNNKKLAR D ELYMGNKFSRIRGKQYDDFLEKFIKAVKKV
Mycobacterium_tuberculosis LYTAGGGVDPRRCLAVSLDVGTDNEQLLA D PFYLGNRHARRRGREYDEFVSRYIETAQRL
Bacillus_subtilis LFDQLAGIS---GIPILLDTS-------- - ----------DPEEIIKTVKHI
Bacillus_stearothermophilus LFKEFAGVD---AFPICLDTK-------- - ----------DTEEIIQIVKAI
Haemophilus_influenzae LFKKFAGIN---VFDIEVNEH-------- - ----------DPDKLVDIIASL
Tetramer Interface
• D194 in Pigeon Liver ME
• D231 in AsME

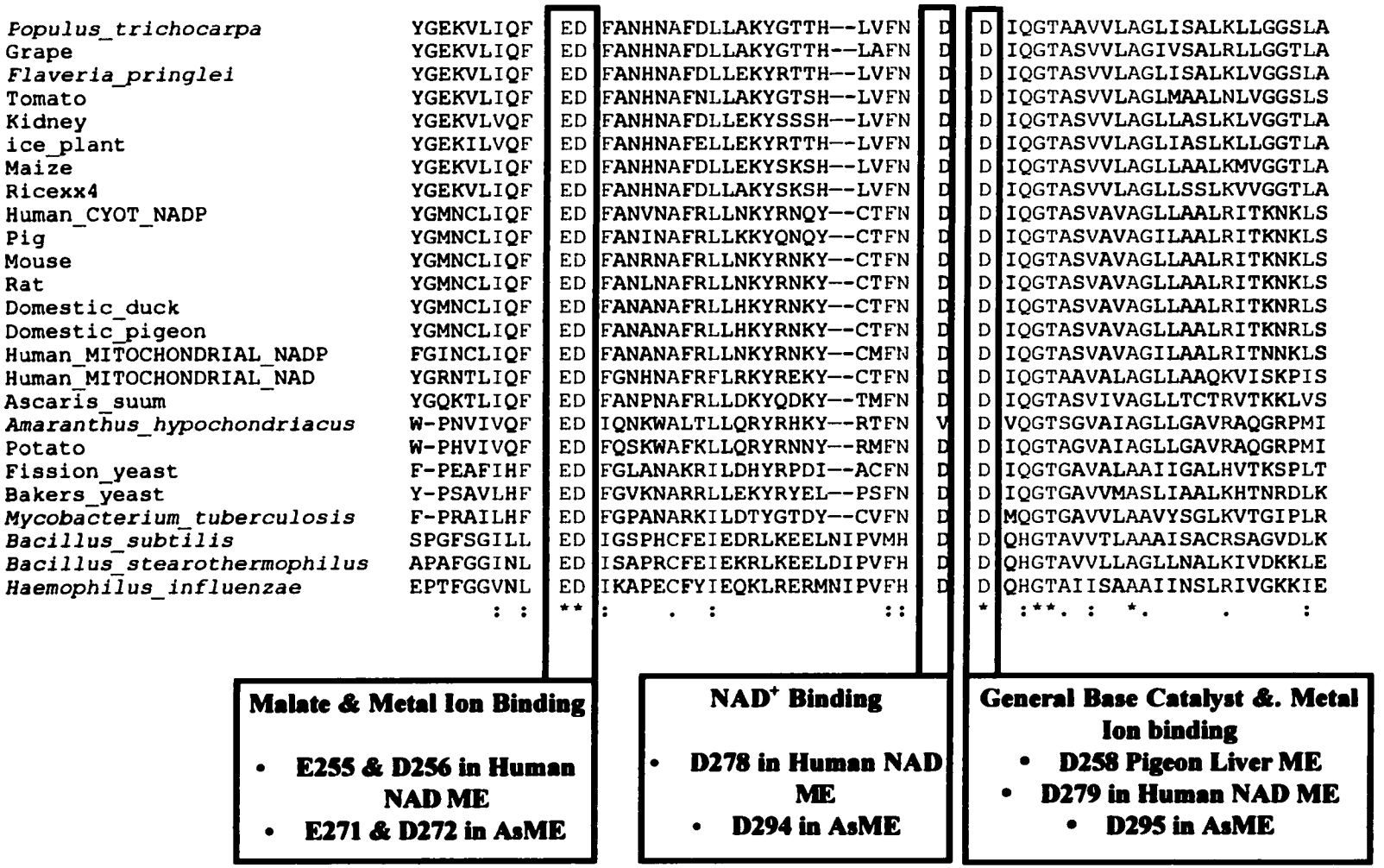
Populus_trichocarpa YGEKVLIQF ED FANHNAFDLLAKYGTTH--LVFN D D IQGTAAVVLAGLISALKLLGGSLA
Grape YGEKVLIQF ED FANHNAFDLLAKYGTTH--LAFN D D IQGTASVVLAGIVSALRLLGGTLA
Flaveria_pringlei YGEKVLIQF ED FANHNAFDLLEKYRTTH--LVFN D D IQGTASVVLAGLISALKLVGGSLA
Tomato YGEKVLIQF ED FANHNAFNLLAKYGTSH--LVFN D D IQGTASVVLAGLMAALNLVGGSLS
Kidney YGEKVLVQF ED FANHNAFDLLEKYSSSH--LVFN D D IQGTASVVLAGLLASLKLVGGTLA
ice_plant YGEKILVQF ED FANHNAFELLEKYRTTH--LVFN D D IQGTASVVLAGLIASLKLLGGTLA
Maize YGEKVLIQF ED FANHNAFDLLEKYSKSH--LVFN D D IQGTASVVLAGLLAALKMVGGTLA
Ricexx4 YGEKVLIQF ED FANHNAFDLLAKYSKSH--LVFN D D IQGTASVVLAGLLSSLKVVGGTLA
Human_CYOT_NADP YGMNCLIQF ED FANVNAFRLLNKYRNQY--CTFN D D IQGTASVAVAGLLAALRITKNKLS
Pig YGMNCLIQF ED FANINAFRLLKKYQNQY--CTFN D D IQGTASVAVAGILAALRITKNKLS
Mouse YGMNCLIQF ED FANRNAFRLLNKYRNKY--CTFN D D IQGTASVAVAGLLAALRITKNKLS
Rat YGMNCLIQF ED FANLNAFRLLNKYRNKY--CTFN D D IQGTASVAVAGLLAALRITKNKLS
Domestic_duck YGMNCLIQF ED FANANAFRLLHKYRNKY--CTFN D D IQGTASVAVAGLLAALRITKNRLS
Domestic_pigeon YGMNCLIQF ED FANANAFRLLHKYRNKY--CTFN D D IQGTASVAVAGLLAALRITKNRLS
Human_MITOCHONDRIAL_NADP FGINCLIQF ED FANANAFRLLNKYRNKY--CMFN D D IQGTASVAVAGILAALRITNNKLS
Human_MITOCHONDRIAL_NAD YGRNTLIQF ED FGNHNAFRFLRKYREKY--CTFN D D IQGTAAVALAGLLAAQKVISKPIS
Ascaris_suum YGQKTLIQF ED FANPNAFRLLDKYQDKY--TMFN D D IQGTASVIVAGLLTCTRVTKKLVS
Amaranthus_hypochondriacus W-PNVIVQF ED IQNKWALTLLQRYRHKY--RTFN V D VQGTSGVAIAGLLGAVRAQGRPMI
Potato W-PHVIVQF ED FQSKWAFKLLQRYRNNY--RMFN D D IQGTAGVAIAGLLGAVRAQGRPMI
Fission_yeast F-PEAFIHF ED FGLANAKRILDHYRPDI--ACFN D D IQGTGAVALAAIIGALHVTKSPLT
Bakers_yeast Y-PSAVLHF ED FGVKNARRLLEKYRYEL--PSFN D D IQGTGAVVMASLIAALKHTNRDLK
Mycobacterium_tuberculosis F-PRAILHF ED FGPANARKILDTYGTDY--CVFN D D MQGTGAVVLAAVYSGLKVTGIPLR
Bacillus_subtilis SPGFSGILL ED IGSPHCFEIEDRLKEELNIPVMH D D QHGTAVVTLAAAISACRSAGVDLK
Bacillus_stearothermophilus APAFGGINL ED ISAPRCFEIEKRLKEELDIPVFH D D QHGTAVVLLAGLLNALKIVDKKLE
Haemophilus_influenzae EPTFGGVNL ED IKAPECFYIEQKLRERMNIPVFH D D QHGTAIISAAAIINSLRIVGKKIE
: : ** : . : :: * :**. : *. . :
Malate & Metal Ion Binding
• E255 & D256 in Human NAD ME
• E271 & D272 in AsME
NAD+ Binding
• D278 in Human NAD ME
• D294 in AsME
General Base Catalyst &. Metal Ion binding
• D258 Pigeon Liver ME
• D279 in Human NAD ME
• D295 in AsME

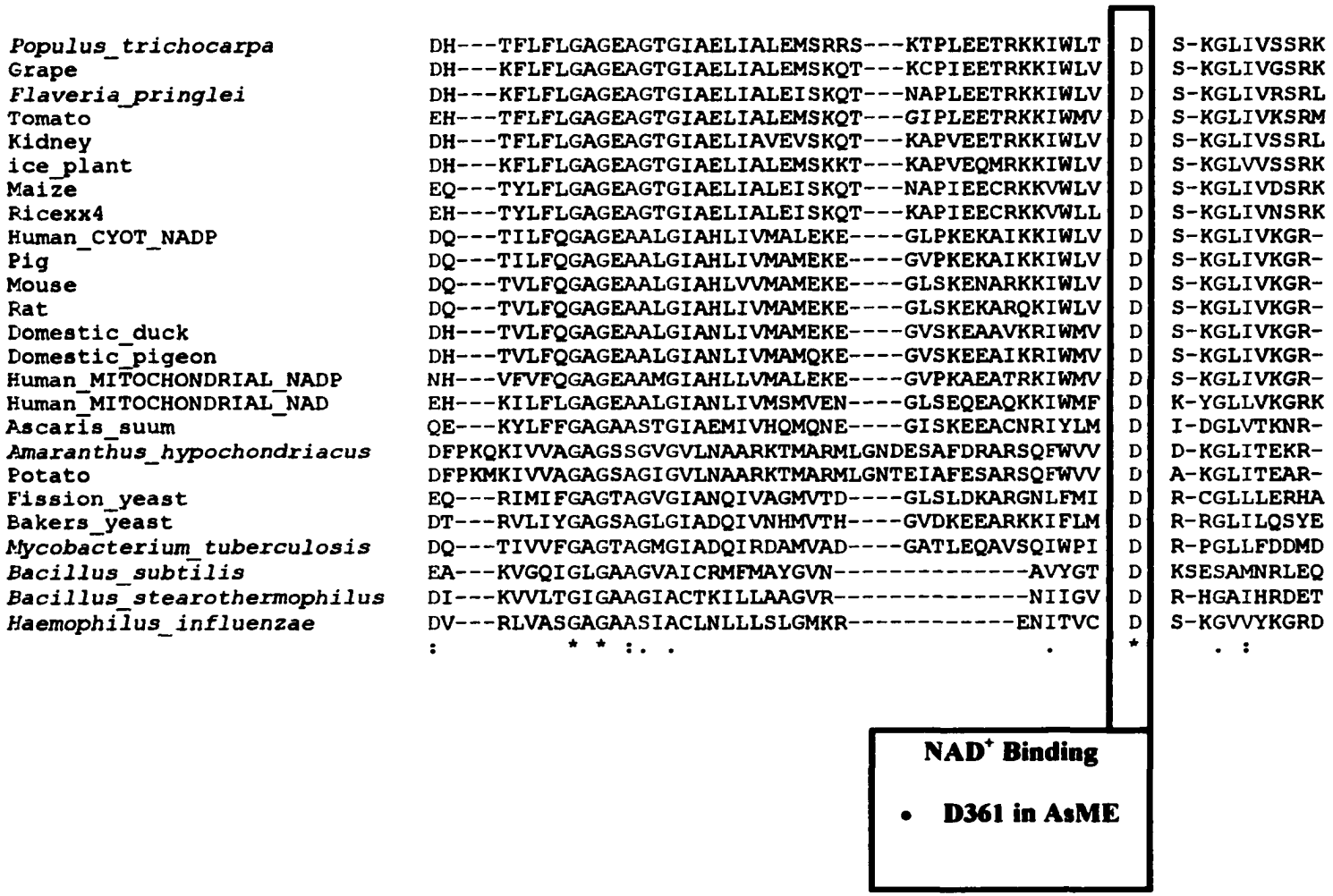
Populus_trichocarpa DH---TFLFLGAGEAGTGIAELIALEMSRRS---KTPLEETRKKIWLT D S-KGLIVSSRK
Grape DH---KFLFLGAGEAGTGIAELIALEMSKQT---KCPIEETRKKIWLV D S-KGLIVGSRK
Flaveria_pringlei DH---KFLFLGAGEAGTGIAELIALEISKQT---NAPLEETRKKIWLV D S-KGLIVRSRL
Tomato EH---TFLFLGAGEAGTGIAELIALEMSKQT---GIPLEETRKKIWMV D S-KGLIVKSRM
Kidney DH---TFLFLGAGEAGTGIAELIAVEVSKQT---KAPVEETRKKIWLV D S-KGLIVSSRL
ice_plant DH---KFLFLGAGEAGTGIAELIALEMSKKT---KAPVEQMRKKIWLV D S-KGLVVSSRK
Maize EQ---TYLFLGAGEAGTGIAELIALEISKQT---NAPIEECRKKVWLV D S-KGLIVDSRK
Ricexx4 EH---TYLFLGAGEAGTGIAELIALEISKQT---KAPIEECRKKVWLL D S-KGLIVNSRK
Human_CYOT_NADP DQ---TILFQGAGEAALGIAHLIVMALEKE----GLPKEKAIKKIWLV D S-KGLIVKGR-
Pig DQ---TILFQGAGEAALGIAHLIVMAMEKE----GVPKEKAIKKIWLV D S-KGLIVKGR-
Mouse DQ---TVLFQGAGEAALGIAHLVVMAMEKE----GLSKENARKKIWLV D S-KGLIVKGR-
Rat DQ---TVLFQGAGEAALGIAHLIVMAMEKE----GLSKEKARQKIWLV D S-KGLIVKGR-
Domestic_duck DH---TVLFQGAGEAALGIANLIVMAMEKE----GVSKEAAVKRIWMV D S-KGLIVKGR-
Domestic_pigeon DH---TVLFQGAGEAALGIANLIVMAMQKE----GVSKEEAIKRIWMV D S-KGLIVKGR-
Human_MITOCHONDRIAL_NADP NH---VFVFQGAGEAAMGIAHLLVMALEKE----GVPKAEATRKIWMV D S-KGLIVKGR-
Human_MITOCHONDRIAL_NAD EH---KILFLGAGEAALGIANLIVMSMVEN----GLSEQEAQKKIWMF D K-YGLLVKGRK
Ascaris_suum QE---KYLFFGAGAASTGIAEMIVHQMQNE----GISKEEACNRIYLM D I-DGLVTKNR-
Amaranthus_hypochondriacus DFPKQKIVVAGAGSSGVGVLNAARKTMARMLGNDESAFDRARSQFWVV D D-KGLITEKR-
Potato DFPKMKIVVAGAGSAGIGVLNAARKTMARMLGNTEIAFESARSQFWVV D A-KGLITEAR-
Fission_yeast EQ---RIMIFGAGTAGVGIANQIVAGMVTD----GLSLDKARGNLFMI D R-CGLLLERHA
Bakers_yeast DT---RVLIYGAGSAGLGIADQIVNHMVTH----GVDKEEARKKIFLM D R-RGLILQSYE
Mycobacterium_tuberculosis DQ---TIVVFGAGTAGMGIADQIRDAMVAD----GATLEQAVSQIWPI D R-PGLLFDDMD
Bacillus_subtilis EA---KVGQIGLGAAGVAICRMFMAYGVN----------AVYGT D KSESAMNRLEQ
Bacillus_stearothermophilus DI---KVVLTGIGAAGIACTKILLAAGVR----------NIIGV D R-HGAIHRDET
Haemophilus_influenzae DV---RLVASGAGAASIACLNLLLSLGMKR----------ENITVC D S-KGVVYKGRD
: * * :. . . * . :
NAD+ Binding
• D361 in AsME

```
Populus_trichocarpa                ESLQHFKKPWAHEHEPVK--------GLLEVVKAIKPIVLIGTSGVGKTFTKEVIEAMAS
Grape                              DSLQQFKKPWAHEHEPVK--------DLLDAVKVIKPTVLIGSSGVGKAFTKEVIEAMAS
Flaveria_pringlei                  DSLQHFKKPWAHDHEPVN--------KFLDAVKAIKPTVLIGSSGAGQTFTKEVVEAMSS
Tomato                             EMLQHFKRPWAHDHEPVQ--------ELVNAVKSIKPTVLIGSSGAGRTFTKEVVQAMAT
Kidney                             ESLQQFKKPWAHEHEPVK--------GLLEAVKAIKPTVLIGSSGAGKTFTKEVVETMAS
ice_plant                          ETLQQFKLPWAHEHEPIT--------TLIDAVQAIKPTVLIGTSGKGKQFTKEVVEAMAN
Maize                              GSLQPFKKPWAHEHEPLK--------TLYDAVQSIKPTVLIGTSGVGRTFTKEIIEAMSS
Ricexx4                            ESLQAFKKPWAHEHEPVT--------TLLDAVQSIKPTVLIGTSGVGKTFTKEVIEAMAS
Human_CYOT_NADP                    ASLTQEKEKFAHEHEEMK--------NLEAIVQEIKPTALIGVAAIGGAFSEQILKDMAA
Pig                                AALTNEKEEFAHEHEEMK--------NLEAIVQDIKPTALIGVAAIGGAFSEQILKDMAA
Mouse                              ASLTEEKEVFAHEHEEMK--------NLEAIVQKIKPTALIGVAAIGGAFTEQILKDMAA
Rat                                ASLTEEKEVFAHEHEEMK--------NLEAIVQKIKPTALIGVAAIGGAFTEQILKDMAA
Domestic_duck                      ASLTAEKTRFAHEHAEMK--------NLEDIVKDIKPSVLIGVAAIGGAFTKEILQDMAA
Domestic_pigeon                    ASLTPEKEHFAHEHCEMK--------NLEDIVKDIKPTVLIGVAAIGGAFTQQILQDMAA
Human_MITOCHONDRIAL_NADP           SHLNHEKEMFAQDHPEVN--------SLEEVVRLVKPTAIIGVAAIAGAFTEQILRDMAS
Human_MITOCHONDRIAL_NAD            AKIDSYQEPFTHSAPESIPD------TFEDAVNILKPSTIIGVAGAGRLFTPDVIRAMAS
Ascaris_suum                       KEMNPRHVQFAKDMPETT--------SILEVIRAARPGALIGASTVRGAFNEEVIRAMAE
Amaranthus_hypochondriacus         ANLDPEVQPFAWKENEISLQGLNEGAKLVEVVRQVKPDVLLGLSAYGGLFSKEVLEALKD
Potato                             ENVDPDARPFARKIKEIERQGLSEGATLAEVVREVKPDVLLGLSACGGLFSKEVLEALKH
Fission_yeast                      KIATDGQKPFLKKDSDFKEVPSGD-INLESAIALVKPTILLGCSGQPGKFTEKAIREMSK
Bakers_yeast                       ANSTPAQHVYAKSDAEWAGINTR---SLHDVVENVKPTCLVGCSTQAGAFTQDVVEEMHK
Mycobacterium_tuberculosis         DLR-DFQVPYAKNRHQLGVAVGDR-VGLSDAIKIASPTILLGCSTVYGAFTKEVVEAMTA
Bacillus_subtilis                  YG--------GQAVS-------------SIEELMETCDIVIATTGVPGLIKPAFVR----
Bacillus_stearothermophilus        YEN-PYWQEYAQLTNPDNL-------KGSLSDVIAGADVFIGVS-APGILKVEDVKKMA-
Haemophilus_influenzae             DK---MDQTKKEYAIEDNG-------WRKLADAIPNADIFLGCS-AAGALTQDMVKSMA-
                                                                    .:. :     :.   :.
```

```
Populus_trichocarpa              FN-EKPLILALSNPTSQS  E  CTAQEAYTWTKGKAIFASGSPFDPVEYE-GKVFVPGQSNNA
Grape                            CN-EKPLILALSNPTSQS  E  CTAEEAYTWTQGRAIFASGSPFDPVEYN-GKTFVPGQANNA
Flaveria_pringlei                FN-EKPIILALSNPTSQS  E  CTAEQAYTWSEGRTIFASGSPFAPVEYN-GKVYVSGQSNNA
Tomato                           FN-EKPIIFALSNPTSQS  E  CTAEEAYSWSEGRAIFASGSPFAPVEYN-GKVYASGQANNA
Kidney                           LN-EKPLILALSNPTSQS  E  CTAEEAYTWSKGRAIFASGSPFDPVEYE-GKLFVPGQANNA
ice_plant                        IN-AKPLILALSNPTSQS  E  CTAEEAYTWSQGHAIFASGSPFDPVEYE-GRTFVPGQANNA
Maize                            FN-ERPIIFSLSNPTSHS  E  CTAEQAYTWSQGRSIFASGSPFAPVEYE-GKTFVPGQSNNA
Ricexx4                          FN-ERPVIFSLANPTSHS  E  CTAEEAYNWSQGRAVFASGSPFDPVEYN-GKIHVPGQSNNA
Human_CYOT_NADP                  FN-ERPIIFALSNPTSKA  E  CSAEQCYKITKGRAIFASGSPFDPVTLPNGQTLYPGQGNNS
Pig                              FN-ERPIIFALSNPTSKA  E  CTAERGYTLTQGRAIFASGSPFDPVTLPSGQTLYPGQGNNS
Mouse                            FN-ERPIIFALSSPTSKA  E  CSADECYKVTKGRAIFASGSPFDPVTLPDGRTLFPGQGNNS
Rat                              FN-ERPIIFALSNPTSKA  E  CSAEECYKVTKGRAIFASGSPFDPVTLPDGRTLFPGQGNNS
Domestic_duck                    FN-KRPIIFALSNPTSKA  E  CTAEQCYKYTEGRGIFASGSPFDPVTLPNGKTLYPGQGNNS
Domestic_pigeon                  FN-KRPIIFALSNPTSKA  E  CTAEQLYKYTEGRGIFASGSPFDPVTLPSGQTLYPGQGNNS
Human_MITOCHONDRIAL_NADP         FH-ERPIIFALSNPTSKA  E  CTAEKCYRVTEGRGIFASGSPFKSVTLEDGKTFIPGQGNNA
Human_MITOCHONDRIAL_NAD          IN-ERPVIFALSNPTAQA  E  CTAEEAYTLTEGRCLFASGSPFGPVKLTDGRVFTPGQGNNV
Ascaris_suum                     IN-ERPIIFALSNPTSKA  E  CTAEEAYTFTNGAALYASGSPFPNFELN-GHTYKPGQGNNA
Amaranthus_hypochondriacus       STSTRPAIFAMSNPTKNA  E  CTPEEAFSIVGDHVVYASGSPFKDVDLGNGKIGHVNQGNNM
Potato                           STSTRPAIFPMSNPTRNA  E  CTPEEAFSILGENIIFASGSPFKDVDLGNGHVGHCNQANNM
Fission_yeast                    HV-ERPIIFPISNPTTLM  E  AKPDQIDKWSDGKALIATGSPLPPLNRN-GKKYVISQCNNA
Bakers_yeast                     HN-PRPIIFPLSNPTRLH  E  AVPADLMKWTNNNALVATGSPFPPVDG-----YRISENNNC
Mycobacterium_tuberculosis       SC-KHPMIFPLSNPTSRM  E  AIPADVLAWSNGRALLATGSPVAPVEFD-ETTYVIGQANNV
Bacillus_subtilis                ---SGQVILALSNPKPEI  E  PEAALQAG--------------AAYAAD-GRS-----VNNV
Bacillus_stearothermophilus      ---RDPIVFAMANPIPEI  D  PELAEPY---------------VRVMAT-GRSDYPNQINNV
Haemophilus_influenzae           ---AHPIILALANPNPEI  T  PPEAKAVRP-------------DAIVCT-GRSDYPNQVNNV
                                       ::.::.*                                              **
```

NAD$^+$ Binding

- **E427 in Human NAD ME**
- **E440 in AsME**

```
Populus_trichocarpa                YIFPGLGLGLVISGAIRVHDDMLLAAAEALAGQ-IKEEYLAKGL------------IYPP
Grape                              YIFPGLGMGLVISGAIRVHDEMLLAASEALARQ-VTQENFDKGL------------IYPP
Flaveria_pringlei                  YIFPGFGLGLIISGAIRVHDEMLLAASEALAEQ-VTQEHFDNGL------------IYPP
Tomato                             YIFPGFGLGLIISGAIRVHDDMLLVASEALADE-VSQENFEKGT------------HIPP
Kidney                             YIFPGFGLGLIMSGAIRVRDEMLLAASEALAAQ-VSEENYDKGL------------IYPP
ice_plant                          YIFPGFGLGLIMCGAIRVHDDMLLAASEALASQ-VTGEHFIKGL------------IYPP
Maize                              YIFPGLGLGLVISGAVRVHEDMLLAASKALADQ-ATQDNFEKGS------------IFPP
Ricexx4                            YIFPGFGLGVVISGAVRVHEDMLLAASETLADQ-ATQENFEKGS------------IFPP
Human_CYOT_NADP                    YVFPGVALGVVACGLRQITDNIFLTTAEVIAQQ-VSDKHLEEGR------------LYPP
Pig                                YVFPGVALAVVACGLRHITDKIFLTTAEVIAQQ-VSDKHLEEGR------------LYPP
Mouse                              YVFPGVALGVVACGLRHIDDKVFLTTREVISQQ-VSDKHLQEGR------------LYPP
Rat                                YVFPGVALGVVACGLRHINDSVFLTTAEVISQQ-VSDKHLEEGR------------LYPP
Domestic_duck                      YVFPGVALGVIACGLKHIGEDVFLTTAEVIAEQ-VSEENLQEGR------------LYPP
Domestic_pigeon                    YVFPGVALGVISCGLKHIGDDVFLTTAEVIAQE-VSEENLQEGR------------LYPP
Human_MITOCHONDRIAL_NADP           YVFPGVALGVIAGGIRHIPDEIFLLTAEQIAQE-VSEQHLSQGR------------LYPP
Human_MITOCHONDRIAL_NAD            YIFPGVALAVILCNTRHISDSVFLEAAKALTSQ-LTDEELAQGR------------LYPP
Ascaris_suum                       YIFPGVALGTILFQIRHVDNDLFLLAAKKVASC-VTEDSLKVGR------------VYPQ
Amaranthus_hypochondriacus         YLFPGIGLGVLLSGSRIISDSMFQAAAERLAGY-MTDEEVINGV------------IYPS
Potato                             FLFPGIGLGTLLSGSRIVSDGMLQAAAECLAAY-ITEEEVLKGI------------IYPS
Fission_yeast                      LLYPALGVACVLSRCKLLSDGMLKAASDALATV-PRSLFAADEA------------LLPD
Bakers_yeast                       YSFPGIGLGAVLSRATTITDKMISAAVDQLAELSPLREGDSRPG------------LLPG
Mycobacterium_tuberculosis         LAFPGIGLGVIVAGARLITRRMLHAAAKAIAHQ--ANPTNPGDS------------LLPD
Bacillus_subtilis                  LGFPGIFRGALNAKSTEINHDMLVAAAEAIAACTKQGD------------------VVP
Bacillus_stearothermophilus        LCFPGIFRGALDCRAREINEEMKLAAAKAIASVVTEDEL--------------NETYIIP
Haemophilus_influenzae             LCFPFIFRGALDVGATTINEEMKRAAVYAIADLALEEQNEVVTSAYGGEGATFGADYVIP
                                     :* .  . :      :   :   :   ::
```

```
Populus_trichocarpa                LSNIRKISVQIAANVAAKAYELGLATRLPRPE----------------NLVKHAESCMYS
Grape                              FSNIRKISAHIAANVAAKAYELGLATRLPQPE----------------NLVKYAESCMYS
Flaveria_pringlei                  FTNIRKISAHIAAKVAAKAYELGLASRLPQPE----------------NLVAYAESCMYS
Tomato                             FSNIRKISAHIA-KVAAKAYELGLATRLPQPK----------------DLVAYAESCMYS
Kidney                             FTNIRKISANIAAKVAAKAYDLGLASHLKRPK----------------DLVKYAESCMYS
ice_plant                          FKDIRKISAHIAAGVAAKAYELGLASRLPQPA----------------DLVKFAESCMYN
Maize                              FTSIRKISAHIAAAVAGKAYELGLATRLPPPS----------------DLVKYAENCMYT
Ricexx4                            FTNIRKISARIAATVAAKAYELGLATRLPQPR----------------DLEKYAESCMYT
Human_CYOT_NADP                    LNTIRDVSLKIAEKIVKDAYQEKTATVYPEPQ----------------NKEAFVRSQMYS
Pig                                LNTIRDVSLKIAEKIVRDAYQEKTATIYPEPS----------------NKEAFVRSQMYS
Mouse                              LNTIRGVSLKIAVKIVQDAYKEKMATVYPEPQ----------------NKEEFVSSQMYS
Rat                                LNTIRDVSLKIAVKIVQDAYKEKMATVYPEPQ----------------NKEEFVSSQMYS
Domestic_duck                      LVTIQHVSLKIAVRIAEEAYRNNTASTYPQPK----------------DLEAFIQSQIYS
Domestic_pigeon                    LVTIQQVSLKIAVRIAKEAYRNNTASTYPQPE----------------DLEAFIRSQVYS
Human_MITOCHONDRIAL_NADP           LSTIRDVSLRIAIKVLDYAYKHNLASYYPEPK----------------DKEAFVRSLVYT
Human_MITOCHONDRIAL_NAD            LANIQEVSINIAIKVTEYLYANKMAFRYPEPE----------------DKAKYVKERTWR
Ascaris_suum                       LKEIREISIQIAVEMAKYCYKNGTANLYPQPE----------------DLEKYVRAQVYN
Amaranthus_hypochondriacus         ISRIRDITKEVAAAVIKEAVEEDLAEGYRDMDA------RELQKLNEEQILEYIEKNMWN
Potato                             ISRIRDITKEVAAAVVKEAIEEDLAEGYREMDS------RELRKLDEAQISEFVENNMWS
Fission_yeast                      LNNAREISRHIVFAVLKQAVSEGMS--------------TVDLPKDDAKLKEWIIEREWN
Bakers_yeast                       LDTITNTSARLATAVILQALEEGTARIEQEQVPGGAPGETVKVPRDFDECLQWVKAQMWE
Mycobacterium_tuberculosis         VQNLRAISTTVAEAVYRAAVQDGVA------------------SRTHDDVRQAIVDTMWL
Bacillus_subtilis                  QPLDSKVHHAVAAAVEHAAL-TAVK----------------------------------
Bacillus_stearothermophilus        SVFNSKVVERVRQAVVEAAYRTGVARKDNIP----------------VGGYTGQ-----
Haemophilus_influenzae             RPFDPRLIVRIAPAVAKAAMESGVATRPIQN----------------WDAYVEKLTQFV
                                             :   :
```

```
Populus_trichocarpa          PAYRYYR-------------------------------------------------------
Grape                        PVYRSYR-------------------------------------------------------
Flaveria_pringlei            PKYRNYR-------------------------------------------------------
Tomato                       PAYRSYR-------------------------------------------------------
Kidney                       PGYRSYR-------------------------------------------------------
ice_plant                    PTYRSFR-------------------------------------------------------
Maize                        PVYRNYR-------------------------------------------------------
Ricexx4                      PVYRSYR-------------------------------------------------------
Human_CYOT_NADP              TDYDQILPDCYSWPEEVQ----KIQTKVDQ---------------------------------
Pig                          TDYDQILPDGYSWPEEAQ----KIQTKLD----------------------------------
Mouse                        TNYDQILPDCYPWPAEVQ----KIQTKVNQ---------------------------------
Rat                          TNYDQILPDCYSWPEEVQ----KIQTKVNQ---------------------------------
Domestic_duck                TDYNSFVADSYTWPEEAM----KVKL-------------------------------------
Domestic_pigeon              TDYNCFVADSYTWPEEAM----KVKL-------------------------------------
Human_MITOCHONDRIAL_NADP     PDYDSFTLDSYTWPKEAM----NVQTV------------------------------------
Human_MITOCHONDRIAL_NAD      SEYDSLLPDVYEWPESAS----SPPVITE----------------------------------
Ascaris_suum                 TEYEELINATYDWPEQDMRHGFPVPVVRHDSMDG------------------------------
Amaranthus_hypochondriacus   PEYPTLVYKKR---------------------------------------------------
Potato                       PDYPTLVYKKD---------------------------------------------------
Fission_yeast                PEYKPFV-------------------------------------------------------
Bakers_yeast                 PVYRPMIKVQHDPSVHTNQL------------------------------------------
Mycobacterium_tuberculosis   PAYD----------------------------------------------------------
Bacillus_subtilis            ----------------------------------------------------------------
Bacillus_stearothermophilus  ----------------------------------------------------------------
Haemophilus_influenzae       YKTSLFMRP-IFSQAKSAKQRIILAEGEENKALHATQEVISMGLANPILIGRRSVIEEKI
```

Haemophilus_influenzae KKLGLRLTAGVDFEIVDNEDNPRYEECWKHYYELTKRKGITPAIAKRVVRSNTTVLASTL

Haemophilus_influenzae LSLGYADALVCGLFGSYGKHLASIRDIIGLKDGVKTAAALNSLVLPTGNVFLTDTHVNSN

Haemophilus_influenzae PTAEELAEITLMAAEEIHRFGIEPAVALLSHSNFGSSDSLGAPKMREVLQIVKERNPHLM

Haemophilus_influenzae IDGEMRGDLAMNEAHRKELMPDSPLKGSANLLVFPDLSASRISYSLLRGTTTAITVGPIL

Haemophilus_influenzae MGMNKSAHILNPGASVRRIINMIAYAAVKAQQE

- **Alignment data :**

  Alignment length : 1053
  Identity (*) : 22 is 2.09 %
  Strongly similar (:) : 43 is 4.08 %
  Weakly similar (.) : 22 is 2.09 %
  Different : 966 is 91.74 %
  Sequence 0001 : *Populus_trichocarpa* (591 residues).
  Sequence 0002 : Grape (591 residues).
  Sequence 0003 : *Flaveria_pringlei* (647 residues).
  Sequence 0004 : Tomato (573 residues).
  Sequence 0005 : Kidney (589 residues).
  Sequence 0006 : ice_plant (585 residues).
  Sequence 0007 : Maize (636 residues).
  Sequence 0008 : Ricexx4 (638 residues).
  Sequence 0009 : Human_CYOT_NADP (572 residues).
  Sequence 0010 : Pig (557 residues).
  Sequence 0011 : Mouse (572 residues).
  Sequence 0012 : Rat (572 residues).
  Sequence 0013 : Domestic_duck (557 residues).
  Sequence 0014 : Domestic_pigeon (557 residues).
  Sequence 0015 : Human_MITOCHONDRIAL_NADP (604 residues).
  Sequence 0016 : Human_MITOCHONDRIAL_NAD (584 residues).
  Sequence 0017 : Ascaris_suum (643 residues).
  Sequence 0018 : *Amaranthus_hypochondriacus* (623 residues).
  Sequence 0019 : Potato (626 residues).
  Sequence 0020 : Fission_yeast (565 residues).
  Sequence 0021 : Bakers_yeast (669 residues).
  Sequence 0022 : *Mycobacterium_tuberculosis* (652 residues).
  Sequence 0023 : *Bacillus_subtilis* (439 residues).
  Sequence 0024 : *Bacillus_stearothermophilus* (478 residues).
  Sequence 0025 : *Haemophilus_influenzae* (756 residues)

- **Domain seperation point are determined upon Human NAD Malic Enzyme structure.**